ACD-8569

MICROMINIATURE RATE-OF-TURN SENSOR

FINAL REPORT

SEPTEMBER 1967

CONTRACT NO. NAS8-20618
CONTROL NO. 1-6-40-62363(1F) and S2(1F)

NATIONAL AERONAUTICS AND
SPACE ADMINISTRATION
GEORGE C. MARSHALL SPACE FLIGHT CENTER
HUNTSVILLE, ALABAMA

Prepared by

GENERAL ELECTRIC COMPANY
AVIONIC CONTROLS DEPARTMENT
BINGHAMTON, NEW YORK

Author

S. B. HAMILTON

ABSTRACT

A laboratory model of a single-axis vibratory angular rate servo has been developed, designed, and built. The vibrating element is a "free-free" metal beam mounted at its first mode nodal points and is vibrated by piezoelectric transducers mounted on the beam faces. Changes in the beam vibration produced to Coriolis forces due to applied angular rates are detected by other piezoelectric transducers. Electronics are used to provide voltages to vibrate the beam and to amplify and demodulate the sensor voltage output.

The major emphasis in the model development was placed on improving the threshold and null stability of the sensor. To achieve this, the new flexural pivot mounting method was developed which stabilized the drift characteristics of the sensor and improved the external vibration performance. Also, electronics were developed that provided a more accurate driving signal and a study was made of cross-couplings effects in the beam. The results of this work was at least at 5 to 1 improvement in sensor threshold and a corresponding improvement in null stability.

FOREWORD

This report was prepared by the General Electric Company, Avionic Controls Department, Binghamton, New York, on Contract Number NAS8-20618, "Microminiature Rate-of-Turn Sensor", administered by the National Aeronautics and Space Administration, Marshall Space Flight Center. The contract was initiated under Control Number 1-6-40-62363(1F) and S2(1F).

This is the final report covering the sensor development work for the fifteen month period from June 1966 to September 1967.

The contract work was a group effort, with the following principle contributors and their field of effort: S. B. Hamilton, Program Management and Analysis; J. N. Russell, Electronics Design; W. D. Gates and P. R. Danyluk, Mechanical Design; T. F. Conroy and G. Macko, Mechanical Details and Assembly.

This report is published by the Avionic Controls Department under publication number ACD 8569.

TABLE OF CONTENTS

LIST OF ILLUSTRATIONS

LIST OF ILLUSTRATIONS (cont'd)

Section 1

INTRODUCTION AND SUMMARY

This report describes the development, design, fabrication, and testing of a laboratory model for a single-axis vibratory angular rate sensor. The vibrating element of the sensor is a "free-free" metal beam of approximately a square cross-section that is mounted at its first mode nodal points, and is vibrated by piezoelectric transducers. The transducers, bonded to each of the four faces of the beam, are also used to detect changes in the direction of beam vibration due to angular rates about the longitudinal axis of the beam which is the sensitive axis. Electronics, utilizing microelectronic operational amplifiers, produce the voltages which excite the transducers, and also amplify and demodulate the sensor output signal.

The impetus behind the development of vibratory angular rate sensors in general, and the "free-free" beam sensor in particular, is the potential long-life and excellent operating characteristics of this type of sensor when compared to conventional angular rate sensors with rotating elements. The absence of bearings and requirements for absolute dimensional stability, combine to make the expected life of a vibratory sensor much greater than its conventional counterpart. This, coupled with the accuracy, wide dynamic range, low power, dc operation, and wide bandwidth of the device, make the vibratory or "solid-state" sensor applicable for long duration space missions. The principle limitations of the "free-free" angular rate at the present time are its environmental performance, specifically temperature, and its "threshold" or ability to measure very slow rates-of-turn. The second of these was the subject of the work on this contract.

A picture of the laboratory model is shown in Figure 1, and consists of the mechanical assembly of beam, mount, and transducers and the associated electronics. Table 1 is a summary of the model characteristics as determined by test. The threshold/resolution of this particular unit is approximately 0.002 deg/sec and the null uncertainty is 0.15 deg/sec. These parameters are an improvement by an order of magnitude as a result of the analysis and testing accomplished during this contract. The specific design changes to the "free-free" beam sensor which resulted in the improvement were the following:

1. Development of the flexural pivot mount for the beam. This approach allows the interaction between the beam and mount to be minimized and held constant.

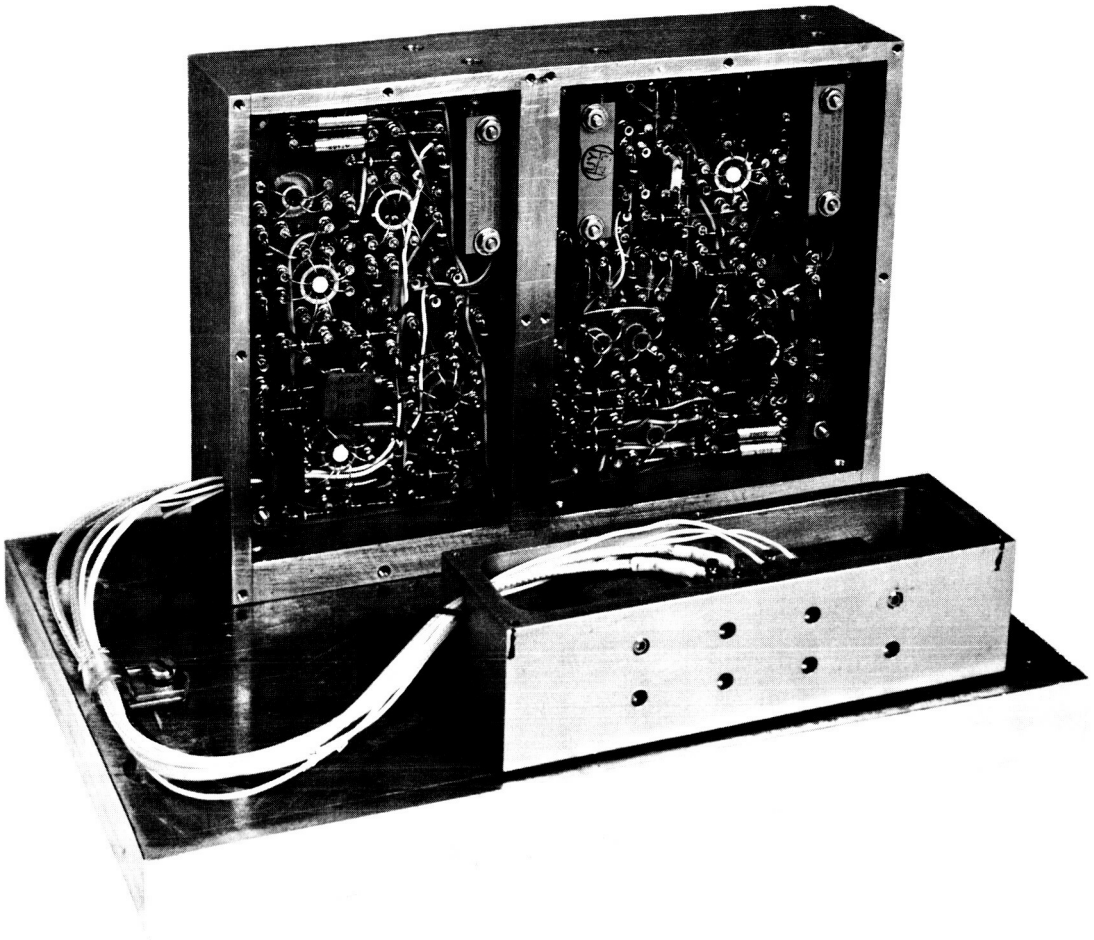

Solid-State Sensor, Laboratory Model

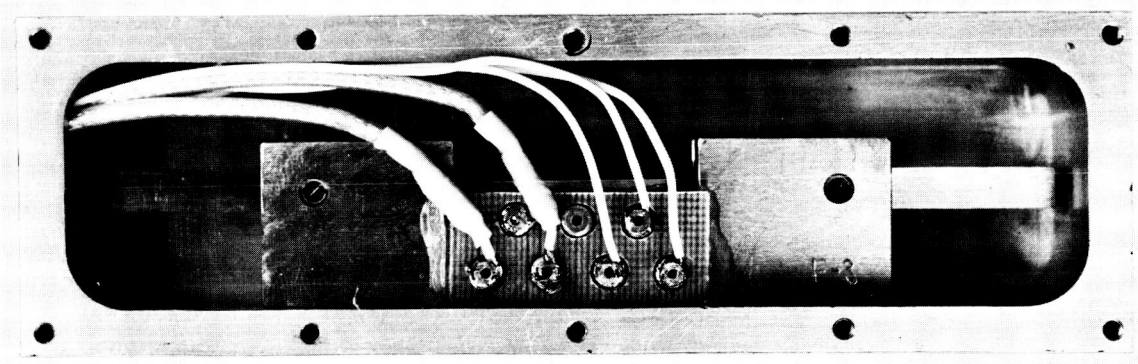

Figure 1. Solid-State Sensor Mechanical Assembly

2. Minimization of cross-coupling between input and output vibration to reduce sensor noise threshold.

3. Development and design of improved drive electronics. The reduction of harmonic content and improved regulation reduce sensor noise.

Scale Factor:	0.395 volt/deg/sec
Full Scale Rate:	± 25 deg/sec
Linearity:	≤ 1% (point-for-point)
Frequency Response:	1 db to 40 Hz
Natural Frequency:	63 Hz
Damping Ratio:	0.6
Threshold and Resolution:	~ 0.002 deg/sec
Null Uncertainty:	0.15 deg/sec
Output Voltage:	± 10 volts dc
Output Impedance:	< 500 ohms
Power:	2 watts at ± 15 volts dc
Null Shift with Temp: ($-10^{o}C$ to $+70^{o}C$)	< ± 6 deg/sec
Null Shift with Vibration: 1g (0 to 1500 Hz)	< 0.25 deg/sec

Laboratory Model Performance Parameters

TABLE 1

Section 2

THEORY OF OPERATION

The operation of a vibratory angular rate sensor depends upon the motion of individual mass particles in a rotating frame of reference. The mass can be vibrating in any one of many modes (extensionally, bending, torsionally, etc.) at small amplitudes such that the particle motion is approximately linear and varying sinusoidally with time. Usually, the vibrational motion is constrained so that the mass particles can move only in one plane. The following paragraphs contain a description of particle motion and derivation of the vibratory sensor sensitivity.

DERIVATION OF GENERAL EQUATIONS OF MOTION

If the mass particle position in a moving co-ordinate system with unit vectors, $\bar{i}$, $\bar{j}$, $\bar{k}$ is given by

$$\bar{r} = \bar{i}x + \bar{j}y + \bar{k}z \tag{1}$$

and if the motion of the $\bar{i}$, $\bar{j}$, $\bar{k}$ triad with respect to the inertial triad, $\bar{I}$, $\bar{J}$, $\bar{K}$, is described by the angular velocity vector

$$\bar{\omega} = \bar{i}\omega_x + \bar{j}\omega_y + \bar{k}\omega_z \tag{2}$$

then the velocity and acceleration of the mass particle are given by

$$\bar{v} = \frac{d\bar{r}}{dt} = \frac{\partial \bar{r}}{\partial t} + \bar{\omega} \times \bar{r} \tag{3}$$

$$\bar{a} = \frac{d\bar{v}}{dt} = \frac{\partial^2 \bar{r}}{\partial t^2} + 2\bar{\omega} \times \frac{\partial \bar{r}}{\partial t} + \frac{\partial \bar{\omega}}{\partial t} \times \bar{r} + \bar{\omega} \times \bar{\omega} \times \bar{r} \tag{4}$$

where $\frac{\partial \bar{r}}{\partial t}$ is the rate of change of position with respect to the moving co-ordinate system.

$$\frac{\partial \bar{r}}{\partial t} = \bar{i}\dot{x}(t) + \bar{j}\dot{y}(t) + \bar{k}\dot{z}(t) \tag{5}$$

If the particle mass is m and the general force on the particle is $\overline{F}$, then the equation of motion is

$$\frac{1}{m}\overline{F} = \frac{\partial^2 \overline{r}}{\partial t^2} + 2\overline{\omega} \times \frac{\partial \overline{r}}{\partial t} + \frac{\partial \overline{\omega}}{\partial t} \times \overline{r} + \overline{\omega} \times \overline{\omega} \times \overline{r} \tag{6}$$

In Equation (6), the Coriolis acceleration is given by

$$A_c = 2\overline{\omega} \times \frac{\partial \overline{r}}{\partial t} \tag{7}$$

Equation (6) can be expanded and re-written in matrix form as

$$\frac{1}{m}\begin{bmatrix} F_x \\ F_y \\ F_z \end{bmatrix} = \begin{bmatrix} \ddot{x} \\ \ddot{y} \\ \ddot{z} \end{bmatrix} + \begin{bmatrix} 0 & -2\omega_z & 2\omega_y \\ 2\omega_z & 0 & -2\omega_x \\ -2\omega_y & 2\omega_x & 0 \end{bmatrix} \begin{bmatrix} \dot{x} \\ \dot{y} \\ \dot{z} \end{bmatrix}$$

$$+ \begin{bmatrix} -(\omega_y^2 + \omega_z^2) & \omega_x\omega_y - \dot{\omega}_z & \omega_x\omega_z + \dot{\omega}_y \\ \omega_x\omega_y + \dot{\omega}_z & -(\omega_x^2 + \omega_z^2) & \omega_y\omega_z - \dot{\omega}_x \\ \omega_x\omega_z - \dot{\omega}_y & \omega_y\omega_z + \dot{\omega}_x & -(\omega_x^2 + \omega_y^2) \end{bmatrix} \begin{bmatrix} x \\ y \\ z \end{bmatrix} \tag{8}$$

The specific case of Equation (8) that applies to the general vibratory angular rate sensor is the case when the particles are constrained to move in the y - z plane, and the angular rate $\overline{\omega}$ has only one component, ω_z. Hence, the equations simplify to

$$\frac{1}{m}\begin{bmatrix} F_y \\ F_z \end{bmatrix} = \begin{bmatrix} \ddot{y} \\ \ddot{z} \end{bmatrix} + \begin{bmatrix} 0 & -2\omega_x \\ 2\omega_x & 0 \end{bmatrix} \begin{bmatrix} \dot{y} \\ \dot{z} \end{bmatrix} + \begin{bmatrix} -\omega_x^2 & -\dot{\omega}_x \\ \dot{\omega}_x & -\omega_x^2 \end{bmatrix} \begin{bmatrix} y \\ z \end{bmatrix} \tag{9}$$

The generalized forces F_y and F_z consist primarily of internal damping and restraint forces of the vibrating material, and external forces produced by electrical, magnetic, or mechanical transducers. It is assumed here that the amplitudes of any movement are small enough so that the y and z damping and restraint forces are independent. Therefore,

$$\begin{bmatrix} F_y \\ F_z \end{bmatrix} = \underset{\text{Transducer}}{\begin{bmatrix} f_y \\ f_z \end{bmatrix}} - \underset{\text{Damping}}{\begin{bmatrix} C_y \dot{y} \\ C_z \dot{z} \end{bmatrix}} - \underset{\text{Restraint}}{\begin{bmatrix} K_y y \\ K_z z \end{bmatrix}} \tag{10}$$

Equations (9) and (10) combined yield the following particle equations of motion

$$\frac{1}{m} \begin{bmatrix} f_y \\ f_z \end{bmatrix} = \begin{bmatrix} \ddot{y} \\ \ddot{z} \end{bmatrix} + \begin{bmatrix} \frac{\omega_c}{Q_c} & -2\omega_x \\ 2\omega_x & \frac{\omega_o}{Q_o} \end{bmatrix} \begin{bmatrix} y \\ z \end{bmatrix}$$

$$+ \begin{bmatrix} \left(\omega_c^2 - \omega_x^2\right) & -\dot{\omega}_x \\ \dot{\omega}_x & \left(\omega_o^2 - \omega_x^2\right) \end{bmatrix} \begin{bmatrix} y \\ z \end{bmatrix} \tag{11}$$

where

$$\frac{C_y}{m} = \frac{\omega_c}{Q_c}, \quad \frac{C_z}{m} = \frac{\omega_o}{Q_o}, \quad \frac{K_y}{m} = \omega_c^2, \quad \frac{K_z}{m} = \omega_o^2 \tag{12}$$

The above equations are the basic operating relationships for a vibratory angular rate sensor. For convenience and purposes of definition, the 'y' axis is designated as the "vibrational" axis, the 'z' axis as the "output" axis, and the 'x' axis as the "input" axis. For example, if a free-free beam vibrating in its fundamental bending mode is chosen as the vibrating mass, the sensor axis would be defined as shown in Figure 2.

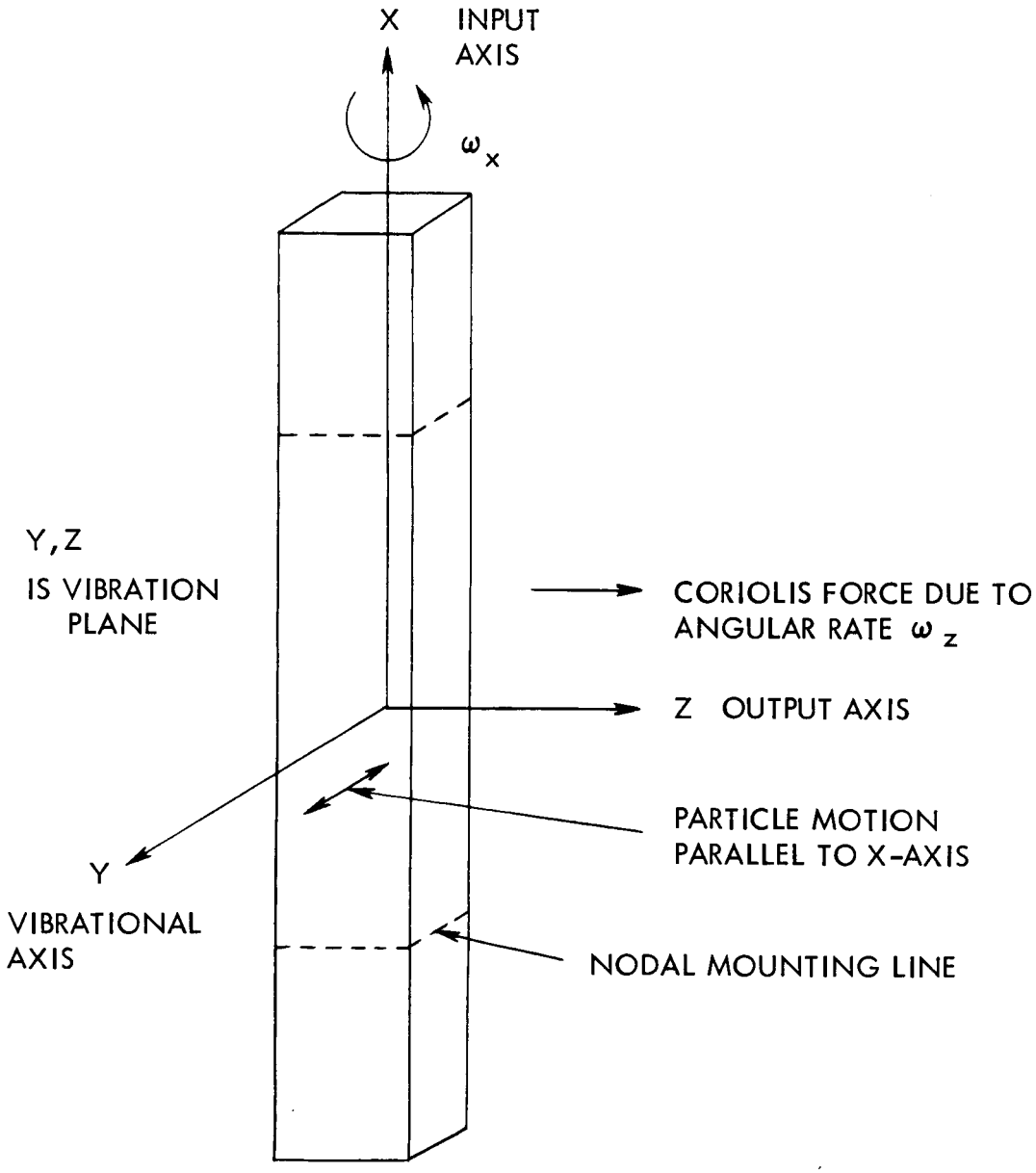

Figure 2. Sensor Axes

The parameters for the vibratory sensor are chosen such that the centrifugal and Coriolis forces due to motion in the 'z' axis or output axis in the vibrational axis are negligible.

Therefore,

$$y(t) \quad >> \quad z(t)$$

$$\dot{y}(t) \quad >> \quad \dot{z}(t)$$

$$\omega_c^2 \quad >> \quad \omega_x^2$$

$$\omega_o^2 \quad >> \quad \omega_x^2$$

The above conditions yield a lower limit for the possible mechanical resonant frequencies for a sensor with a given dynamic range. It will be shown in the following paragraphs that the sensor scale factor is proportional to $\frac{\omega_x}{\omega_c}$. If ω_c is chosen too small, the output motion is significant for high applied angular rates and the sensor output is non-linear due to the centrifugal and Coriolis forces. For instance, mechanical resonant frequencies of at least 1000 Hz are needed for a sensor to be linear for angular rates of 1000 deg/sec.

SENSITIVITY TO A CONSTANT ANGULAR RATE

If the moving co-ordinate frame is rotating at a constant angular rate ω_z, then the Coriolis acceleration of a particle is given by $\omega_z y(t)$ where $y(t)$ is the amplitude of an externally induced vibration along the vibrational axis. The motion of the particle along the output axis is determined by this acceleration and the output axis dynamics of the particle. If the external force, f_y, is controlled such that

$$y(t) = y_o \cos \omega_c t \tag{13}$$

then $z(t)$ is the solution to the equation

$$-2\omega_z \omega_c y_o \sin \omega_c t = \ddot{z}(t) + \frac{\omega_o}{Q_o} \dot{z}(t) + \omega_o^2 z(t) \tag{14}$$

The steady state solution to the preceding equation is

$$z(t) = \frac{-2y_o\omega_x}{\omega_c\left[\left(1 - \frac{\omega_c^2}{\omega_o^2}\right)^2 + \left(\frac{\omega_c}{\omega_o Q_o}\right)^2\right]^{1/2}} \sin(\omega_c t - \phi_c) \qquad (15)$$

$$\text{where } \phi_c = \arctan\left[\frac{\omega_c\omega_o}{Q_o(\omega_o^2 - \omega_c^2)}\right]$$

Equation (15) is the basic sensitivity expression for a vibratory angular rate sensor. The output motion is proportional to both the input or induced motion and the angular rate ω_z, and is also dependent upon the relative location of the two resonant frequencies, ω_c and ω_o.

BANDWIDTH - SENSOR RATE FREQUENCY RESPONSE

The rate frequency response of a vibratory sensor with separated frequencies can be shown qualitatively and quantitatively to be approximately that of a lightly-damped second-order system with the natural frequency being the separation frequency, ω_s. If the sensor is subjected to an oscillating input rate of frequency, ω_i, about its sensitive axis, then the Coriolis force acting along the output axis is amplitude-modulated with a carrier frequency, ω_c. The force then has two sidebands, $\omega_c + \omega_i$ and $\omega_c - \omega_i$ which are amplified and phase-shifted by the dynamics of the structure in the output direction. If the sensor is designed for a frequency separation such that there is a minimal coupling ($\phi_c \approx 0$), then the rate frequency response depends almost entirely on the upper sideband ($\omega_c + \omega_i$) response. As the input frequency, ω_i, increases, the lower sideband is attenuated and remains at approximately zero degrees phase shift. As $\omega_c + \omega_i$ approaches ω_o, the upper sideband is amplified by the high Q of the output axis. The rate frequency response of the vibratory sensor therefore exhibits a resonance when $\omega_i = \omega_s$ due to this upper sideband amplification. Accordingly, the transfer function of the

sensor will be shown to be approximately

$$z(s) = \frac{1}{1 + \frac{S}{Q_s \omega_s} + \frac{S^2}{\omega_s^2}} \omega(s) \tag{16}$$

where Q_s is related to Q_o.

The equation of motion in the 'z' direction is given by

$$\ddot{z}(t) + \frac{\omega_o}{Q_o} \dot{z}(t) + \omega_o^2 z(t) = \frac{f_c(t)}{m} \tag{17}$$

where $f_c(t)$ is the Coriolis force.

In Laplace transform notation, Equation (17) becomes

$$z(s) = G(s) \frac{F_c(s)}{m\omega_o^2}, \text{ where } G(s) = \frac{1}{1 + \frac{S}{\omega_o Q_o} + \frac{S^2}{\omega_o^2}}$$

If Q_o is large and the operating frequencies are near the resonant frequency, ω_o, then

$$G(j\omega) \cong \frac{1}{2\left[1 - \frac{\omega}{\omega_o}\right] + j\frac{1}{Q_o}} \tag{18}$$

and

$$\left|G(j\omega)\right| \cong \frac{1}{\left[4\left(1 - \frac{\omega}{\omega_o}\right)^2 + \frac{1}{Q_o^2}\right]^{1/2}} = B(\omega) \tag{19}$$

$$\text{ARG } G(j\omega) = -\tan^{-1}\left[\frac{1}{2Q_o\left(1 - \frac{\omega}{\omega_o}\right)}\right] = \phi(\omega) \tag{20}$$

If the input rate and induced motion are

$$\omega_x(t) = \omega_{xo} \cos \omega_i t \tag{21}$$

$$y(t) = y_o \sin \omega_c t, \tag{22}$$

then the Coriolis force $f_c(t)$ is given by

$$f_c(t) = -2mx_o\omega_{xo}\omega_c \cos \omega_i t \cos \omega_c t \tag{23}$$

$$f_c(t) = -my_o\omega_{xo}\omega_c \left[\cos (\omega_c + \omega_i) t + \cos (\omega_c - \omega_i) t\right] \tag{24}$$

For this force, the steady-state solution of Equation (17) is found to be

$$z(t) = B_u \cos \left[(\omega_c + \omega_i) t + \phi_u\right] + B_\ell \cos \left[(\omega_c - \omega_i) t + \phi_\ell\right]$$

where

$$B_u = -\frac{y_o\omega_{xo}\omega_c}{\omega_o^2} B (\omega_c + \omega_i),\ \phi_u = \phi(\omega_c + \omega_i) \tag{25}$$

$$B_\ell = -\frac{y_o\omega_{xo}\omega_c}{\omega_o^2} B (\omega_c - \omega_i),\ \phi_\ell = \phi (\omega_c - \omega_i)$$

In order to provide sensor null stability as previously described, the resonant frequencies are separated such that $\omega_o > \omega_c$ and $\phi (\omega_c) \cong 0$. Therefore, the lower sideband phase-shift is always approximately zero.

$$\phi_\ell \cong 0 \text{ for all } \omega_i$$

Using this fact and expanding Equation (25), it becomes

$$z(t) = B_u \cos \phi_u \cos \omega_i t \cos \omega_c t - B_u \cos \phi_u \sin \omega_i t \sin \omega_c t$$

$$-B_u \sin \phi_u \sin \omega_i t \sin \omega_c t - B_u \sin \phi_u \sin \omega_i t \cos \omega_c t$$

$$+B_\ell \cos \omega_i t \cos \omega_c t + B_\ell \sin \omega_i t \sin \omega_c t \qquad (26)$$

A typical vibratory sensor uses a phase-sensitive demodulator to reduce harmonic noise and null shifts. The only components of z(t) that produce a rate output are those which are in quadrature with the induced motion y(t) (terms containing cos $\omega_c t$). If $z_o(t)$ is the demodulated output of the sensor, then

$$z_o(t) = A(\omega_i) \cos \left[\omega_i t - \theta(\omega_i)\right] \qquad (27)$$

where

$$A(\omega_i) = \left[(B_u \cos \phi_u + B_\ell)^2 + (B_u \sin \phi_u)^2\right]^{1/2} \qquad (28)$$

$$\theta(\omega_i) = \arctan \left[-\frac{B_u \sin \phi_u}{B_u \cos \phi_u + B_\ell}\right] \qquad (29)$$

If the expressions for B_u, B_ℓ, etc. are substituted into Equation (27), then

$$A(\omega_i) \cong \frac{y_o \omega_{xo} \omega_c}{\omega_o(\omega_s)\left[4\left(1 - \frac{\omega_i}{\omega_s}\right)^2 + \frac{1}{Q_i^2}\right]^{1/2}} \cdot$$

$$\left[1 + \frac{1 - \frac{\omega_i}{\omega_s}}{1 + \frac{\omega_i}{\omega_s}} + \frac{4\left(1 - \frac{\omega_i}{\omega_s}\right)^2 + \frac{1}{Q_i^2}}{4\left(1 + \frac{\omega_i}{\omega_s}\right)^2}\right]^{1/2} \qquad (30)$$

$$\theta(\omega_i) \cong \arctan\left[\frac{1}{2Q_i\left(1 - \frac{\omega_i}{\omega_s}\right)}\right] \tag{31}$$

where

$$Q_i = \frac{Q_o \omega_s}{\omega_o} \tag{32}$$

The gain and phase of the output given above are approximately those of a second order system with a resonant frequency of ω_s and a quality factor Q_i. For example, if $Q_o = 750$, $\omega_o = 1540$ Hz, $\omega_c = 1500$ Hz, then $\omega_s = 40$ Hz and $Q_i = 19.5$.

DESCRIPTION OF SINGLE-AXIS FREE-FREE BEAM VIBRATORY ANGULAR RATE SENSOR

GENERAL

A single-axis sensor, consisting of a free-free metal beam mounted at its nodal points and vibrated at its fundamental bending frequency, is considered superior to other potential sensor configurations because of its basic simplicity and its theoretical insensitivity to external vibrations or accelerations. Piezoelectric transducers, mounted on the four beam faces, are used to produce the motion along the vibrational axis and to detect the motion along the output axis. This transducer configuration minimizes the sensitivity of the sensor to dimensional stabilities between the beam and the external case. The following paragraphs contain an analytical description of the force transmission from the transducers to the beam, and the subsequent motions and voltages.

The free-free beam and its attached transducers are depicted in Figure 3 with the associated nomenclature. The driven motion along the vibrational axis is produced by applying a voltage to the drive transducer which exerts a force on the outside of the beam, which tends to contract or expand the skin of the beam between the nodal or mounting points. This force results in an effective torque on the beam about the nodes, and tends to bend the beam in its characteristic first mode shape as shown in Figure 4. If the frequency of the applied voltage is chosen to be the first natural frequency of the beam, then vibrational resonance occurs and the beam has the motion envelope as shown in Figure 4. If an angular rate is applied thru the mounting points to the longitudinal axis of the beam, the Coriolis forces produced by the velocity of the beam in the vibrational axis, cause the beam to vibrate

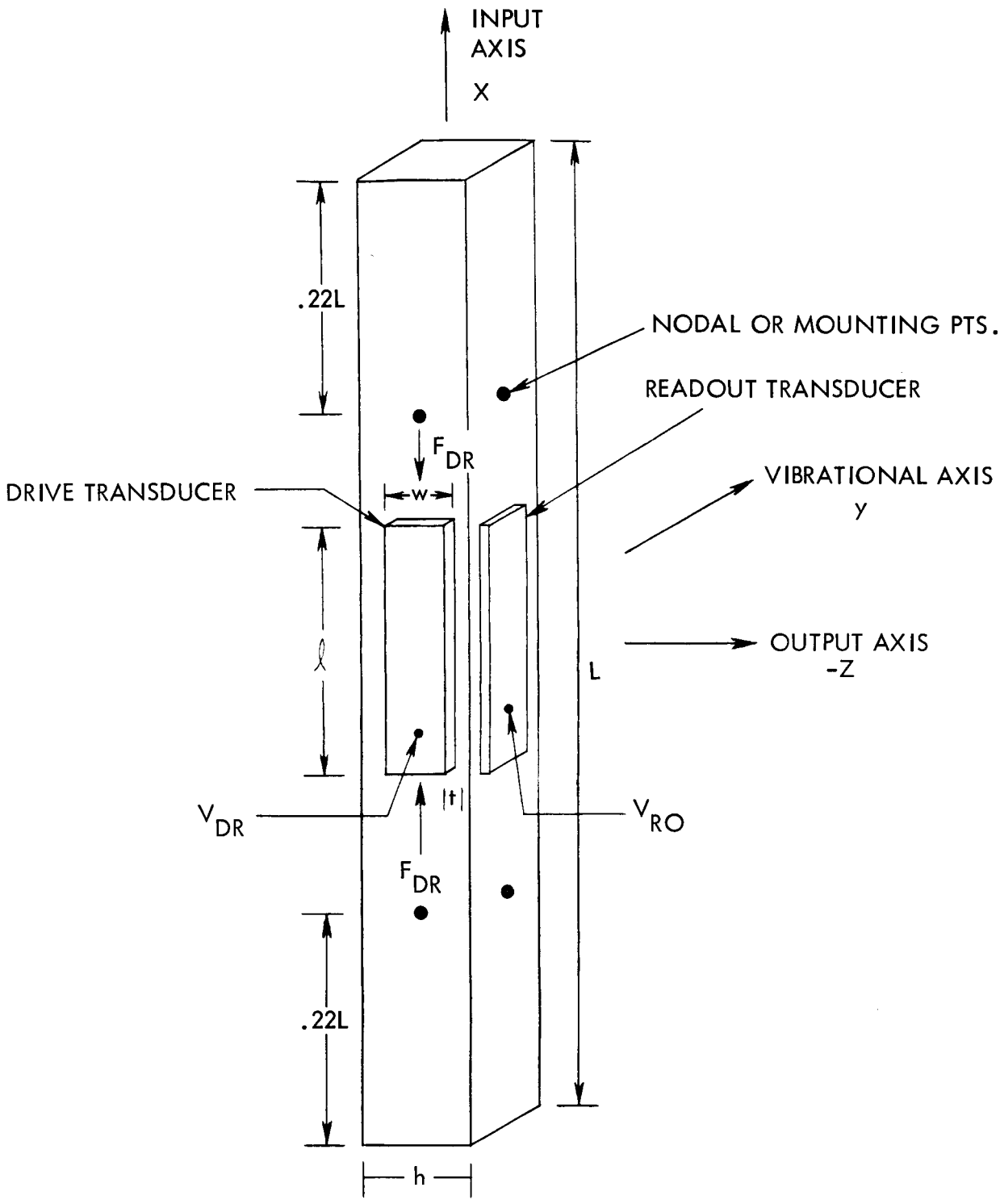

Figure 3. Free-free Beam & Transducer

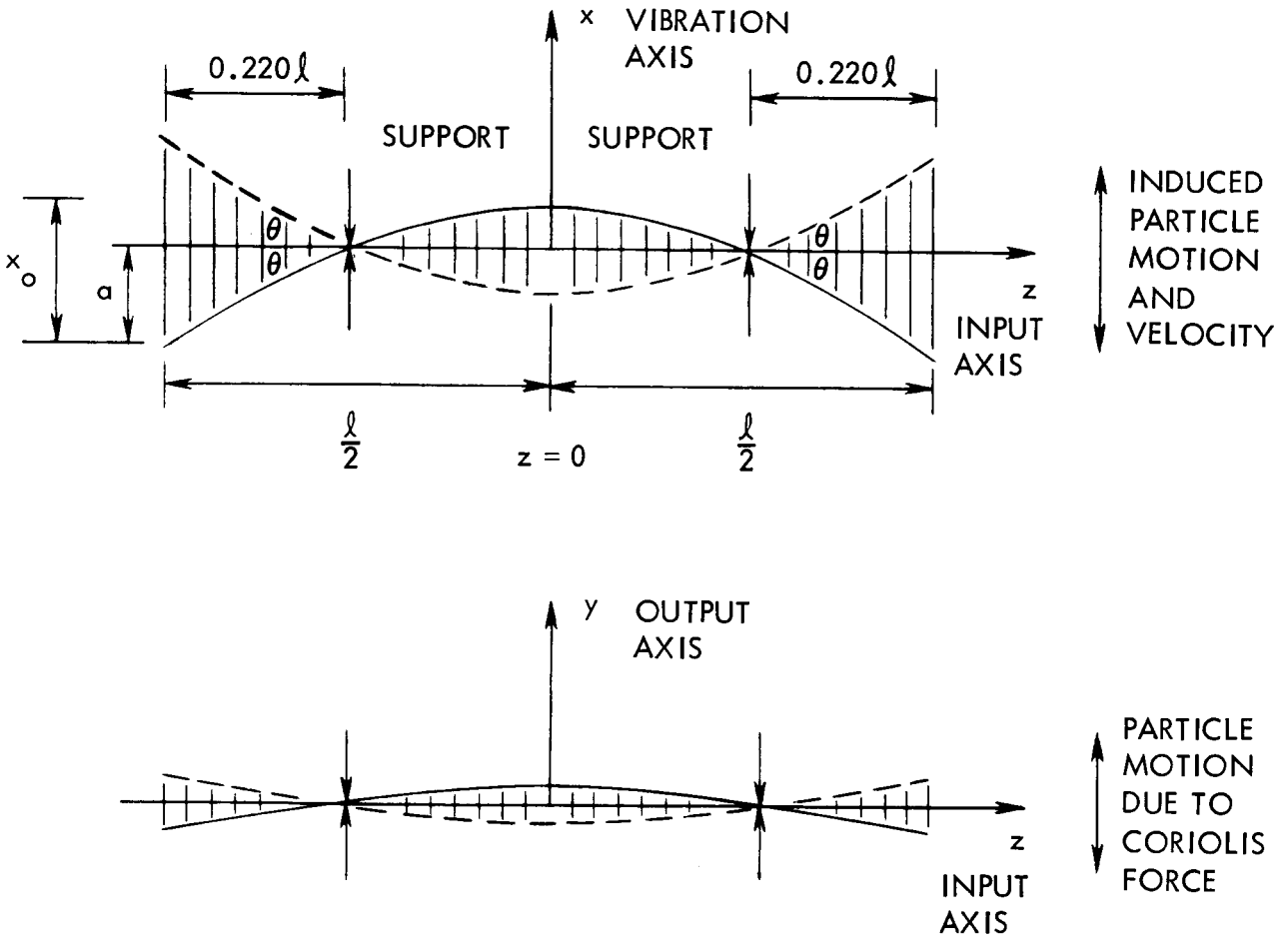

Figure 4. Beam Vibration Envelope

along the output axis. This vibration bends the output piezoelectric transcuder which produces an ac output voltage whose amplitude is proportional to the applied angular rate. Typical vibration envelopes for the free-free beam are shown in Figure 4 for both the vibrational axis and the output axis.

INDUCED BEAM VIBRATION ALONG VIBRATIONAL AXIS - TRANSDUCER FORCE-VOLTAGE RELATIONSHIPS

The induced beam vibration as referred to in the previous sections is produced by applying an ac voltage to the "drive" piezoelectric transducer. The effective force produced between the ends of the transducer is given by

$$F_{DR} = \frac{W}{K_e g_{31}} V_{DR} \tag{33}$$

where W is the width of the transducer, V_{DR} is the applied voltage, g_{31} is the transducer 'g' constant, and K_e is the transmission factor which takes into account the mounting method for the transducer. This force produces a torque on the beam about the mounting points because of the beam thickness. Referring to the nomenclature of Figure 3, the torque is given by

$$T_{DR} = \frac{2\,\ell\,Fh}{3\,L} \tag{34}$$

The angular deflection of the beam about its mounting points away from its equilibrium position can be approximately described by the differential equation

$$T_{DR} = I_B \ddot{\theta}_y + C\,\dot{\theta}_y + K_B \theta_y \tag{35}$$

where I_B is the inertia of one-half the beam about the mounting point and K_B is the rotational spring constant of the beam. Therefore,

$$\theta_y(s) = \frac{\frac{T_{DR}(s)}{K_B}}{1 + \frac{s}{\omega_y Q_y} + \frac{s^2}{\omega_y^2}} \tag{36}$$

where

$$\omega_y^2 = \frac{K_B}{I_B}, \quad \omega_y Q_y = \frac{K_B}{C} \tag{37}$$

The deflection angle θ is shown in Figure 4. The quality factor Q_y is usually very high (~1000) and represents only the material damping effects.

If the deflection angle, $\theta_y(t)$ is known, then both the maximum deflection of the beam at the center and the extension of the "feedback transducer" can be found. These are both important parameters since the first determines the sensor scale factor and the second influences the drive circuit design.

If the first mode deflection curve of the beam is assumed to be approximately

$$y(x, t) = \left[\left(y_o \sin \frac{\pi x}{L} - \frac{2}{\pi}\right) \cos \omega_y t\right] \tag{38}$$

(See Appendix A)

then the mode deflection angle θ_y is related to y_o by the equation

$$y_o \cong \frac{1.3L}{\pi} \theta_y \tag{39}$$

and

$$y_o(s) = \frac{\frac{2.6\, \ell\, h\, w}{3\pi\, K_e g_{31}} V_{DR}(s)}{1 + \frac{s}{\omega_y Q_y} + \frac{s^2}{\omega_y^2}} \tag{40}$$

If the drive voltage is designed to be generated at the resonant frequency ω_y, Q_y and

$$V_{DR}(t) = V_{DRO} \cos \omega_y t \tag{41}$$

then

$$y_o = \frac{2.6\, \ell\, h\, w\, Q_y}{3\pi\, K_e g_{31}} \tag{42}$$

Equation (42) gives the maximum beam drive deflection in terms of the drive voltage amplitude applied to the drive transducer. When the beam is driven along the vibrational axis using the drive transducer, then the "feedback" transducer (transducer on the opposite side of the beam from the drive transducer) is extended and contracted as the beam moves. This extension/contraction produces a voltage on the feedback transducer that is proportional to the amplitude motion, and may be used electronically for amplitude and frequency control of the beam motion. The feedback voltage is related to angular deflection by

$$V_{FB}(t) = \frac{th}{Ld_{31}}\,\theta_y(t) \qquad \text{(refer to Figure 3 for nomenclature)} \tag{43}$$

and therefore,

$$V_{FB}(s) = \frac{\dfrac{2\ell\ th^2 w}{3L^2 K_B K_e d_{31} g_{31}}}{1 + \dfrac{s}{\omega_y Q_y} + \dfrac{s^2}{\omega_y^2}}\ V_{DR}(s) \tag{44}$$

This is the steady-state transfer function on "gain" of the beam-transducers along the vibrational axis. It plays an important part in the evaluation of a given sensor and the design of the electronics that produce the drive voltage.

OUTPUT AXIS MOTIONS DUE TO ANGULAR RATE

With the above information, the beam deflection along the output axis for a given applied angular rate may be calculated as well as the corresponding voltage output of the readout transducer. For a constant input angular rate, Ω_x, about the x-axis, the Coriolis force acting on the beam per unit length along the beam is given by

$$f_{cz}(t) = 2\mu\Omega_x\,\dot{y}(t) \tag{45}$$

where

$$y(t) = \omega_y y_o\,(\sin\frac{\pi x}{L} - \frac{2}{\pi})\cos\omega_y(t) \tag{46}$$

or

$$f_{ct}(t) = 2\mu\Omega_x\omega_y y_o\,(\sin\frac{\pi x}{L} - \frac{2}{\pi})\cos\omega_y t = A(t)\,(\sin\frac{\pi x}{L} - \frac{2}{\pi}) \tag{47}$$

The corresponding torque in the output plane about the mounting points or nodes is found by integrating this unit Coriolis force.

$$T_z = \int_0^{L/2} x\, f_{cz}(x,t)\, dx = A(t) \int_0^{L/2} x \left(\sin \frac{\pi x}{L} - \frac{2}{\pi}\right) dx \tag{48}$$

This results in

$$T_z(t) = \frac{2L^2}{\pi^2}\left[1 - \frac{\pi}{4}\right]\mu\Omega_x\omega_y y_o \cos \omega_y t \tag{49}$$

The angular deflection response in the output axis is described by a differential equation similar to the one used for the vibrational axis.

$$T_z(t) = I_B \ddot{\theta}_z(t) + C\dot{\theta}_z(t) + K_B\theta_z(t) \tag{50}$$

or alternately

$$\theta_z(s) = \frac{\frac{1}{K_B} T_z(s)}{1 + \frac{s}{\omega_z Q_z} + \frac{s^2}{\omega_z^2}} \tag{51}$$

where

$$\omega_z^2 = \frac{K_B}{I_B} \qquad \omega_z Q_z = \frac{K_B}{C}$$

If only the steady-state (or sinusoidal) operation is considered and the drive frequency ω_y is significantly different from the output axis resonance ω_z, then the peak angular deflection and the torque are given by the approximate relation.

$$\theta_{z_o} = \frac{T_{z_o}}{2K_B\left(1 - \frac{\omega_y}{\omega_z}\right)} \tag{52}$$

The maximum beam deflection is related to angular nodal deflection by

$$z_o \cong \frac{1.3L}{\pi} \theta_{z_o} \tag{53}$$

if the first mode beam deflection is given by

$$z(x,t) = \left[z_o \frac{\sin \pi x}{L} - \frac{2}{\pi} \right] \cos \omega_y t \tag{54}$$

Therefore,

$$z_o \cong \frac{1.3L^3}{\pi^3} \left[1 - \frac{\pi}{4} \right] \frac{\mu \omega_y y_o}{K_B \left(1 - \frac{\omega_y}{\omega_z} \right)} \Omega_x \tag{55}$$

where y_o is related to the drive voltage V_{DR}.

The bending of the beam along the output axis also bends the "readout transducer" and produces a voltage proportional to the amount of bending, and thus, to applied angular rate. The readout voltage V_{RO} is related to the angular deflection in the readout plane by

$$V_{RO}(t) = \frac{\text{th } \theta_z}{L K_e d_{31}} \tag{56}$$

from which the sensor scale factor (volts/deg/sec) may be found.

The relationships established in the previous paragraphs serve the purpose of a foundation from which to study sensor operation from the point of view of developing design criteria and analyzing possible sources of sensor null shift, noise, and drift.

The important facts that should be remembered from the preceding text are:

1. The main component of sensor vibratory motion is at mechanical resonance.
2. The output or angular rate sensitive motion is of resonance and approximately in quadrature time-phase with the main component.

The following paragraphs examine the causes of sensor null shifts and noise, in general, and then examine the electrical and mechanical design of the sensor in detail.

SOURCES OF SENSOR NULL SHIFTS AND NOISE

The primary sources of vibratory sensor null shifts and noise are directly related to or can be represented by changes or anomalies in the piezoelectric transducers or external distrubances such as mount vibration. For instance, if the force or torque produced by the drive transducer is not exactly aligned with the vibrational axis, then beam vibration will occur along the output axis that cannot be distinguished from the vibration produced by an applied angular rate. Factors such as uneven bonding between transducer and beam or a nonhomogeneous transducer can cause the above. The major sources of sensor drift and noise are listed below.

1. Variation in the direction of drive transducer force with time or environment.

2. Quadrature coupling between the vibrational and output axes.

3. Beam vibrations induced by external accelerations.

The sensitivity of the sensor voltage output to changes in the direction of drive torque or force may be represented by differences in applied voltage for parts of the drive transducer or differences in coupling factors. The force-voltage relationship

$$F_{DR} = \frac{W V_{DR}}{K_e g_{31}} \tag{57}$$

was used in the previous work in this section as the basis for sensor operation. If the coupling factor K_e is not constant across the width of the transducer, then there is torque produced in the z (output) axis as well as the y (vibrational) axis. For simplicity, this situation may be represented by a split transducer with the two halves having different applied voltages as depicted in Figure 5.

The total torque acting on the beam in the output axis is

$$T_z = T_1 - T_2 = \frac{W^2}{36 K_e g_{31}} \left[V_1 - V_2 \right] \tag{58}$$

and the resulting output voltage from the readout transducer due to beam bending is

$$V_{RO} \cong \frac{th\, T_z}{2L\, K_e K_B g_{31} \left(1 - \frac{\omega_y}{\omega_z}\right)} \tag{59}$$

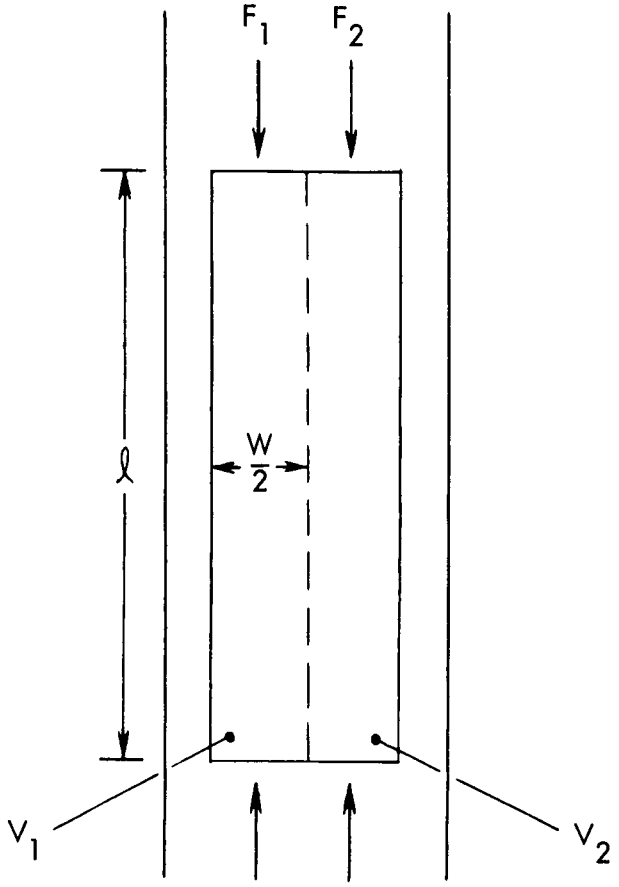

$$F_1 = \frac{W V_1}{2K_1 g_{31}} , \quad T_1 = \frac{W^2 V_1}{36K g_{31}}$$

$$F_2 = \frac{W V_2}{2K_2 g_{31}} , \quad T_2 = \frac{W^2 V_2}{36K g_{31}}$$

Figure 5. Split Transducer

$$V_{RO} = \frac{th\, W^2 \left[V_1 - V_2\right]}{72\, L\, K_e^{\,2} K_B g_{31} d_{31} \left(1 - \frac{\omega_y}{\omega_z}\right)} \tag{60}$$

This output voltage is either in phase or out-of-phase with the drive voltage and therefore, cannot be distinguished from an output voltage due to an input angular rate. Therein lies the sensor null shift problem. Changes in transducer parameters such as coupling factors, d and g constants with environmental and time, may be represented by changes in the effective applied voltage. The actual magnitude of this sensitivity, which will be calculated in the Sensor Design, Section 3, in connection with a self-test method, is large enough to pinpoint this sensitivity as the major limitation of sensor performance. Sensor parameters such as threshold and null stability are affected by this drive transducer stability problem.

The quadrature coupling, between the vibrational and output axes, makes the sensor null voltage output sensitive to changes in the amplitude of the driven vibration. As was noted in a previous discussion, the output motion is approximately but not exactly in quadrature with the input motion. The degree of exactness of this phase relationship depends upon the difference of the two natural frequencies and the associated quality factors. From the sensor gain equation given in this Section, the output motion of the beam drive to an angular rate can be approximated by

$$z(x, t) = \frac{y_o \Omega_x}{\omega_s} \left[\sin \frac{\pi x}{L} - \frac{2}{\pi}\right] \sin\left(\omega_y t - \frac{\omega_y}{Q_z \omega_s}\right) \tag{61}$$

where y_o is the amplitude of the beam motion in the vibrational axis, Ω_x, is the input angular rate, and ω_s if the beam separation frequency.

The principal causes of crosscoupling between input and output are the small phase shift indicated in the above expression and the actual response of the output transducer. The transducer that senses the output motion cannot be made completely insensitive to the motion in the vibrational axis. Because of the sizeable difference between the amplitudes of input and output motion (10^4) this sensitivity can be extremely important when considering sensor performance at null or very low rates. The output of the readout transducer may be represented as

$$V_O(t) = K_z\, z(t) + K_y\, y(t) \tag{62}$$

where K_z is the transducer scale factor discussed previously, K_y is the quadrature coupling coefficient, and y(t) is the beam motion along the vibrational axis. Therefore, if

$$y(t) = y_o \cos \omega_y t, \tag{63}$$

then

$$V_O(t) = \frac{K_z y_o \Omega_x}{\omega_s} \sin\left(\omega_y t - \frac{\omega_y}{Q_z \omega_s}\right) + K_y y_o \cos \omega_y t \tag{64}$$

If the phase shift represented by the term $\frac{\omega_y}{Q_z \omega_s}$ is small, so that $\sin \frac{\omega_y}{Q_z \omega_s} \cong \frac{\omega_y}{Q_z \omega_s}$, then referencing to the phase of the output signal,

$$V_O(t) = K_z \left[\frac{y_o \Omega_x}{\omega_s} - \frac{K_y y_o \omega_y}{K_z \omega_s Q_z}\right] \sin \omega_y t_1 + K_y y_o \cos \omega_y t_1 \tag{65}$$

where

$$t_1 = t - \frac{1}{Q_z \omega_s} \tag{66}$$

The resonant mode coupling and the potential cause of null shift or instability is the dependence of the amplitude of the $\sin \omega_y t$, term on y_o. If the null shift of the sensor due to this coupling is to be less than an equivalent angular rate, Ω_x, then

$$\frac{y_o \Omega_x}{\omega_s} \geq \frac{K_y y_o \omega_y}{K_z \omega_s Q_z} \tag{67}$$

or

$$\Omega_x \geq \frac{K_y y_o \omega_y}{K_z Q_z} \qquad \text{Null shift due to coupling} \tag{68}$$

Note that the preceding relationship is independent of the separation frequency ω_s, as long as the approximations are satisfied. These approximations state that the phase shift of the beam motion in the output axis with respect to the drive voltage is small, typically less than 5 degrees. The magnitude of the coupling null shift can be minimized by either trimming the readout transducer or by splitting the readout transducer electrode and nulling the voltage. However, even though trim is possible, the basic coupling still exists and changes in the drive motion amplitude are likely to be reflected in sensor null shifts. The same is true for drive motion amplitude noise which has bearing on the sensor threshold or S/N ratio if coupling is present. The optimum setting for the separation frequency is usually about 20 to 30 Hz for a beam natural frequency of 2000 Hz and a Q of 1000.

The sensitivity of the beam motion to external accelerations introduced through the mounting structure. This sensitivity represents coupling that is a departure from true free-free beam vibration. One of the primary reasons that the use of a free-free beam as a vibratory angular rate sensor should realize better performance than previous vibratory sensor designs is the theoreticle insensitivity of the primary beam motion to accelerations introduced from the mount. As a result of the beam mode shape, as shown in Figure 6 , and the fact that the modes of the first mode are used as mounting points, the instantaneous linear momentum of the beam is zero at any time (ends going down, middle up). If perfect nodal mounting is achieved, the stress on the mounts due to the transducer-driven beam motion is zero, and the interaction between the beam and the external environment is zero. The following analysis is intended to determine the mounting tolerances necessary to minimize vibration sensitivity to explore possible effects on sensor null stability.

Referring to the nomenclature of Figure 6 , the neutral axis of the beam motion is represented by

$$y(x, t) = \left[y_o \sin \frac{\pi x}{\ell} - a \right] \cos \omega_y t \tag{69}$$

where ω_y is the first free-free mode bending frequency. The nominal location of the modes of vibration are at $x = \epsilon_o \cong 0.220\ell$ and $a = a_o = \frac{2y_o}{\pi}$. At this point, the configuration is balanced and the net vertical momentum is zero.

$$M(t) = \mu \int_0^{\ell} \frac{\partial y}{\partial t} \, dx = 0 \tag{70}$$

where μ is the mass per unit length of the beam.

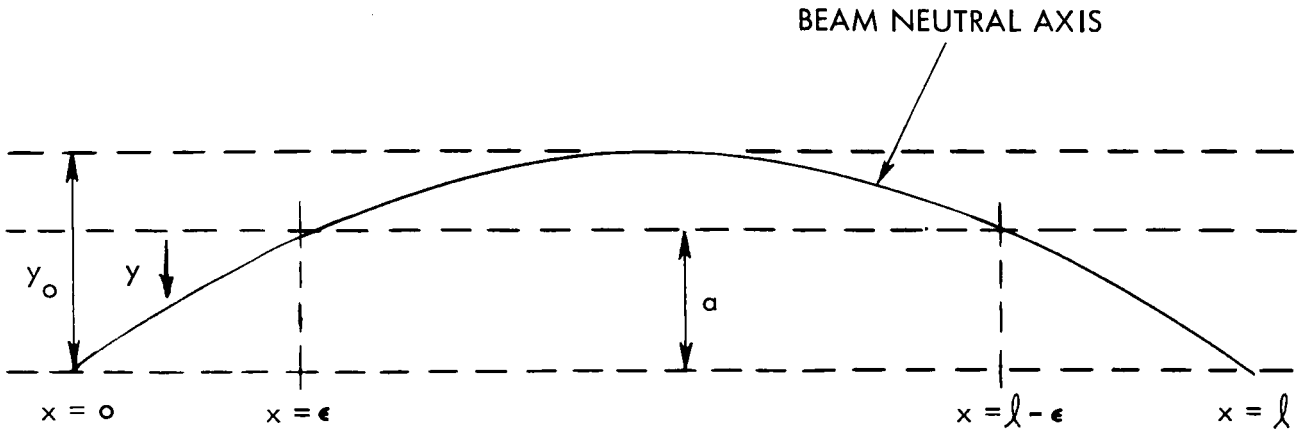

$$y(x,t) \cong \left[y_o \, \text{SIN} \, \frac{\pi x}{\ell} - a \right] \text{COS} \; w_c t$$

Figure 6. Beam Bending

If the beam is mounted at other points such as

$$x = \epsilon = \epsilon_o + \Delta\epsilon \qquad \text{where } a = a_o + \Delta a \tag{71}$$

then there is a resulting unbalance momentum. The modified motion and the resulting momentum are given below

$$y(x, t) = y_o \left[\sin \frac{\pi x}{\ell} - \frac{2}{\pi} - \frac{\pi}{\ell} \cos \frac{\pi \epsilon_o}{\ell} \Delta\epsilon\right] \cos \omega_y t$$

$$M(t) = \pi \mu y_o \omega_y \cos \frac{\pi \epsilon_o}{\ell} \Delta\epsilon \sin \omega_y t \tag{72}$$

The total acceleration on the supports due to this momentum is

$$\alpha_T = \frac{1}{\mu \ell} \frac{dM}{dt} = \pi \omega_y^2 y_o \cos \frac{\pi \epsilon_o}{\ell} \left(\frac{\Delta\epsilon}{\ell}\right) \cos \omega_y t \tag{73}$$

For example, if $\omega_y = 2000$ cps, $y_o = 0.005''$, $\ell = 4.0''$ and the mounting points are each 10 milli-inches ($\Delta\epsilon$) inside the nominal positions, then the total peaks acceleration on the mounts is approximately 12.0 g's. Also, for the example the peak acceleration of the beam at its center is approximately 750.0 g's.

The representative numbers given above point up three potential problem areas with regard to the fabrication and assembly of the vibratory sensor. First, if perfect nodal mounting is not achieved, the sensor will be sensitive to external vibration at its resonance frequency (about 2.0 deg/sec/g of 2000 cps vibration in the readout plane for the above example) and, probably more important, stresses are set up in the mounting structure which may effectively shift the plane of driven vibration and result in significant null shifts of a random nature. Also, the above serves to accentuate the inadequacy of a rubber mount when a high performance sensor is required. Second, at the beam accelerations that are necessary for operation, the stability of the transducer bend is in question. Any change in uniformity or strength will result in large permanent null shifts. Third, if the beam is not balanced, the neutral axis of vibration for the drive and readout planes will not coincide and the nodes for each plane will be in different locations. This fact would complicate the mounting problem.

COMPLETE MATHEMATICAL MODEL FOR THE FREE-FREE BEAM ANGULAR RATE SENSOR

All the sensors parameters and considerations can be combined into a single mathematical model for the free-free beam vibratory angular rate sensor. The ultimate objective of the model is to describe the sensor accurately and in doing so predict the limitations on sensor performance. The results obtained from the hardware during tests will aid this preliminary effort. The following discussion is intended to be qualitative and to define the various aspects of the problem.

The significant segments of a mathematical model for the free-free beam sensor necessarily contain the following:

1. Two dimensional beam dynamics described in fixed beam coordinates.

2. Force-voltage-current relationships of piezoelectric transducers described in transducer coordinates.

3. Electronic transfer functions and noise.

4. Coordinate transformations from transducers to beam as a function of environment.

5. Effects of mount on beam dynamics.

6. Transmission of external accelerations through the mount to the beam.

A block diagram of the mathematical model is shown in Figure 7. The "K" constants represent the transducer gains with associated geometry; the "C's" are transducer coupling constants that are due to misalignments and anomalies; the "H's" are the transfer functions of the electronic circuits. It is evident from Figure 7 that sensor performance is directly related to the stability and magnitude of the coupling C's since they represent the only interactions between drive and readout beam motion besides input angular rate Ω. The beam transfer functions X(s) and Y(s) are limited to first mode dynamics and it will be shown in later work that this representation is valid. External distrubances that act upon the sensor are represented by the noise inputs N and the force inputs F (external accelerations).

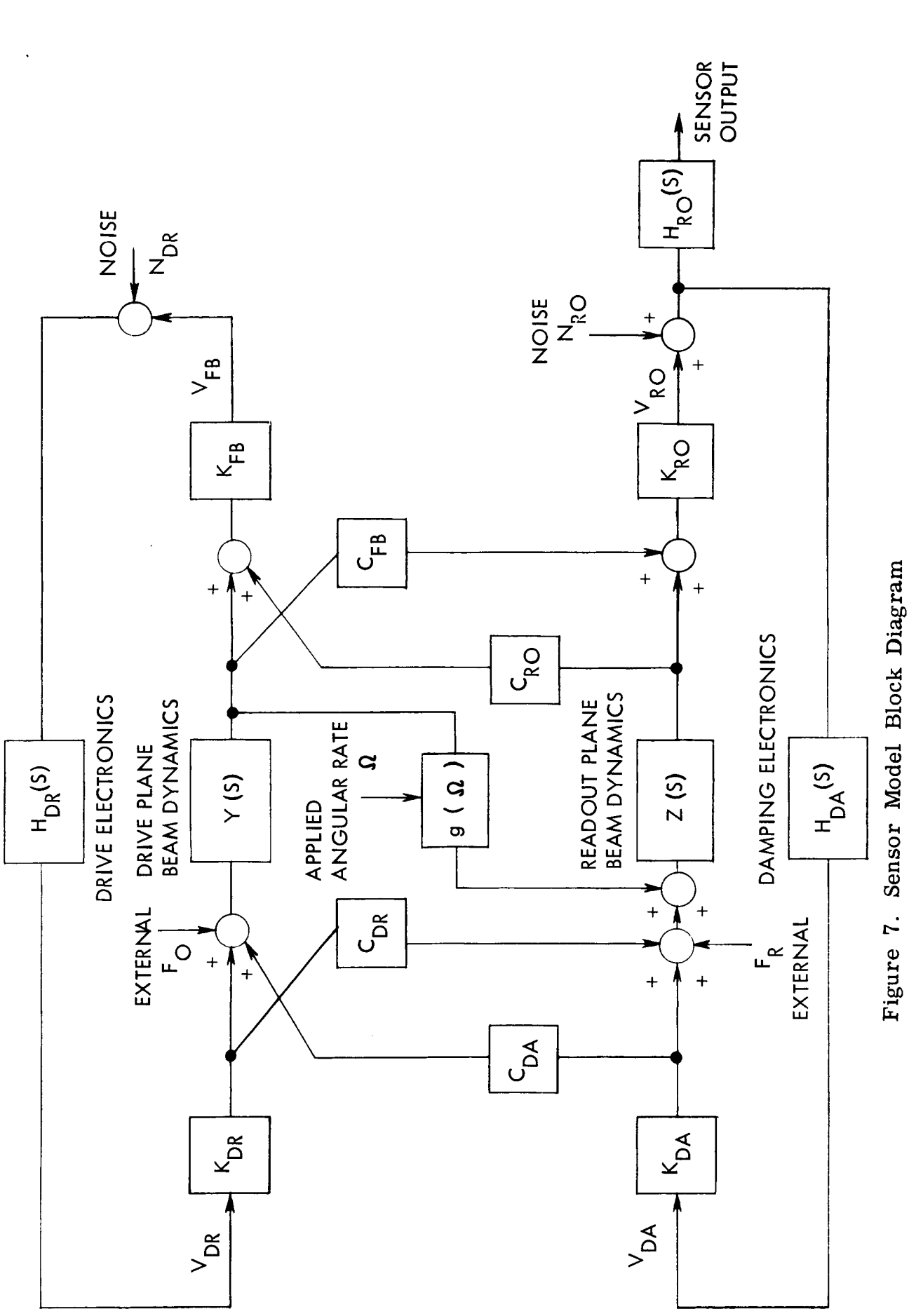

Figure 7. Sensor Model Block Diagram

The various parameters of the model can be evaluated by one or more of the following tests:

1. Open-loop tests of beam and transducers with an audio oscillator (X, Y, K).

2. Calibration of electronic circuits (H, N).

3. Static tests of sensor and electronics - transient responses or modulation (C).

4. Performance tests of sensor in a controlled (K) environment.

5. Environment evaluation of sensor F, $K_{(T)}$.

6. Analysis to extend experimental results.

All of the transfer functions and constants have been developed in the previous paragraphs.

Section 3

SENSOR DESIGN AND ANALYSIS

The following paragraphs contain a description of the various design parameters of the free-free beam vibratory angular rate sensor and the criteria by which they are selected. The discussion is broken into mechanical and electrical sections and is intended as the background for the specific description of the laboratory model and its performance contained in Section 4.

MECHANICAL ANALYSIS AND DESIGN

A sketch of the mechanical design for the laboratory model is shown in Figure 8. The mechanical part of the sensor consists of the beam, the mounting structure for the beam, the four piezoelectric transducers, the bond between the transducers and the beam, and the electrical leads connected to the transducers and brought out to the electronics. The design of the mechanical part of the sensor is a combination of material and parameters selection.

One of the most basic selections for the sensor is that of the first free-free bending mode frequency of the beam and thus, the sensor operating frequency. It is shown in Appendix A that this resonant frequency is given by

$$\omega = \frac{22.4}{L^2} \left(\frac{EI}{\mu} \right)^{1/2} \tag{74}$$

where EI is the flexural rigidity of the beam, μ is the mass of the beam per unit length, and L is the length of the beam. The cross-sectional moment of inertia θ, I, is given by

$$I = \frac{h^4}{12} \tag{75}$$

if the beam cross section is square and of side h. Therefore,

$$\omega = \frac{6.5\, h^2}{L^2} \left(\frac{E}{\mu} \right)^{1/2} \tag{76}$$

and entailed in the frequency selection is the selection of the beam shape (length-to-width ratio).

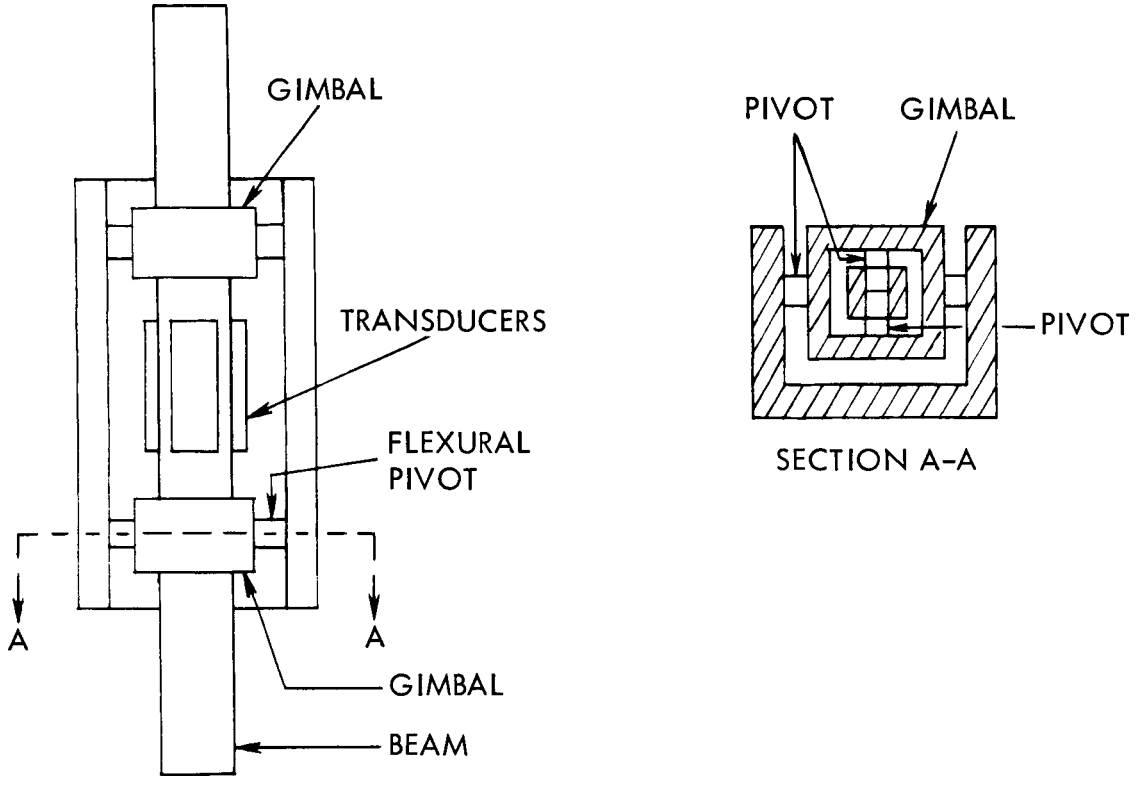

Figure 8. Modified Gimballed Beam and Mount

The general considerations for this selection are the following:

1) Sensor scale factor: Scale factor decreases approximately as $\frac{1}{\omega}$

2) Bandwidth of expected external disturbances: The resonant frequency should be above the expected vibration environment

The selection of beam length-to-width ratio for a specific frequency is dependent on scale factor versus mounting considerations. If the cross section is increased, the sensor scale factor is increased because of the greater transducer bending; however, and increased cross section makes it more difficult to obtain accurate nodal mounting because of the greater surface area.

The separation frequency, or the difference between the vibrational and output resonant frequencies, is determined by making the beam cross section rectangular instead of square. This alters the cross-sectional moment of inertia (or the two axes). Consequently,

$$I_y = \frac{h_y h_z^3}{12} \quad , \quad \omega_z = \frac{6.5}{L^2}\left(\frac{E\, h_y h_z^3}{\mu}\right)^{1/2} \tag{77}$$

$$I_z = \frac{h_z h_y^3}{12} \quad , \quad \omega_y = \frac{6.5}{L^2}\left(\frac{E\, h_z h_y^3}{\mu}\right)^{1/2} \tag{78}$$

Equations (77) and (78) may be combined to yield an expression for the ratio of the two resonant frequencies.

$$\frac{\omega_y}{\omega_z} = \frac{h_y}{h_z} \tag{79}$$

The tolerances on the beam cross-sectional dimensions are established by selecting a tolerance for the sensor separation frequency and then, determining the dimensional tolerance needed to maintain this.

The analysis presented in Section 2 indicated that the sensitivity of the sensor to external disturbances was dependent upon how close the beam mounting points were to the actual nodes of the first free-free beam mode of vibration. In fact, one of the reasons that the free-free beam is considered the best mechanization for a vibratory angular rate sensor is its theoretical intensitivity to external accelerations. When mounted exactly at the first mode nodes, the amplitude of beam vibration at resonance does not depend on mount acceleration because the net beam momentum is always exactly zero. For this reason, second-order effects that result in nodal shifts are of prime interest

in sensor design. The mass of the piezoelectric transducers which are bonded to the beam are one such effect. The nodes of vibration are drawn in significantly by this added mass at beam center. Referring to Figure 9, which shows schematically the beam and transducer, the transducers are centered on the beam and are of length ℓ. If the general first mode shape is given approximately by

$$Y(x) = Y_o \sin \frac{\pi x}{L} - a \tag{80}$$

Where "a" is the constant which defines the nodes of vibration, then the nodes for a beam without transducers are at

$$x_n = \frac{L}{\pi} \sin^{-1}\left(\frac{2}{\pi}\right) \cong 0.22L \tag{81}$$

and

$$x_n = \left[L - \frac{L}{\pi} \sin^{-1}\left(\frac{2}{\pi}\right)\right] \cong 0.78L \tag{82}$$

If transducers are added, the beam is no longer uniform and the extra mass tends to pull the nodes toward the center. Since the nodes are defined as the mounting points for which the net momentum is zero, then Momentum of Beam + Momentum of Transducers = 0, which can be expressed approximately by the equation:

$$M_B \int_o^L \left(y_o \sin \frac{\pi x}{L} - a\right) dx + 4M_T \int_{\frac{L-\ell}{2}}^{\frac{L+\ell}{2}} \left(y_o \sin \frac{\pi x}{L} - a\right) dx = 0 \tag{83}$$

Carrying out the integration and solving for the constant "a",

$$a^* = \frac{2y_o}{\pi} \left[\frac{M_B + 4\,M_T}{M_B + 4\left(\frac{\ell}{L}\right)M_T}\right] \tag{84}$$

where M_B is the mass of the beam

M_T is the mass of one transducer

ℓ is the length of the transducer

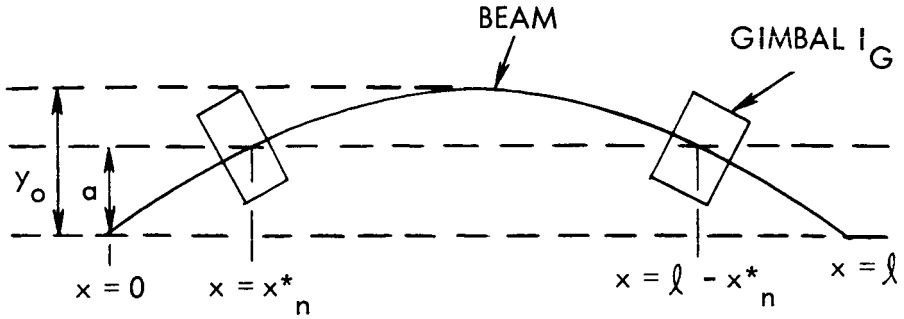

$$y(x) = y_o \text{ SIN } \frac{\pi x}{\ell} - a$$

(a) Beam With Gimbals

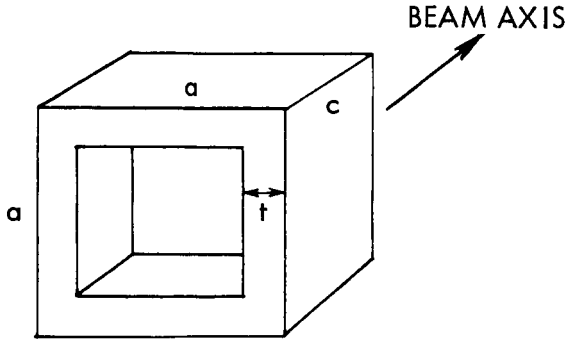

(b) Gimbal With Dimensions

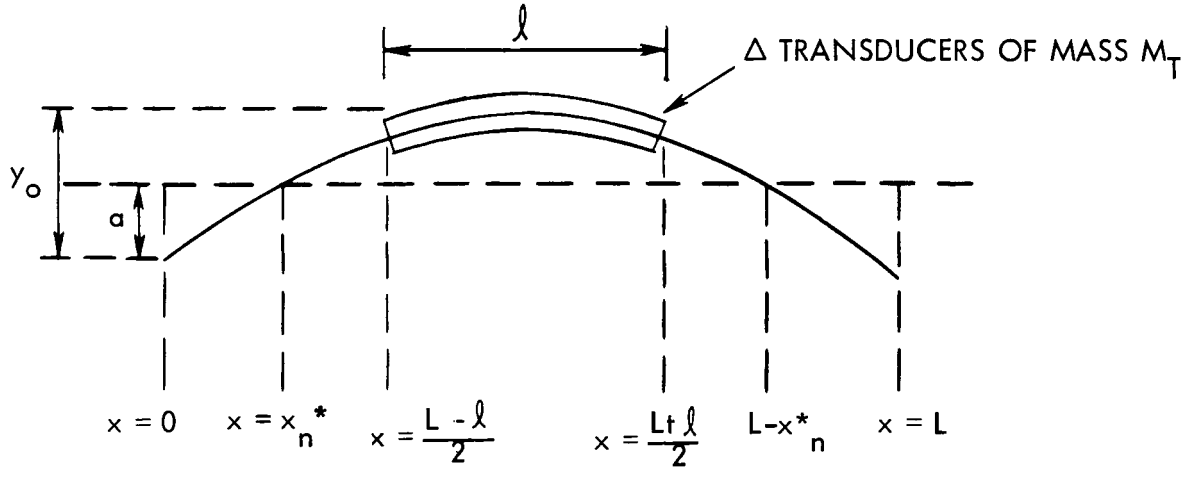

Figure 9. (c) Beam With Transducers

The node location is found to be:

$$x_n^* = \frac{L}{\pi} \sin^{-1} \frac{0.6366(M_B + 4\,M_T)}{M_B + 4\left(\frac{\ell}{L}\right)M_T} \tag{85}$$

As a general rule, the node shift due to transducer mass is approximately 2 to 3% and is particularly important when the beam is hard-mounted such as the gimballed beam described in the Control Loop and Electrical Analysis and Design test that follows.

CONTROL LOOP AND ELECTRICAL ANALYSIS AND DESIGN

The electrical analysis and design for the free-free beam sensor consists of the definition of the control circuits needed to generate the drive voltage, to process the voltage on the readout transducer, and to provide an electrical damping signal for the beam. The gains, frequency responses, and non-linearities of the electronics are directly dependent on the mechanical beam-transducer parameters such as resonant frequencies, and are chosen to minimize sensor output noise and null shift, as well as to fix sensor performance parameters such as scale factor and damping ratio. The electronics are, of necessity, analog because of the amplitude-modulated beam output and are synthesized using an operational amplifier mechanization.

DRIVE LOOP ANALYSIS AND DESIGN

The drive electronics, or drive loop, which provides the drive voltage to vibrate the beam in the vibrational axis, can be generally designed by one of two methods. The first method, which consists of a fixed amplitude-variable frequency oscillator, uses the output of the feedback transducer to determine the frequency of oscillation and to adjust the oscillator frequency to the beam resonance. The second method consists of an analog closed loop oscillator for which the beam-transducer combination is the frequency determining element. As was noted previously, the so-called "gain" or transfer function of the beam-transducers with the drive transducer as input and the feedback transducer for output is very similar to a highly resonant series R-L-C circuit.

For most vibratory sensor designs, the second of the above methods is the most desirable because of the tolerances and variations of the beam-transducer gains and resonant frequencies. Because of the self-tracking nature of the closed-loop oscillator, variations in sensor performance due to aging and environment are minimized by this method. If the resonant frequency of the beam-transducers should shift the oscillator frequency would track it because it is the frequency-determining element. Gain variations can also be compensated for, as will be seen in later paragraphs, by providing a loop gain

much greater than unity, and designing a saturating nonlinearity or regulator control to fix the amplitude of oscillation independent of the beam. The following paragraphs contain a description of the drive loop dynamics as well as the effects of beam-transducer variations such as resonant frequency and gain, and the effects of drive loop noise.

A block diagram of the basic oscillating drive loop is shown in Figure 10 and consists of the beam and transducer dynamics, and the drive electronics. The two functions provided by the drive electronics are filtering of the feedback transducer voltage to assure the correct loop phase for oscillation, and an amplifier to assure a loop gain greater than unity under all conditions. The filter is chosen to be a double pole at the beam resonant frequency instead of an integrator to insure that the loop will not oscillate at any of the higher beam modes (Appendix A). The frequency stability of this loop in terms of its ability to track the beam resonant frequency is dependent on the difference between the beam resonant frequency and the frequency at which the filter provides -90^{o} phase shift. The phase of the beam-transducer transfer function is

$$\phi_y(\omega) = \pi - \tan^{-1}\left[\frac{\omega_y \omega}{Q_y\,(\omega_y^{\,2} - \omega^2)}\right] \tag{86}$$

and the filter pahse shift is

$$\phi_f(\omega) = -2\tan^{-1}\frac{\omega}{\omega_f} \tag{87}$$

where ω_f is usually chosen to coincide with ω_y. The slopes of these phase functions at their respective characteristic frequencies are

$$\left(\frac{d\phi_y}{d\omega}\right)_{(\omega = \omega_y)} = -\frac{2Q_y}{\omega_y} \tag{88}$$

$$\left(\frac{d\phi_f}{d\omega}\right)_{(\omega = \omega_f)} = -\frac{1}{\omega_f} \tag{89}$$

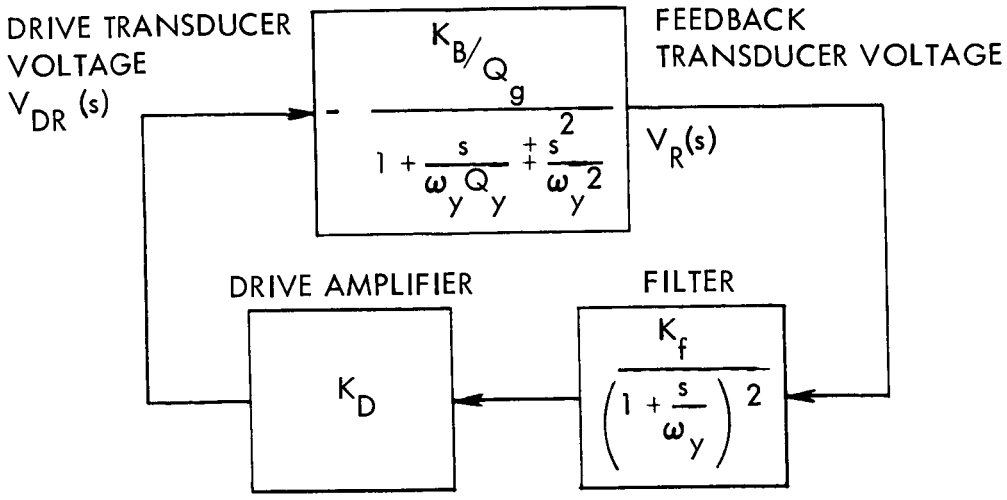

Figure 10. Basic Oscillating Loop

If ω_f and ω_y are close together then both phase characteristics may be approximated by straight lines in this region

$$\phi_y(\omega) \cong \phi_y(\omega_y) + \left(\frac{d\phi_y}{d\omega}\right)_{\omega=\omega_y} (\omega - \omega_y)$$

$$\phi_f(\omega) \cong \phi_f(\omega_f) + \left(\frac{d\phi_f}{d\omega}\right)_{\omega=\omega_f} (\omega - \omega_f)$$

Since $\phi_y(\omega_y) = \frac{\pi}{2}$, and $\phi_f(\omega_f) = -\frac{\pi}{2}$ and the fact that the loop shown in Figure 8 oscillates at a frequency ω_{os} where ω_{os} is determined from the equation

$$\phi_y(\omega_{os}) + \phi_f(\omega_{os}) = 0 \qquad (90)$$

provided that the loop gain is greater than unity. Substituting and solving for ω_{os}, we find that

$$\omega_{os} = \omega_y \left[\frac{1 + 2Q_y}{2Q_y + \frac{\omega_y}{\omega_f}}\right] \cong \omega_y \frac{1}{1 + \frac{\omega_y}{2Q_y\omega_f}} \quad \text{for high Q's} \qquad (91)$$

If the quality factor is approximately 1000, then the frequency of oscillation is always within 0.004% of the natural frequency of the beam, if the difference between the natural frequency and the filter frequency is less than 5%.

The loop in Figure 10 not only sets controls for the frequency of operation, but it also determines the start-up time for the sensor. A good rule of thumb is that for effective loops gains greater than 10, the start-up time is controlled by the beam Q (bandwidth). The amplitude of beam movement rises with an approximate time constant of τ

$$\tau_s \cong \frac{2Q_y}{\omega_y} \quad \text{start-up time constant}$$

For $Q_y \cong 1000$, $\omega_y \cong 1.25 \times 10^4$ rad/sec

$$\tau_s \cong 0.16 \text{ seconds}$$

The previous paragraph describing the oscillator operation did not consider the amplitude of vibration. For a loop such as that shown in Figure 10, the amplitude is determined by the saturation characteristics of the electronics. This saturation produces higher harmonics in the drive voltage that tend to distort the sensor angular rate output and raise its noise content. Also, if saturation characteristics are used for amplitude control, the sensor scale factor which is proportional to the amplitude of beam motion in the vibrational axis becomes very sensitive to changes in the drive transducer and bond. In order to eliminate these problem areas, the drive loop is designed with an automatic gain control which fixes the oscillation at a precise amplitude and maintains sinusoidal operation. A block diagram of this amplitude control is shown in Figure 11, and consists of the basic frequency-determining loop plus an automatic gain control for the drive amplifier. The amplifier gain is controlled with a signal proportional to the difference between the amplitude of the feedback voltage and a chosen reference voltate (ϵ). The gain variation is specified as

$$K(\epsilon) = \frac{1}{K_{Bo}} \quad (m\epsilon + 1) \tag{92}$$

When m is the gain slope and K_{Bo} is the nominal value of beam gain. Using the above and the nomenclature of Figure 11, we find that

$$V_D(t) = \frac{1}{K_{Bo}} \left[1 - mH\,(V_R - V_o) \right] V_R(t) \tag{93}$$

where V_D and V_R are the <u>amplitudes</u> of the drive feedback voltages respectively, and V_o is the reference voltage.

Since it is much easier and more accurate to establish a dc reference instead of ac, the functional block H is of necessity a peak detector and low frequency filter, and may be represented by $H(s) = \frac{1}{1 + \tau s}$ (94)

Since the control loop is nonlinear, stability must be considered in the limits and particularly about the nominal operating point. If

$$V_D(t) = V_{Do} + \triangle V_D(t) \tag{95}$$

$$V_R(t) = V_{Ro} + \triangle V_R(t) \tag{96}$$

and if $V_{Do} >> \triangle V_D(t)$, $V_{Ro} >> \triangle V_R(t)$

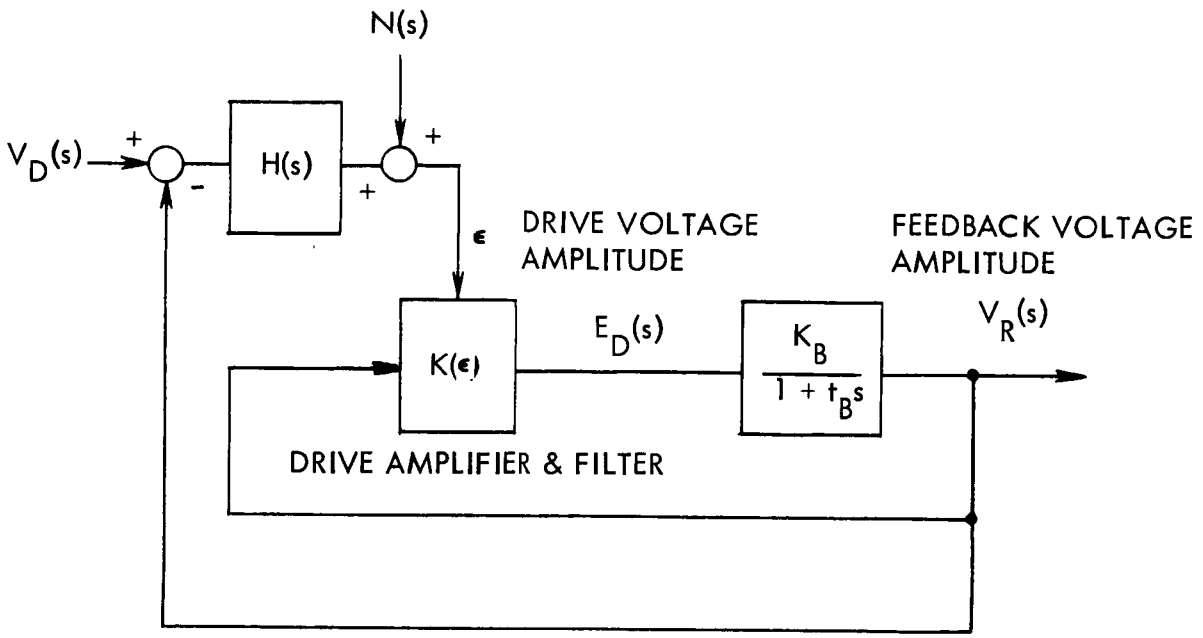

Figure 11. Amplitude Control Block Diagram

then $$\frac{\Delta V_D}{\Delta V_R} = \frac{1}{K_B} (1 - m H V_{Ro}) \quad (97)$$

where $$V_{Ro} = K_B V_{Do} \quad (98)$$

and $$V_{Ro} = V_o \quad (99)$$

Then, the total electronic transfer function for small changes in oscillation amplitude is

$$\frac{\Delta V_D}{\Delta V_R} (s) = \frac{1}{K_B} \left[\frac{1 - m V_{Ro} + \tau s}{1 + \tau s} \right] \quad (100)$$

The beam-transducer amplitude transfer function consists of a single log at the bandwidth of the resonant peak. Amplitude modulation produces sidebands around the resonant carrier which are attenutated the difference between the sideband and the carrier becomes greater. Therefore, the loop of Figure 11 may be written as

$$A(s) = \frac{(m V_{Ro} - 1) \left[1 - \frac{\tau}{m V_{Ro} - 1} s \right]}{(1 + \tau s) (1 + \tau_B s)} \quad (101)$$

A Bode diagram for a typical loop is shown in Figure 12. The RHP zero that is introduced by the filter and variable gain amplifier is always a higher frequency than the filter pole, and selecting parameters for adequate stability is not a problem. The regulating capability of this loop are dependent upon the dc loop gain $(m V_{Ro} - 1)$. The actual regulation in percent in $\frac{10}{m V_{Ro} - 1}$; for a 30% change in beam gain and a loop gain of 10, the feedback voltage amplitude change is approximately 3%.

One of the primary design and analysis considerations for the drive oscillator control loop is its susceptibility to noise, either electrical or mechanical, that could be transferred output axis and affect sensor threshold/resolution. As was shown in Section 1 on Theory of Operation, the drive transducer interface is very sensitive to voltage changes that are reflected in sensor null shifts. Also, the possibility of some noise content at the sensor natural frequency puts a premimum on noise considerations. The noise response of the loop shown in Figure 11 with the noise simulated at the gain control input of the AGC amplifier is

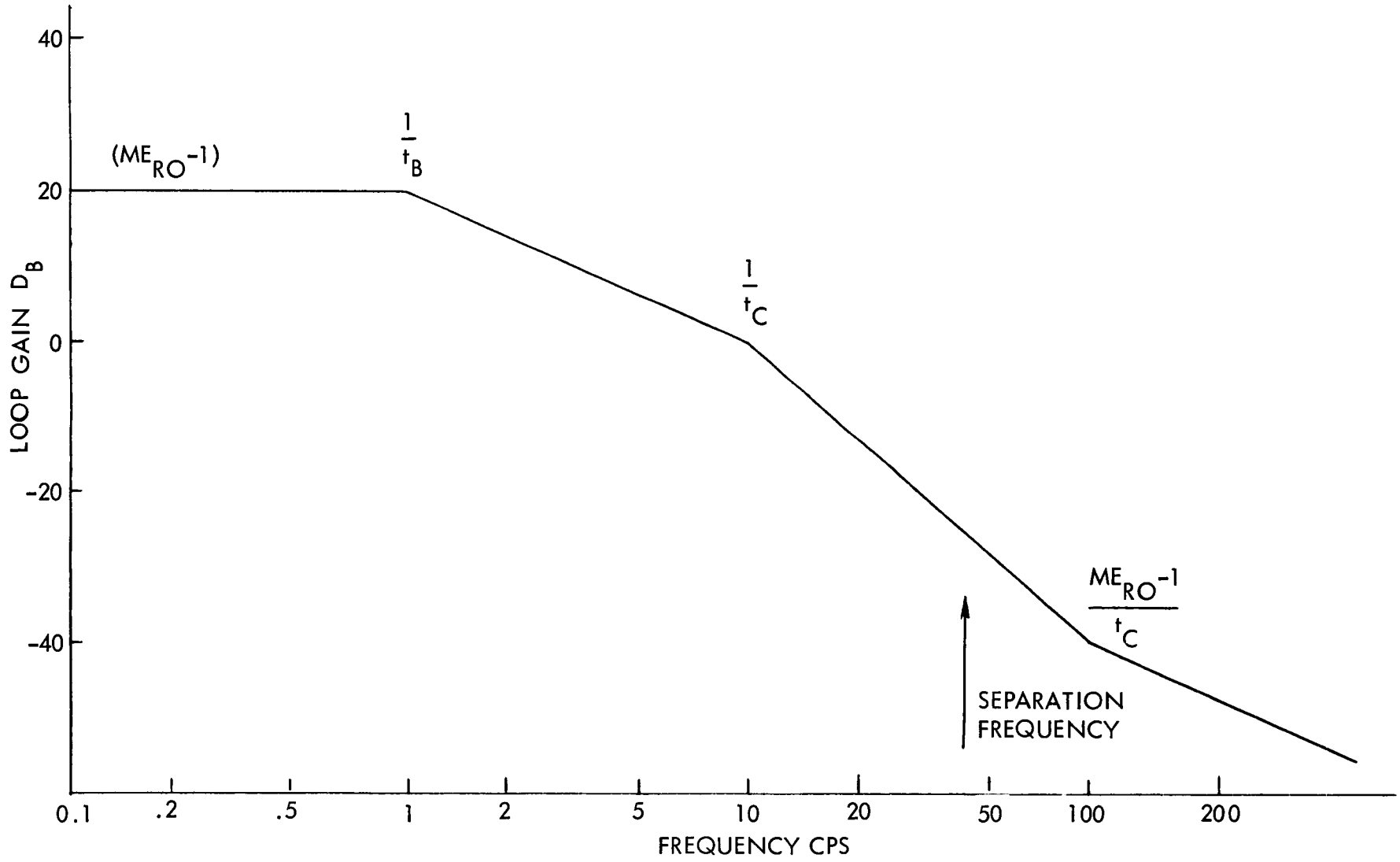

Figure 12. Variation Amplitude Control Bode Diagram

$$\Delta V_D(s) = \frac{\frac{1}{K_B}(1+\tau s)(1+\tau_B s)}{1+\frac{\tau_B}{mV_o}s+\frac{\tau\tau_B}{mV_o}s^2} N(s) \quad (102)$$

If the time constant of the filter H is chosen to yield a critically-damped characteristic, then:

$$\Delta V_D(s) = \frac{\frac{1}{K_B}\left(1+\frac{\tau_B}{4m E_{Vo}}s\right)(1+\tau_B s)}{\left(1+\frac{\tau_B}{2m E_{Vo}}s\right)^2} N(s) \quad (103)$$

where $\tau = \frac{\tau_B}{4m E_{Vo}}$

and

$$A(s) = \frac{(m E_{Vo}-1)\left[1-\frac{\tau_B}{4m E_{Vo}(m E_{Vo}-1)}s\right]}{\left(1+\frac{\tau_B}{4m E_{Vo}}s\right)(1+\tau_B s)} \quad (104)$$

The loop gains and noise responses for various values of $m E_{Vo}$ are shown in Figures 13 and 14 for $\tau_B = 0.08$ sec and $K_B = 1$. These curves point up the fact that the drive loop is susceptible to broad band noise. Random modulations of the drive voltage are especially significant if they excite the readout plane resonance (noise at the separation frequency).

The various typical curves given show that for high loop gains (good feedback voltage and scale factor regulation) that the noise response of the loop degrades especially at higher frequency. This indicates that there is a tradeoff and an optimum setting for regulation versus sensor noise and threshold. This fact will be borne out by the cross coupling data presented in the Testing Section when the sensor is subjected to controlled noise in the drive loop.

READOUT AND DAMPING LOOP ANALYSIS AND DESIGN

The readout or output functions of the sensor consist of amplification and demodulation of the beam-transducer voltage output due to an applied angular rate. Since the beam-transducer system is an ac system with the angular

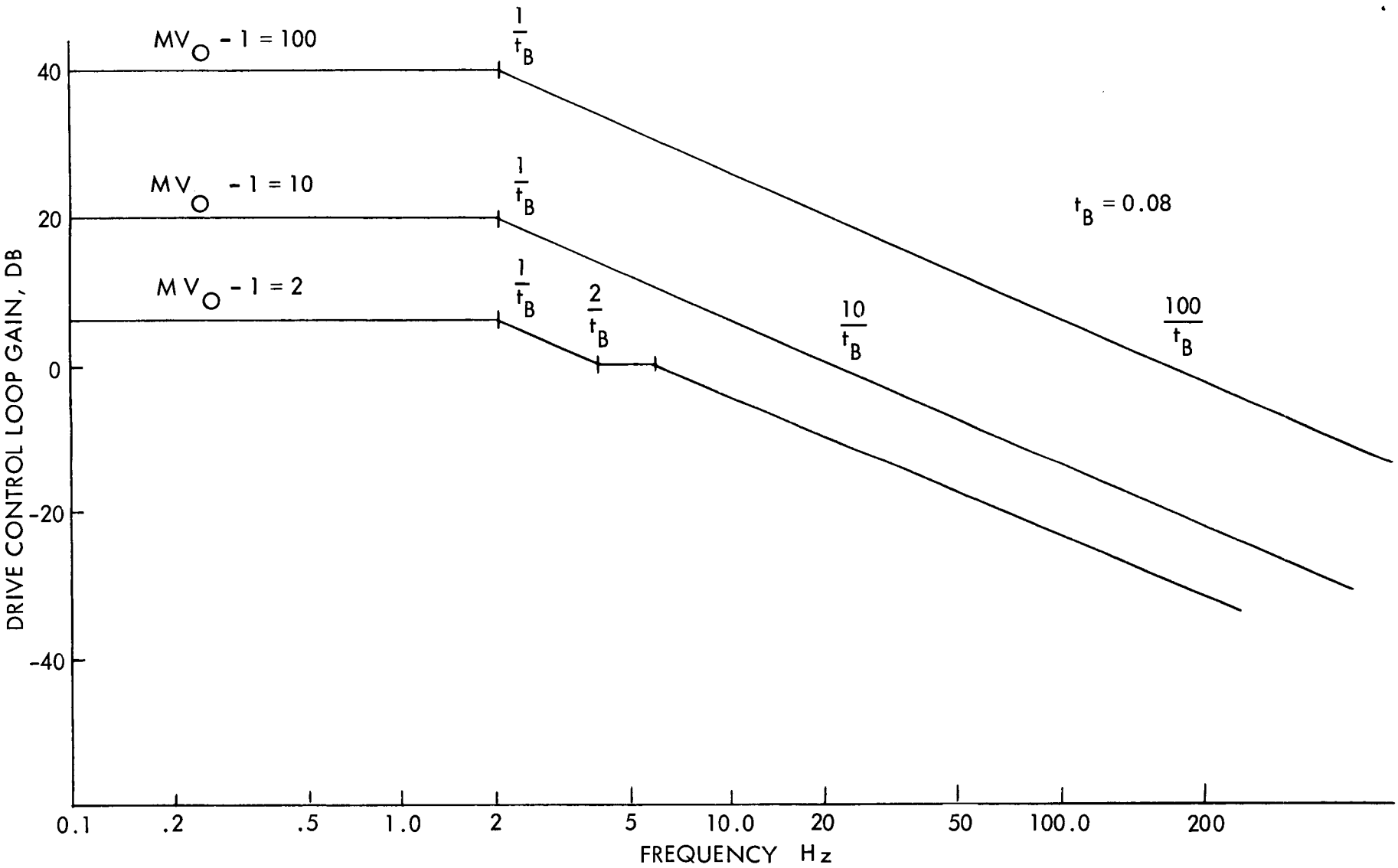

Figure 13. Drive Control Loop Gain

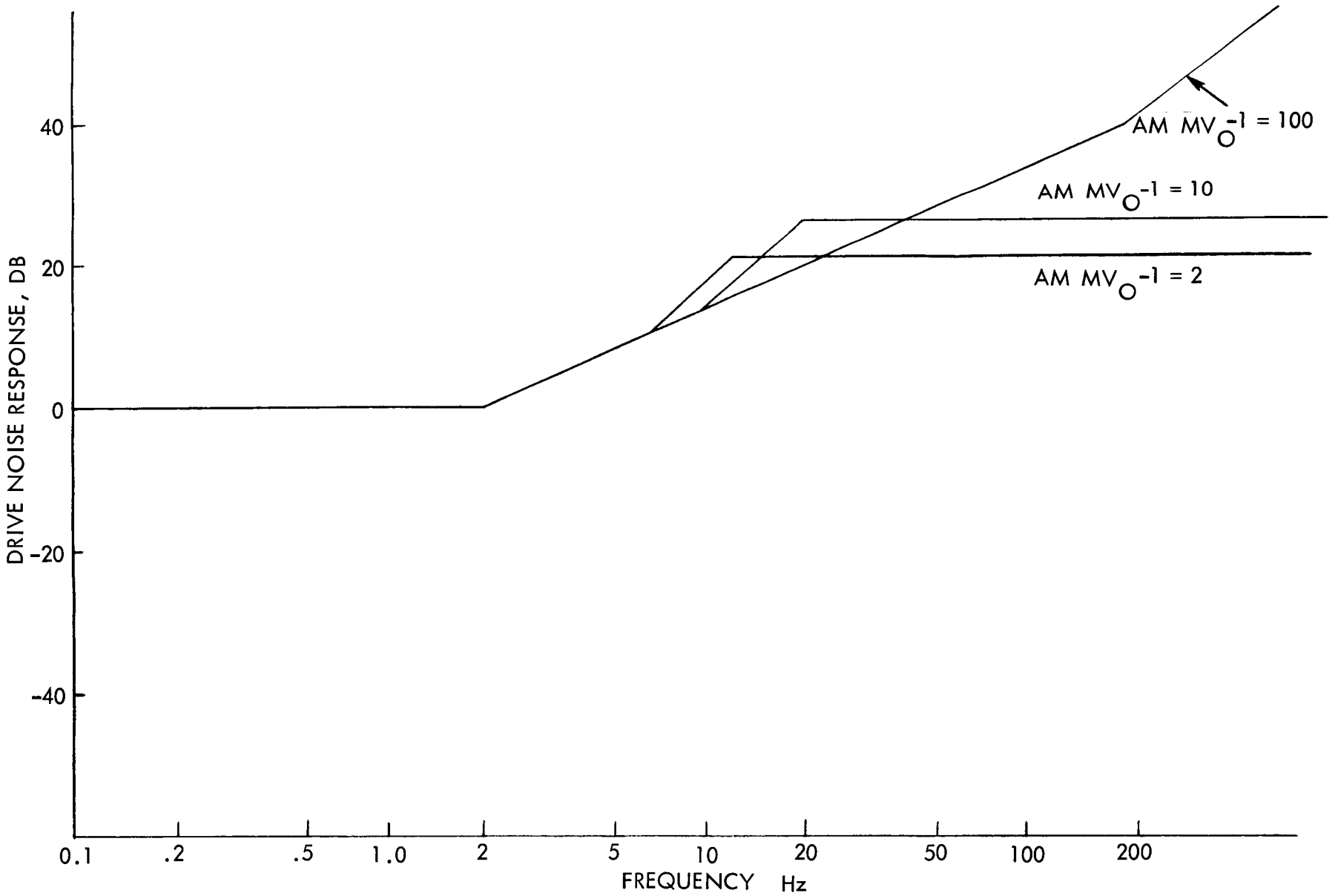

Figure 14. Drive Loop Noise Response

rate information carried as amplitude modulations of the basic oscillator frequency, and is phase sensitive to the direction of the applied angular rate, the drive voltage which was shown to be either in-phase and out-of-phase with the angular rate output can be used as the demodulation reference. This is shown functionally in Figure 15. The sensor transfer function without damping can therefore be represented as

$$E_o(s) = \frac{K_o}{1 + \frac{s}{\omega_s Q_s} + \frac{s^2}{\omega_s^2}} \Omega(s) \qquad (105)$$

where E_o is the transfer function of the demodulated sensor voltage output, K_o is the sensor scale factor in volts/rad/sec and includes both mechanical and electrical gain, ω_s is the separation frequency (difference between vibrational and output frequencies) and Q_s is the output quality factor.

The damping loop, which is also shown functionally in Figure 15, uses the damping transducer to apply an amplitude-modulated voltage to the beam-transducer to increase the basic damping ratio of the above transfer function. The carrier frequency of the damping signal is the basic oscillator frequency. The response of the beam-transducers in the output axis due to a damping signal at the carrier frequency is

$$V_o(j\omega_y) \cong \frac{\frac{2\ell t h^2 w}{3L^2 K_B K_e d_{31} g_{31}}}{(1 - \frac{\omega_y}{\omega_z})} V_{DA}(j\omega_y)$$

This gain must be known to establish the damping loop gain and the effective sensor damping ratio.

The prime design considerations for the damping loop are minimum noise and effective control of damping ratio. The passive filter is designed to be a minimum bandwidth lead-lag such that sufficient phase lead is obtained at the separation frequency. Typically,

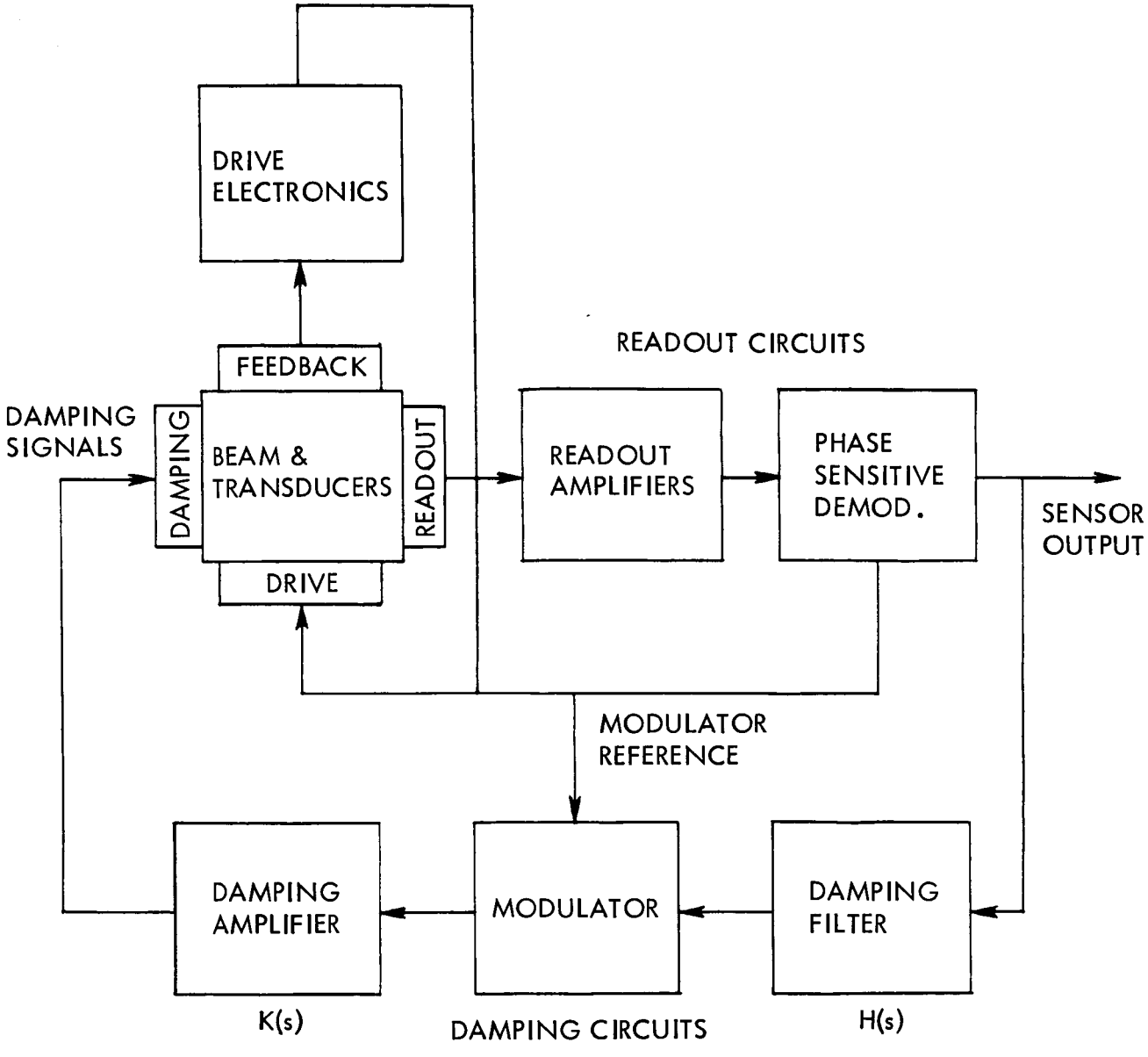

Figure 15. Damping Block Diagram

$$H(s) = \frac{\frac{s}{9\omega_s}}{\left(1 + \frac{s}{3\omega_s}\right)\left(1 + \frac{s}{10\omega_s}\right)^2} \qquad (106)$$

The modulator is used to modulate the damping error signal in phase with the drive voltage and consists of a single transistor chopper. Note that the ac error signal produced by the modulator is a square wave. Band-limiting and noise suppression is also supplied by the damping amplifier to reduce chopper noise. Typically,

$$K(s) = \frac{K_D \frac{5s}{\omega_{cy}}}{\left(1 + \frac{5s}{\omega_y}\right)\left(1 + \frac{s}{5\omega_y}\right)} \qquad (107)$$

Where ω_c is the drive frequency and K_D is the midband gain. The sensor damping ratio can be adjusted from approximately 0.5 to 1.0 by adjusting the damping amplifier gain K_D from 1 to 10.

Any part of the sensor design which affects the sensor separation or natural frequency must be compensated for because of the potential cross-coupling and sensor null shifts. The laboratory model was designed using the gimballed-flexural pivot approach. This design is such that the inertia of the gimbal affects the resonant frequency in one axis but not the other.

The gimbal inertia acts principally in the readout plane of the sensor and tends to lower its resonant frequency with respect to the drive plane, thus widening the frequency separation and sensor bandwidth. This is shown in the following.

The first mode resonant frequency for a perfect free-free is given by:

$$\omega = \frac{22.4}{L^2}\left(\frac{EI}{\mu}\right)^{1/2} \qquad (108)$$

where: L is the length of the beam

μ is the beam mass per unit length

EI is the flexural rigidity

and the beam deflection curve is approximately:

$$y(x) = y_o\left(\sin\frac{\pi x}{L} - \frac{2}{\pi}\right) \qquad \text{(see Figure 9)}$$

The effective rotation of the beam at the nodes is given by:

$$\theta \cong \frac{0.77\pi}{L} \quad y_o$$

and the maximum value of beam potential and kinetic energies are respectively:

$$E_p = \frac{\pi^4 EI y_o^2}{4L^3}, \quad E_K = \mu \omega^2 \; y_o^2 \; L \left[\frac{1}{4} - \frac{2}{\pi^2}\right] \tag{109}$$

Using the above, the resonant frequency can be expressed as:

$$\omega^2 = \frac{K_\theta}{I_B} \tag{110}$$

where K_θ is the effective rotational spring rate of the beam and I_B is the effective beam rotational inertia. If the gimbal inertia is added at the nodes, then the new resonant frequency is:

$$\omega^{*2} = \frac{K_\theta}{I_B + I_G} = \frac{\omega^2}{\left(1 + \frac{I_G}{I_B}\right)} \tag{111}$$

where I_G is the gimbal inertia.

A sketch of the gimbal is shown in Figure 9 with appropriate nomenclature. The inertia is given approximately by:

$$I_G \cong \frac{8\rho}{3g} \; c \; a \; t \left[a(a^2 + c^2) + 3a^2 + c^2\right]$$

where ρ is density of the gimbal material.

As an example, the parameters for the design used for preliminary evaluation where:

$$a = 0.186", \; c = 0.125", \; t = 0.08"$$

$$\rho = 0.3 \text{ lb/in}^3, \; g = 387 \text{ in/sec}^2$$

and

$$I_G = 4.9 \times 10^{-7} \text{ in-lb-sec}^2.$$

For the 4.0" beam with 0.172" cross-section,

$$I_B = 2.48 \times 10^{-5} \text{ in-lb-sec}^2$$

$$K_\theta = 4.5 \times 10^3 \text{ in-lb-rad}$$

Therefore,

$$\omega = 2140 \text{ Hz}$$

and

$$\omega^* = \frac{\omega}{\left(1 + \frac{I_G}{I_B}\right)^{1/2}} \cong 2100 \text{ Hz} \qquad (112)$$

These results are very close to the measured frequency separation which is the combination of non-square beam cross-section and gimbal effects.

Section 4

LABORATORY MODEL DESCRIPTION AND TESTING

DESCRIPTION

The laboratory model of the free-free beam vibratory angular rate sensor was designed with flexural pivot gimballing of the beam and a low-noise set of electronics to allow evaluation of the minimum threshold and resolution. Pictures of the sensor model are shown in Figures 16 and 17, which show an overall view of the beam and electronics, and a close-up of the beam-mount to show details. Figure 18 is a sketch of the cross-section of the beam and mounting channel at one of the mounting points which shows the flexural pivot arrangement.

The gimballed-beam sensor was selected for fabrication because it represented the mounting concept with the best potential for achieving the threshold and null stability requirements. The combination of the "hard" construction and the fact that the configuration could be precisely balanced to reduce external vibration effects make it superior to either a "soft" or rubber-mounted design, or a rigid "clamped-clamped" version. The sketches of Figures 19 thru 24 give the details and dimensions for the design. The pertinent parameters that were selected for the laboratory model were:

Beam:	Material	NiSpan C
	Length L	= 4.00 inches
	Cross-Section	$h_y = h_z$ = 0.172 inches
	Mount Location	x_n^* = 0.92 inches
Gimbal:	Material	303 SS
	Cross-Section	a = 0.377 inches
	Depth	C = 0.172 inches
	Thickness	t = 0.082 inches
Transducers:	Material	PZT-4
	Length	ℓ = 0.75 inches
	Width	W = 0.09 inches
	Thickness	t = 0.02 inches

These parameters were selected to yield beam natural frequencies of approximately 2000 Hz and a separation frequency of 50 Hz. Note that the beam is made square and that the inertia of gimbal gives the desired separation. The mounting locations shown on the sketches are not exact because additional length has been left at the beam ends to allow for trimming during test.

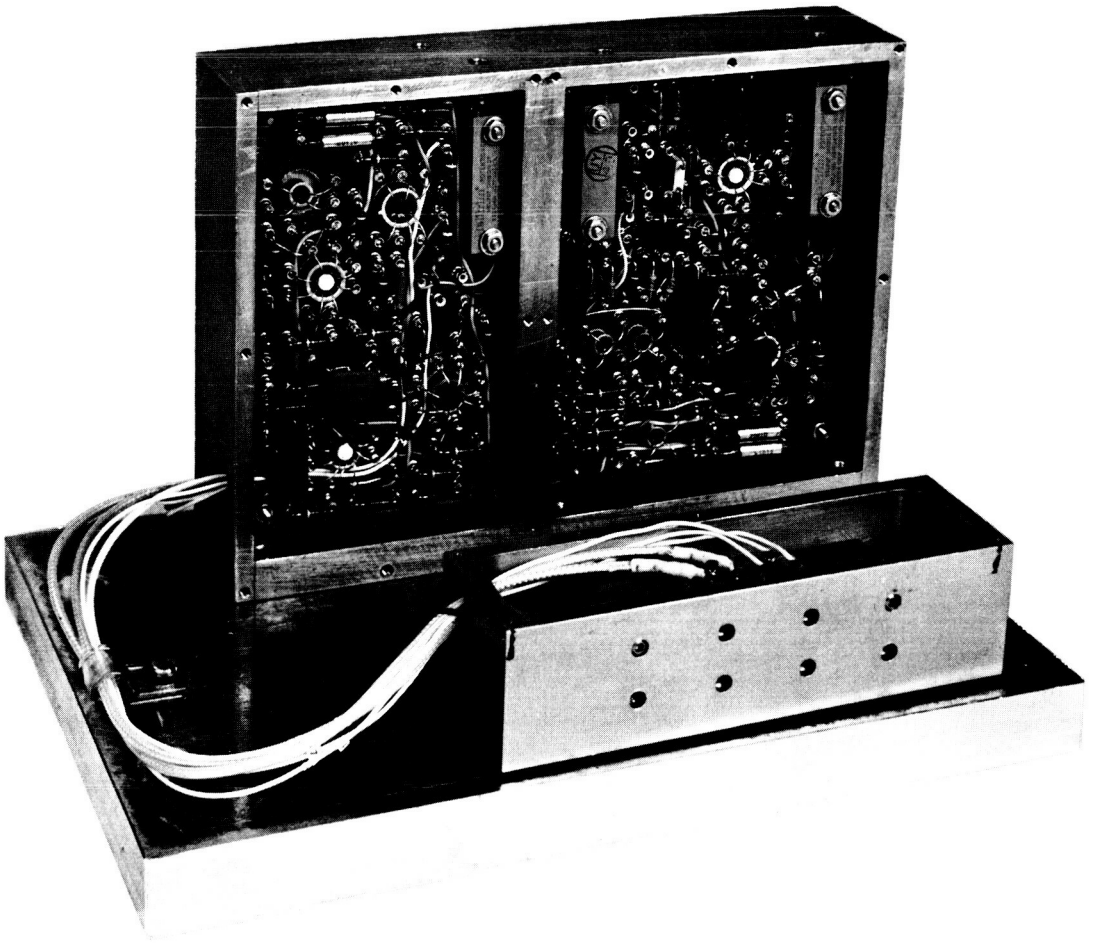

Figure 16. Solid-State Sensor, Laboratory Model

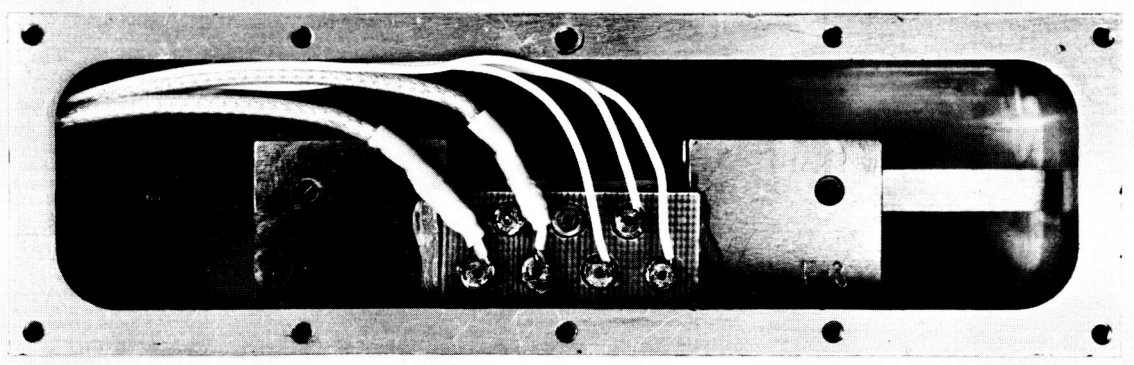

Figure 17. Solid-State Sensor Mechanical Assembly

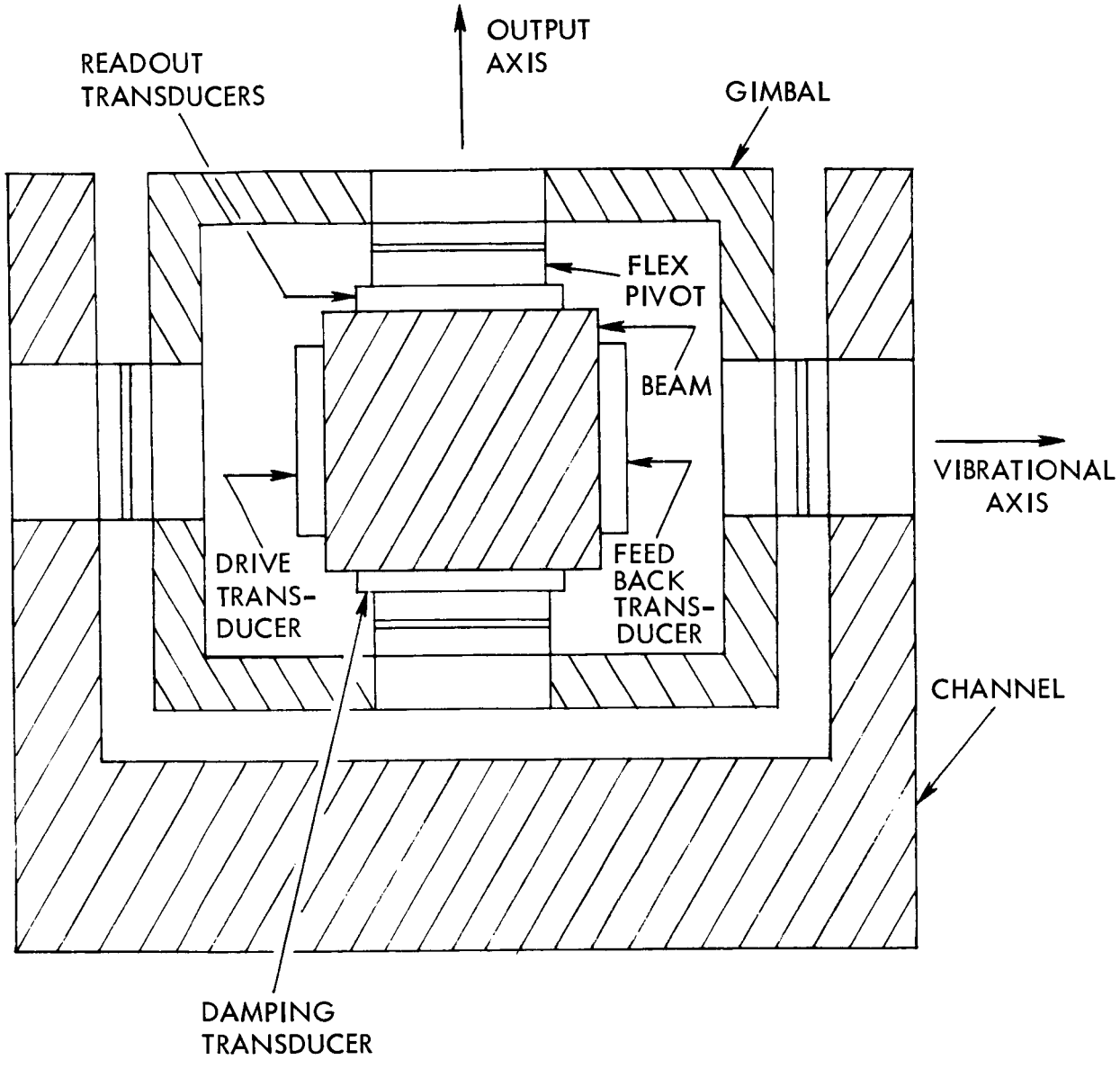

Figure 18. Gimballed Sensor Axes and Transducer Nomenclature

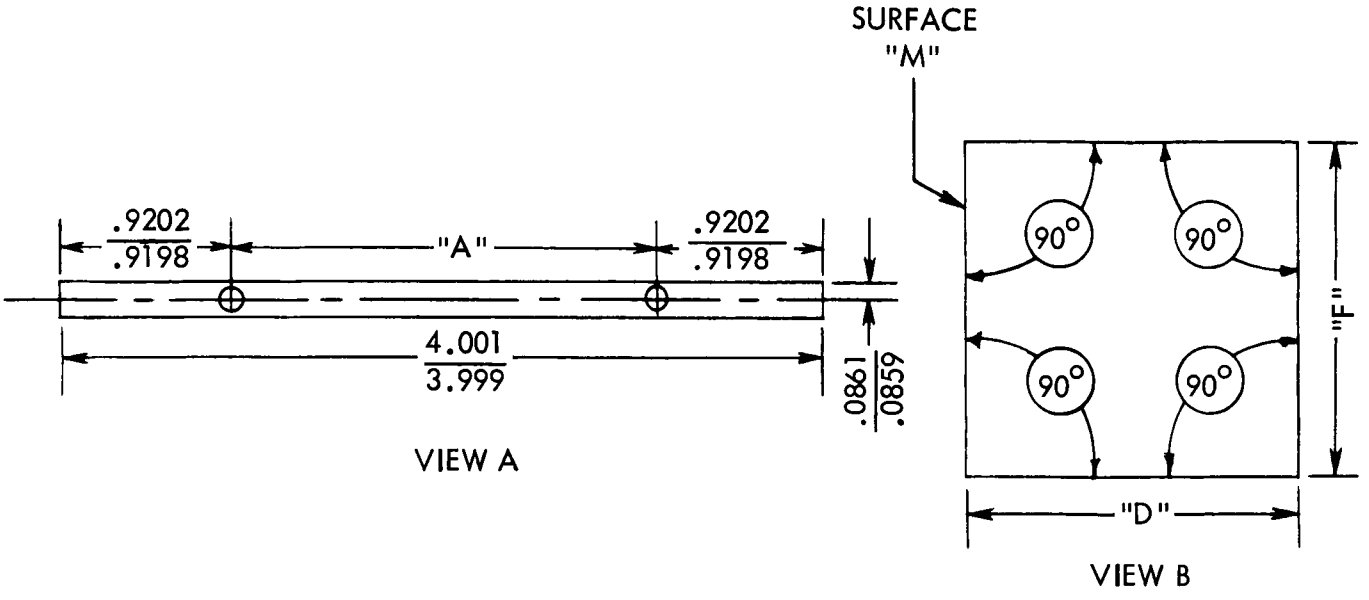

NOTES:

1. THE 2 HOLES TO BE $\frac{.1251}{.1249}$ DIA. & SQUARE TO SURFACE "M" WITHIN .0005 in./in.
2. DIMENSION "A" TO BE $\frac{2.1606}{2\ 1594}$
3. TOLERANCE ON SQUARENESS DESIGNATED BY 90° WITHIN .0005 in/in
4. "D" & "F" SHALL BE $\frac{.173}{.171}$ EXCEPT THAT THEY SHALL NOT DIFFER BY MORE THAN .0002.

BEAM
SCALE - VIEW A 1x
VIEW B 10x
1 REQUIRED
MATERIAL - NI-SPAN C
2-22-67 G. MACKO
3-13-67 GM

Figure 19. Beam

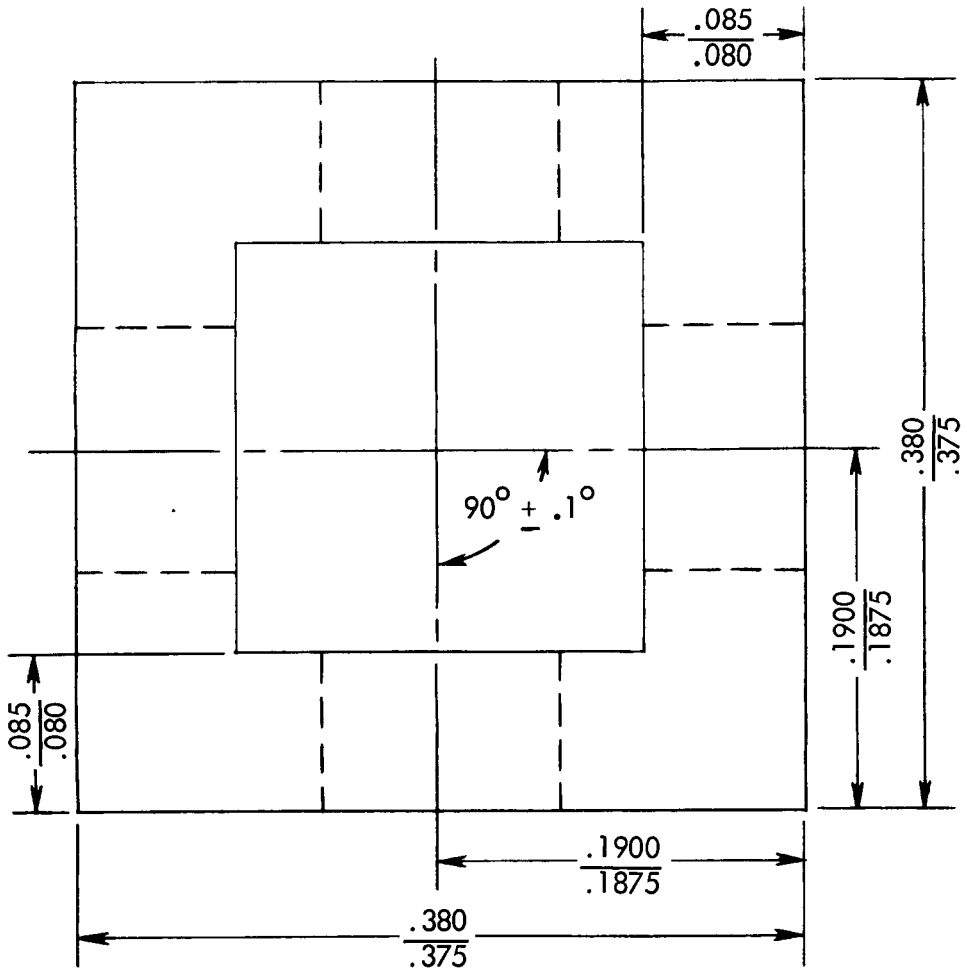

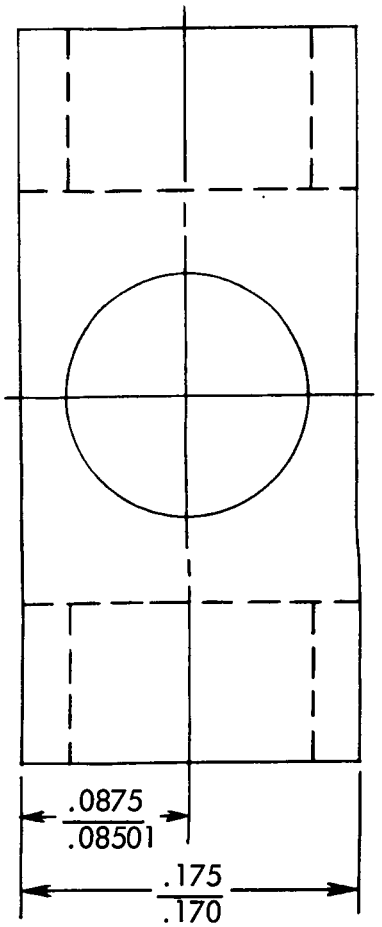

NOTES:

1. ALL 4 HOLES $\frac{.1251}{.1249}$ DIA.
2. ALL 4 INSIDE CORNERS .020 R.

GIMBAL
SCALE - 10X
2 REQUIRED
MATERIAL - 303 SS
2-22-67 G. MACKO

Figure 20. Gimbal

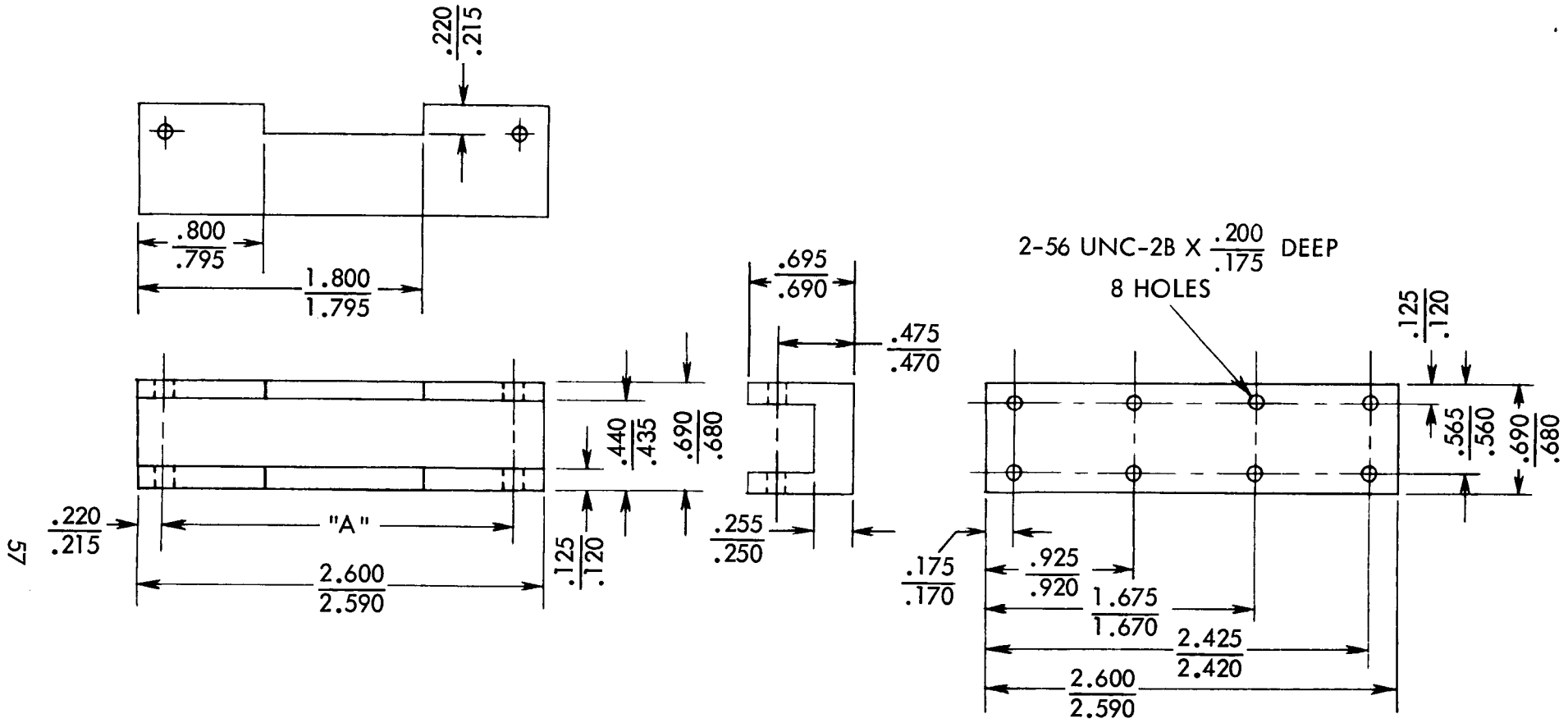

NOTES:

1. ALL 4 HOLES TO BE $\frac{.1251}{.1249}$ DIA.
2. DIMENSION "A" TO BE $\frac{2.1606}{2.1594}$ BUT WILL MATCH CORRESPONDING DIMENSION "A" OF BEAM WITHIN .0002.

BASE
SCALE - 1x1
1 REQUIRED
MATERIAL - 303 SS
2-22-67 G.MACKO

Figure 21. Base

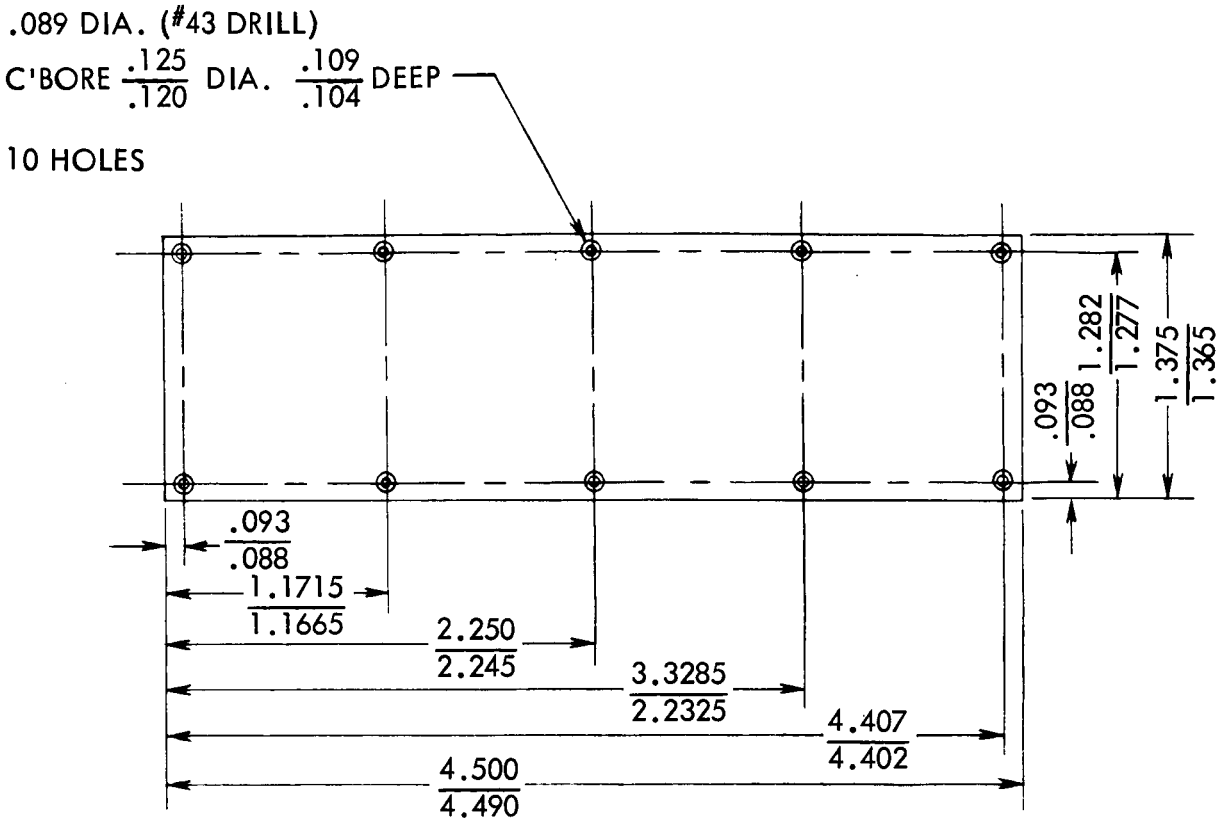

SENSOR BOX COVER
SCALE - 1x1
1 REQUIRED
MATERIAL - AL ALLOY
2-24-67 G. MACKO

NOTES:
1. 3/16 THICK (STOCK)
2. FINISH 125 ALL OVER - ALODINE

Figure 22. Sensor Box Cover

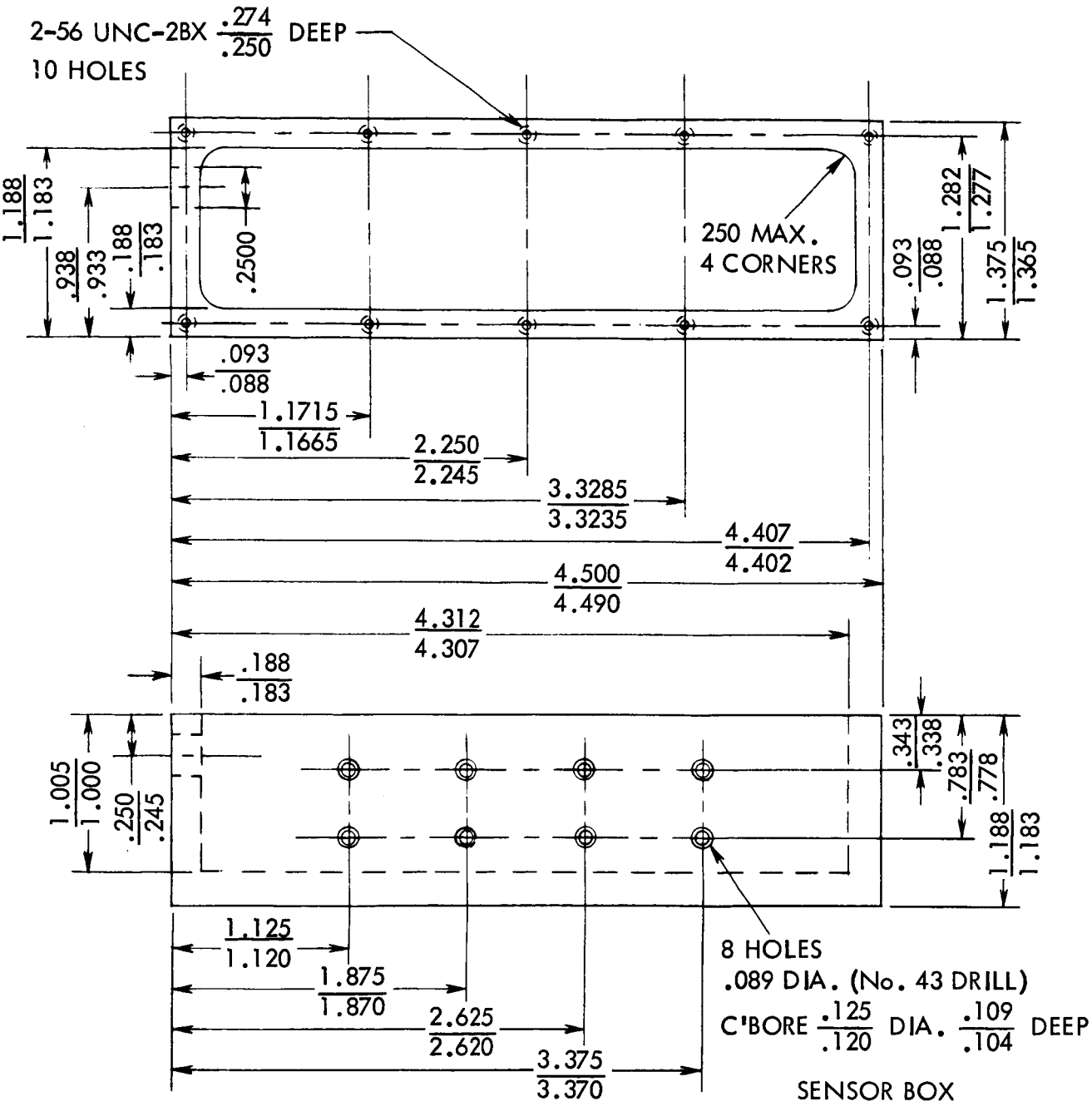

Figure 23. Sensor Box

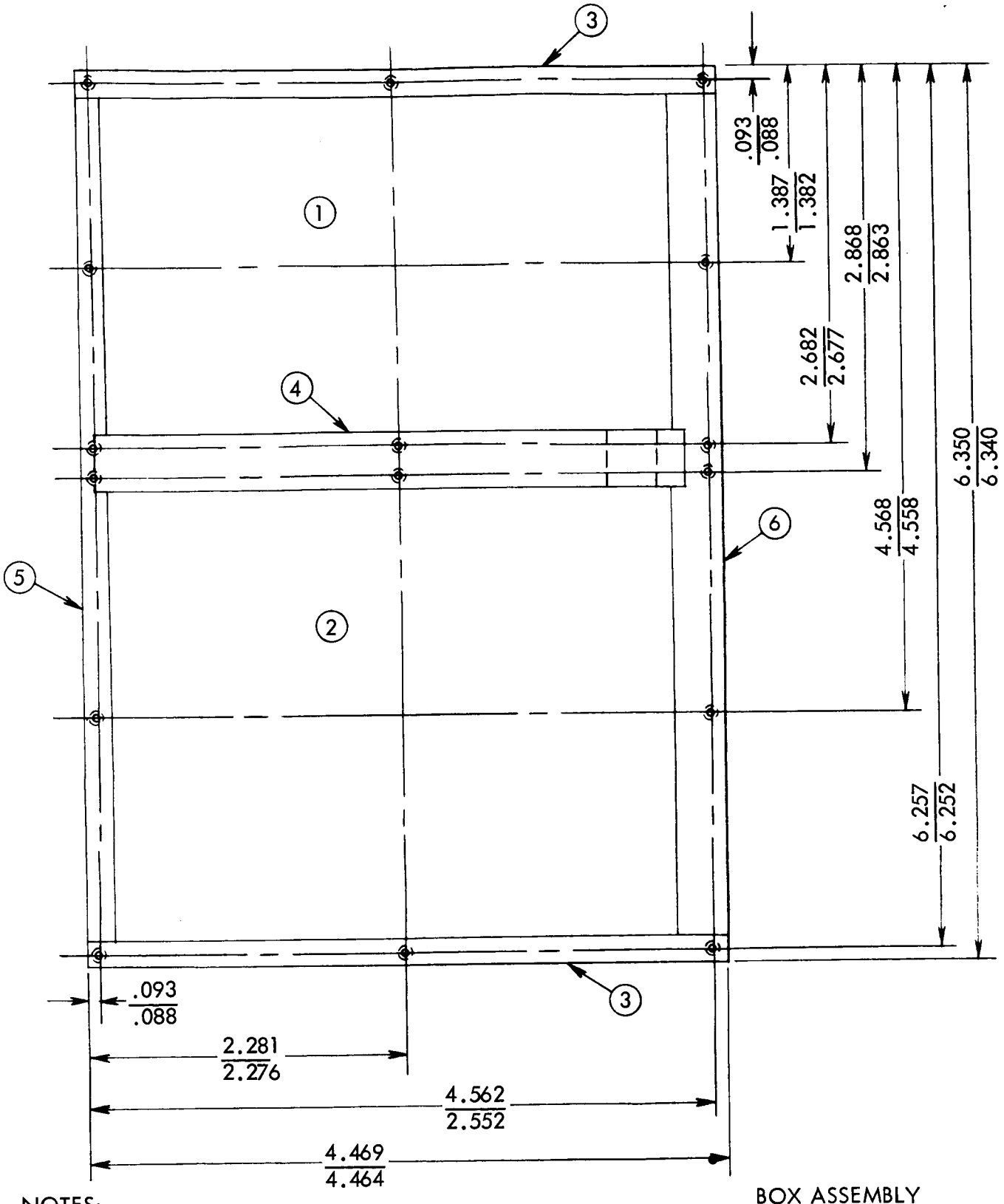

NOTES:

1. ASSEMBLY PARTS AS SHOWN & DIP BRAZE.
2. DRILL & TAP 32 HOLES (16 ON EACH SIDE) 2-56 UNC-2BX $\frac{.375}{.365}$ DEEP.

BOX ASSEMBLY
SCALE - 1x1
1 REQUIRED
FINISH - ALODINE

Figure 24. Box Assembly

The schematics of the sensor laboratory model electronics are shown in Figures 25 thru 28. These electronics are mechanized with 12 microelectronic operational amplifiers and have the advantage that they are easily adaptable to parameter changes during sensor testing. This mechanization, although a hybrid with discrete components for setting gains and compensation, could be extrapolated to an all microelectronic design. The electronics are arranged on four functional boards.

Figure 25 is the basic drive loop circuit which together with the beam forms an amplitude-controlled oscillator that produces a controlled beam vibration at its fundamental frequency. The key element is the AGC amplifier which is controlled by an FET. Figure 26 consists of the circuits which generate the demodulator reference and provide the regulator voltage for the drive loop. Figure 27 shows the buffer amplifiers and preamplifier for the sensor rate output voltage. The use of dual FET's with a microelectronic amplifier reduces the electronic noise present in the output. A quadrature null adjustment is shown before the preamplifier. Figure 28 consists of the demodulator and damping circuits. A dc null adjustment is included before the output amplifier.

The adjustment and calibration of the electronics for the specific beam being used included the following:

1. Selection of vibration amplitude and adjustment of drive loop gain at that amplitude to operate AGC amplifier at approximately the midpoint of its gain range.

2. Quadrature null adjustment after buffer amplifiers.

3. In-phase null adjustment with drive potentiometer and/or output dc null pot.

4. Adjustment of demodulator reference phase for maximum quadrature rejection.

5. Selection of preamplifier gain for desired sensor scale factor.

LABORATORY MODEL TESTS AND EVALUATION

The test and evaluation of the laboratory model consisted of the following:

1. Functional tests of the beam-transducer combination.

2. Calibration and linearity.

3. Threshold and resolution measurements.

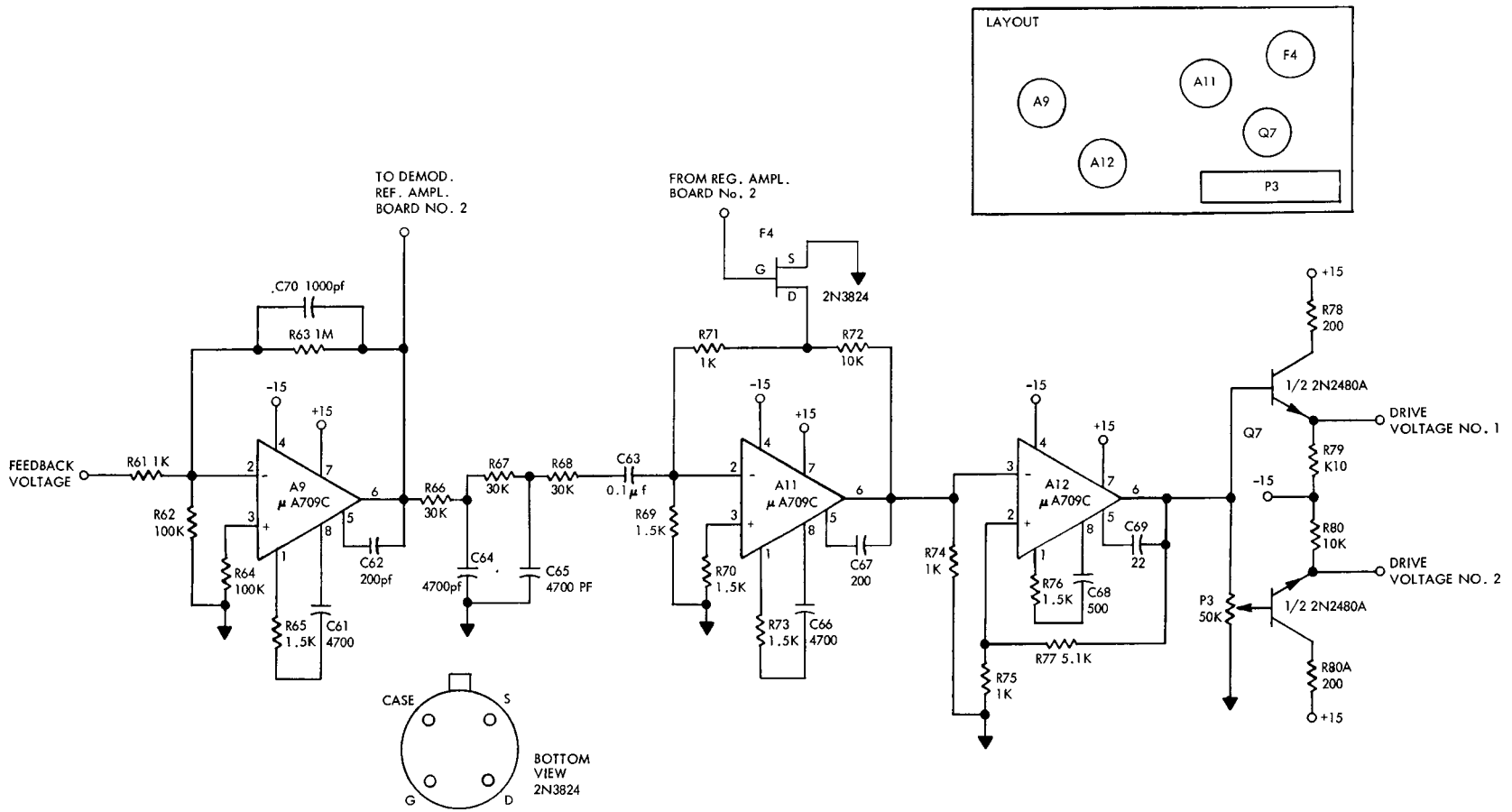

Figure 25. Solid-State Sensor Electronics-Board No. 1 Drive and Feedback

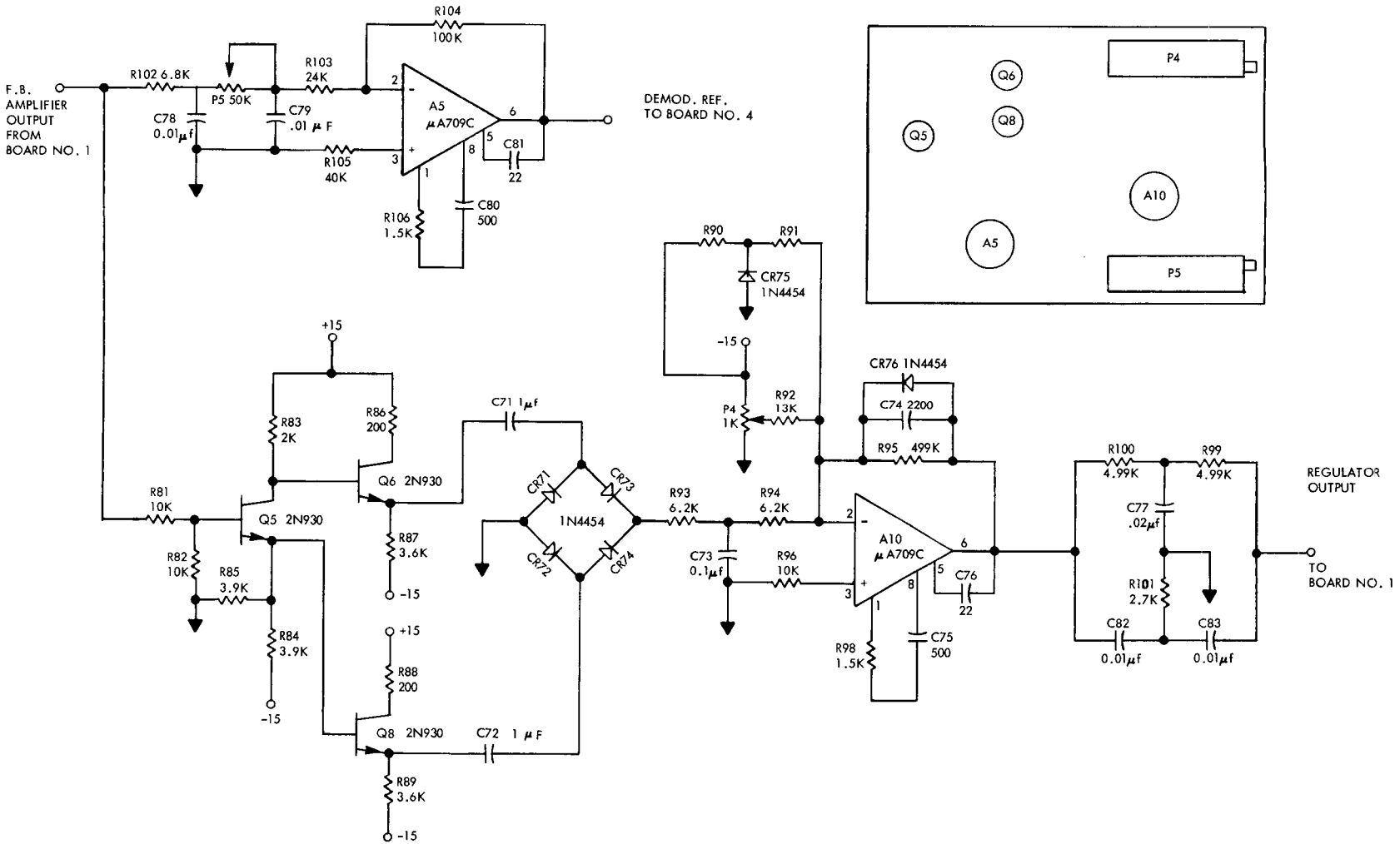

Figure 26. Solid-State Sensor Electronics-Board No. 2 Regulation Regulator and Demod. Ref.

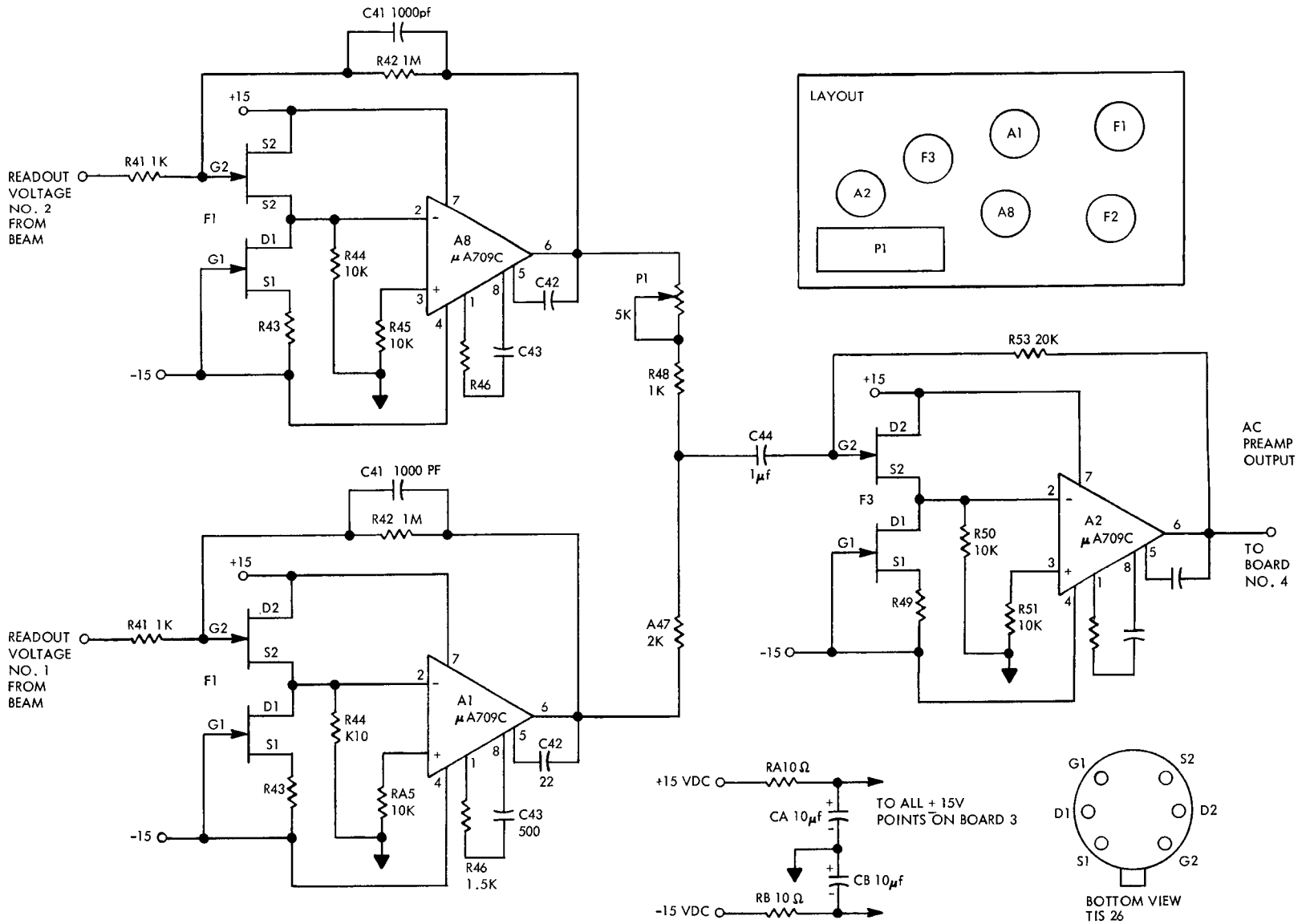

Figure 27. Solid-State Sensor Electronics-Board No. 3 Readout Buffers and Preamplifier

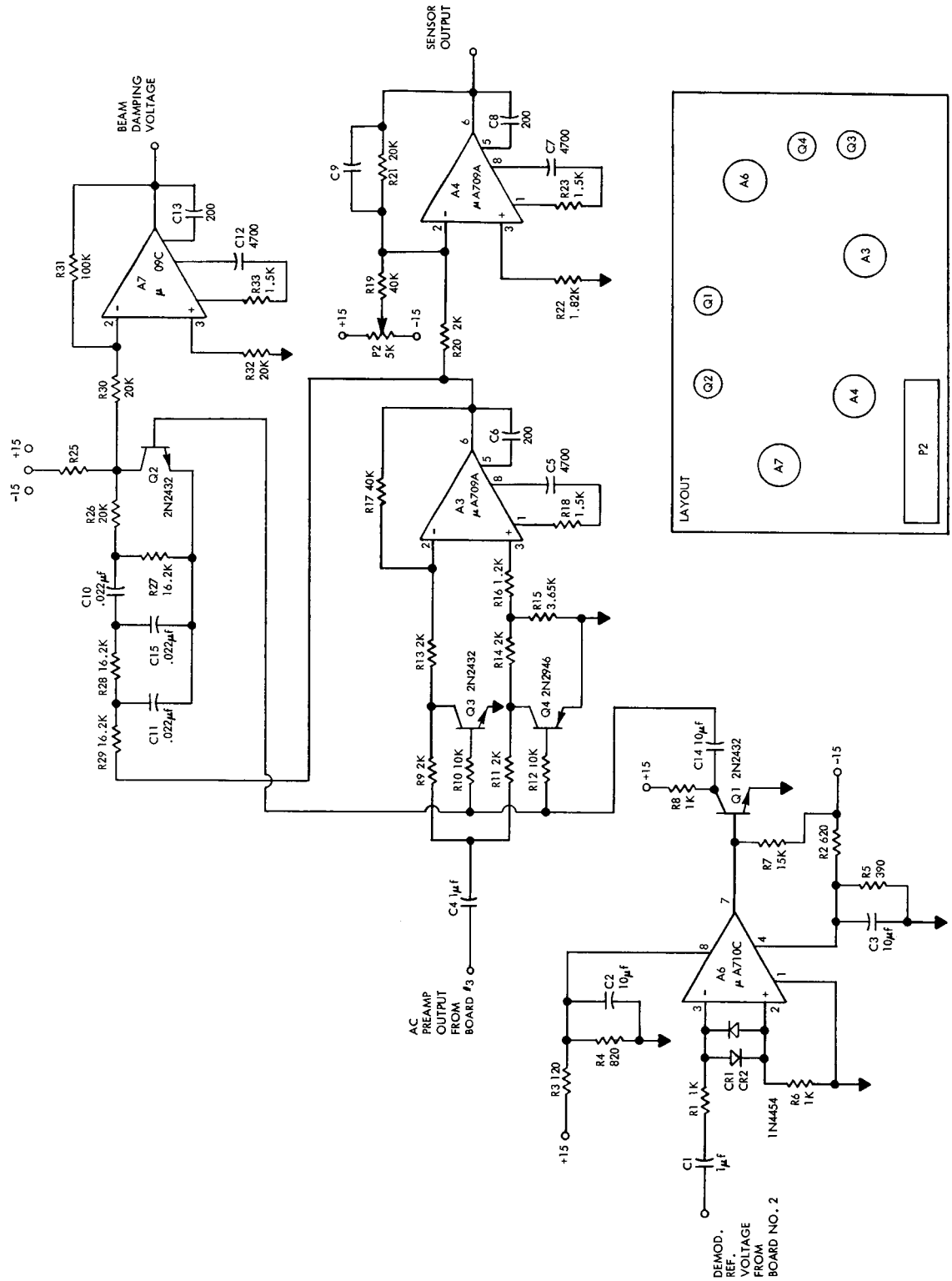

Figure 28. Solid-State Sensor Electronics-Board No. 4
Demodulation and Damping

4. Drift after start-up and long term drift.

5. Null drift with temperature.

6. Frequency response.

7. Null shift due to vibration.

8. Cross-coupling tests.

The functional tests of the mechanical assembly are used for determining whether the beam-transducer configuration is of adequate quality and to determine accurately various parameters such as resonant frequencies and bandwidths. The beam-transducer frequency responses in the drive plane and the readout plane are shown in Figures 29 and 30 . The drive or vibrational axis for the gimballed beam is the inner axis; the readout axis is the outer axis.

Tests were conducted by exciting the drive (damping) transducer with an audio oscillator and monitoring the open or short circuit response of the feedback (readout) transducer as a function of excitation frequency. These tests are significant because the data provides information about sensor quality (transducer gain and bond) proximity of mounting locations to actual vibration nodes, and sensor bandwidth and scale factor. Figure 29 is a plot of the "Q" curve for the drive plane or axis. The beam gain shown is the ratio of the feedback voltage and the drive voltage which are both sinusoidal. The 2KΩ load is used to simulate short-circuit transducer operation. As shown, the "Q" of this unit is unusually high (~ 1300) which is due to the accurate location of the beam nodes ·
A similar plot for the readout plane is shown in Figure 30 and indicates similar results although the Q is lower (~ 860) due to the extra gimbal and pivot effects. The separation frequency or sensor bandwidth for this unit is 63.7 Hz and the scale factor should be between 1.75 and 2.00 millivolts per degree per second at the readout transducer.

The data shown in Figures 31 and 32 exhibits the nonlinearities of the beam vibrational motion due to the flex-pivot mounting. Since the mounting points are fixed rigidly in the frame, large motions of the beam tend to bend the pivots laterally which reduces the actual bending motions of the beam and the equivalent natural frequency. Figure 31 shows both the amplitude and frequency nonlinearities. The beam gain changes approximately 2 to 1 over the range of drive voltages and the maximum change in resonant frequency is approximately 0.1%. Figure 32 shows the reduction in equivalent Q at resonance due to increased beam motion. There is a 50% decrease over the range shown. These nonlinearities do not affect the linearity of the unit when operated as an angular rate sensor because the drive plane is always

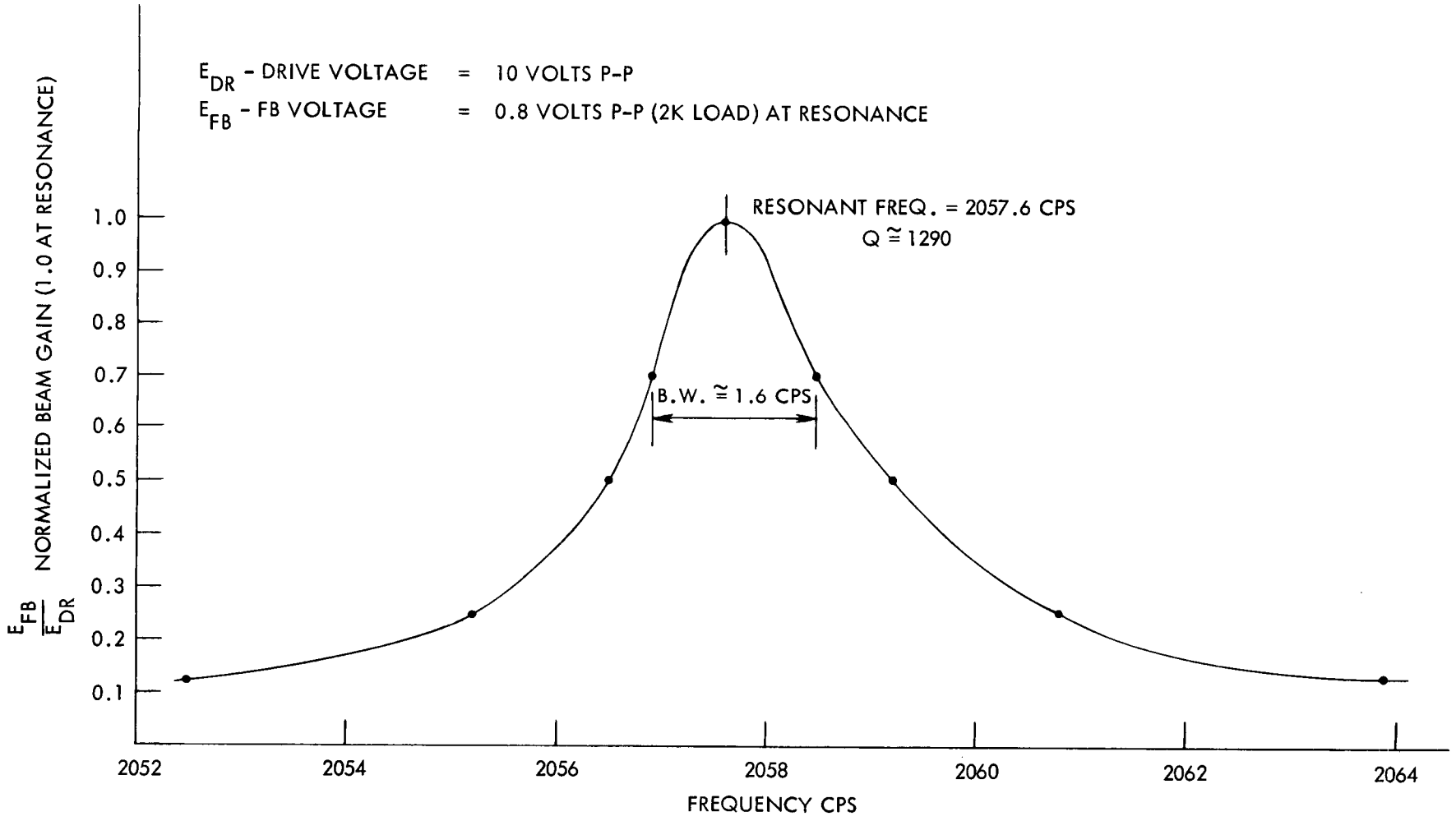

Figure 29. Drive Plane Frequency Response

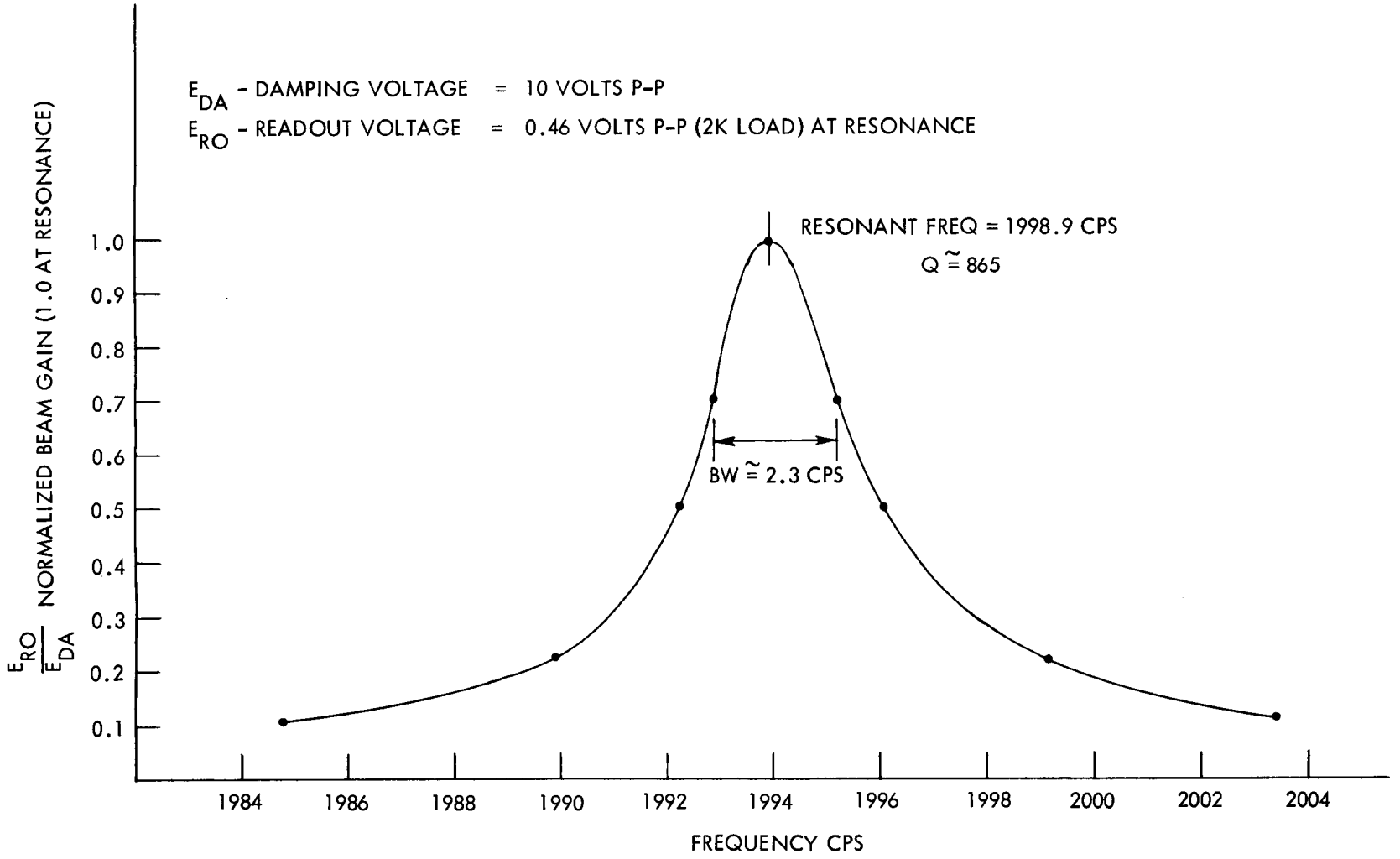

Figure 30. Readout Plane Frequency Response

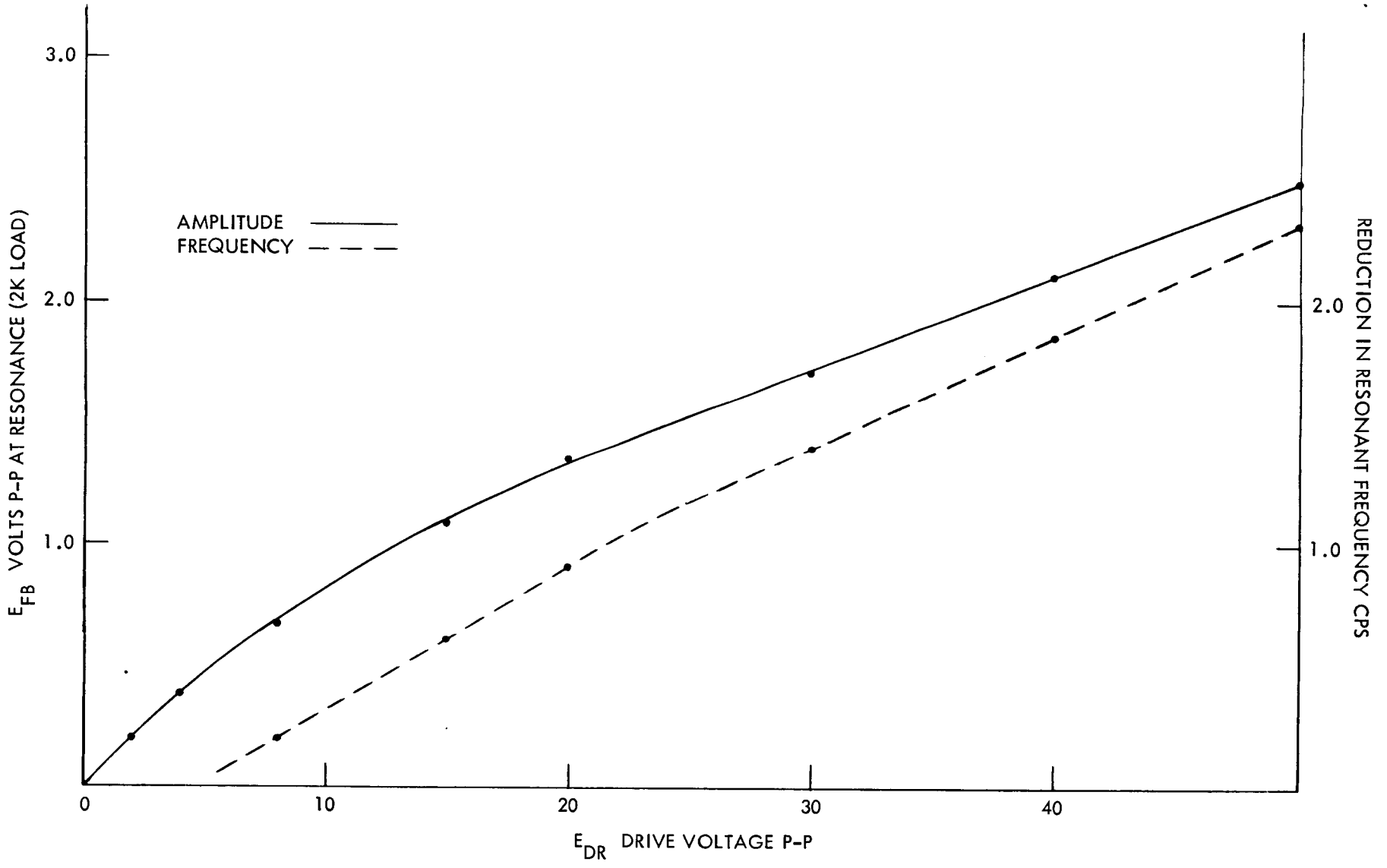

Figure 31. Drive Plane Resonant Response vs Drive Voltage

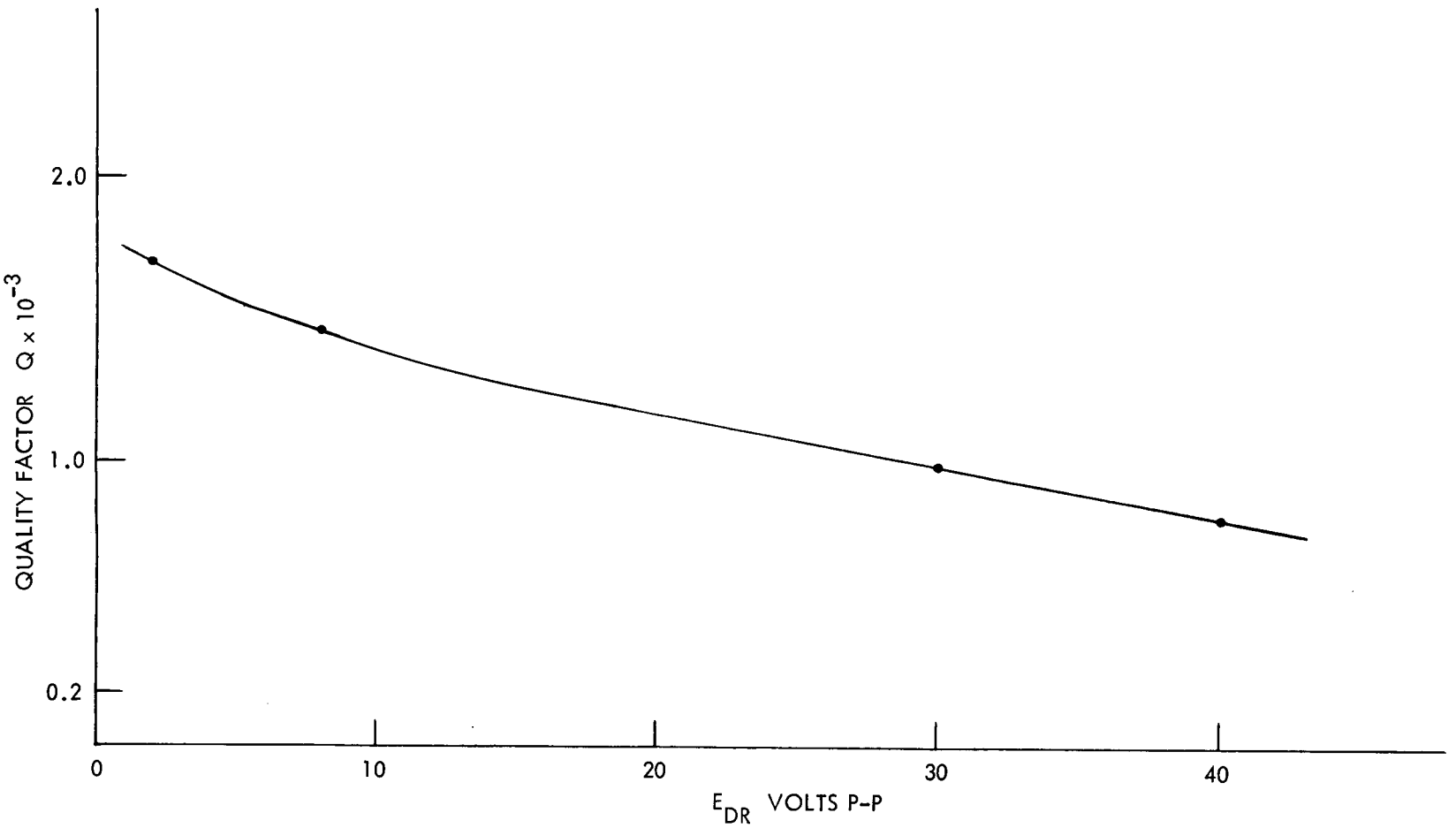

Figure 32. "Q" Variation E With Drive Amplitude

controlled at a specific operating voltage and the readout plane operates at extremely low amplitudes. However, the data shown does imply that the long term stability of the sensor will depend upon the changes in the above curves with environment and time. Further investigation of these effects is planned.

A summary of the laboratory model parameters is given below:

Drive plane (inner axis) at 10 volt excitation

Resonant frequency	2057.6 Hz
Q	1290
Gain (into 2K load) at resonance	0.08 v/v

Readout plane (outer axis) at 10 volt excitation

Resonant frequency	1993.9 Hz
Q	865
Gain (2K load) at resonance	0.05 v/v

Separation frequency = Sensor bandwidth = 63.7 Hz

The free-free beam sensor was calibrated and its linearity measured for input angular rates from 2 deg/sec to 30 deg/sec. The data taken is shown in Table 2 and was obtained with a Genesco Rate-of-Turn table with strobe. The nominal scale factor was set to be approximately 0.4 volt/deg/sec by adjusting the scale factor amplifier gain. For this particular sensor the electronic gain was 300 mv dc/mv p-pac and the actual scale factor at the sensor was approximately 1.3 mv p-pac/deg/sec. The data of Table 1 is plotted in Figure 33 and indicates an average scale factor of 0.395/volt/deg/sec. This scale factor was used to compute the point-for-point linearity of the sensor and electronics. The linearity data is plotted in Figure 34 and represents the point deviation from the average scale factor in deg/sec. The data indicates that the linearity is always better than 1%. The sources of indicated nonlinearity are null shifts and electronic noise; the beam vibrations for input angular rates less than 1000 deg/sec are small enough to yield better than 0.1% linearity.

Some of the most interesting and significant data for the sensor was taken in a series of cross-coupling tests which evaluated the null sensitivity of the sensor. The objective of this evaluation was to find out to what degree the threshold and resolution depended upon the direction of the beam at null. The tests were conducted by modulating the drive voltage, and thus the drive plane motion, at a frequency below or near the separation frequency and

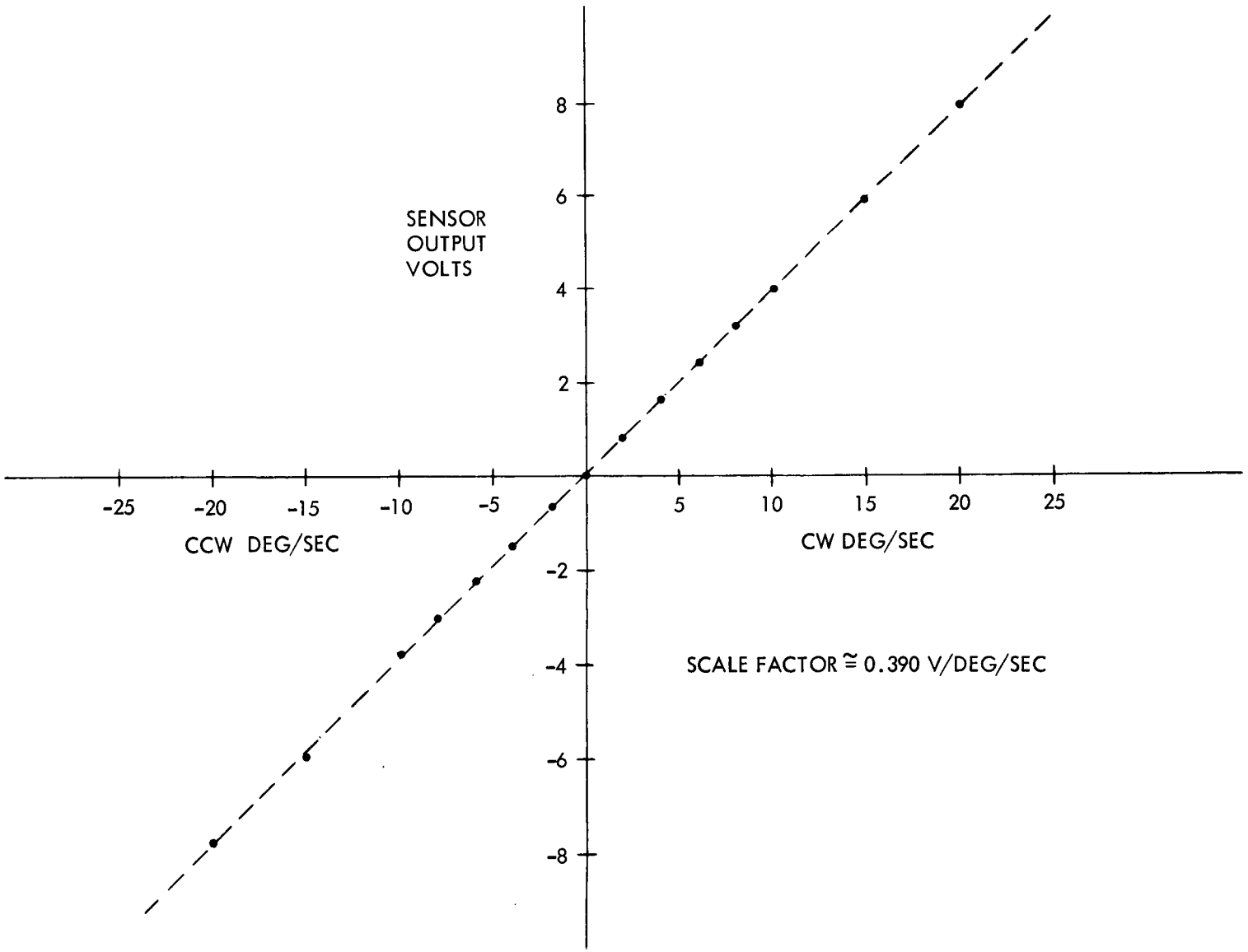

Figure 33. Sensor Output Voltage vs Applied Angular Rate

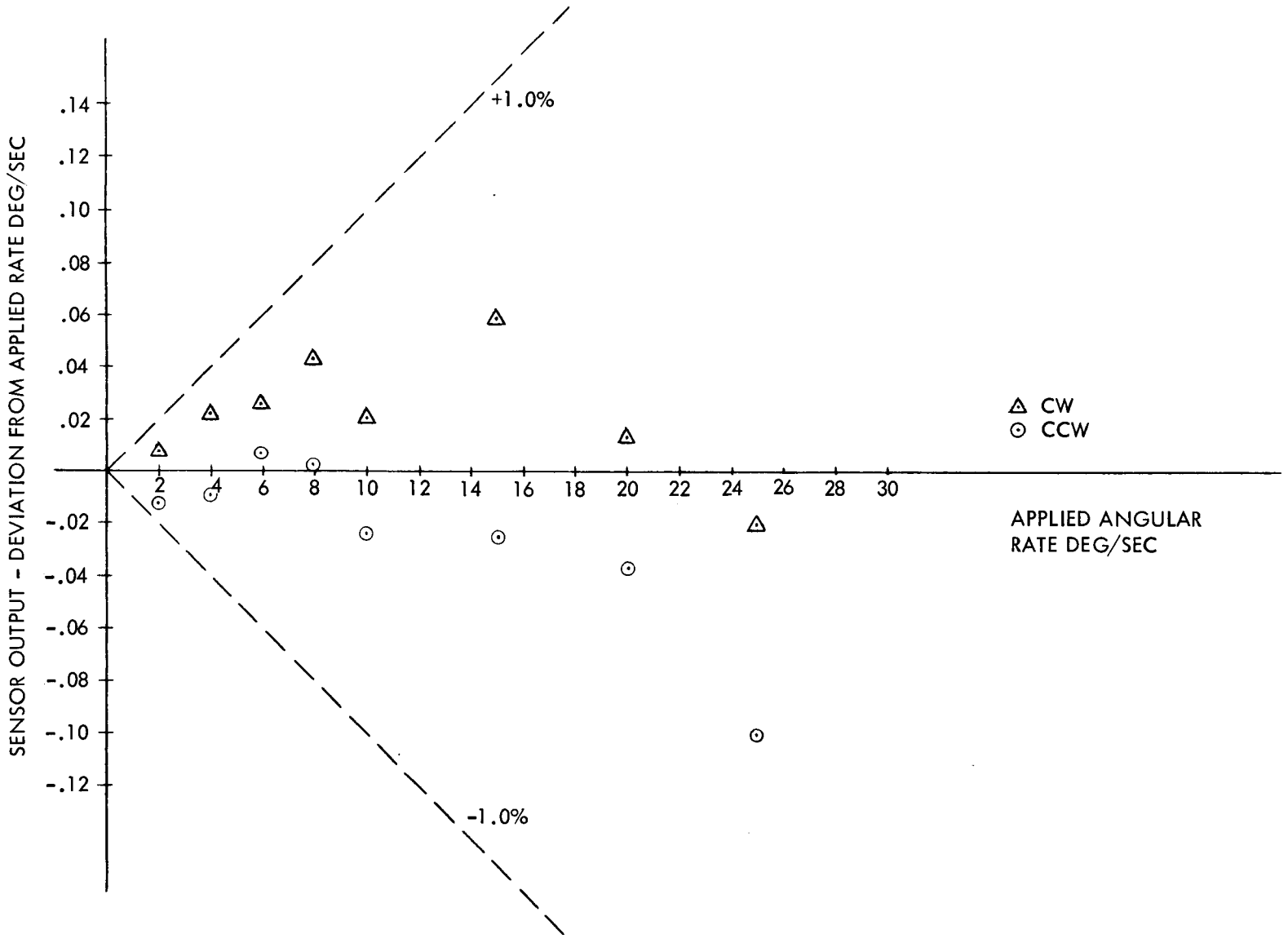

Figure 34. Sensor Linearity

	Angular Rate deg/sec	Sensor Output volts
	30	11.16
	25	9.862
	20	7.906
	15	5.944
CW	10	3.958
	8	3.178
	6	2.380
	4	1.588
	2	.793
	0	.001
	2	.784
	4	1.576
	6	2.374
	8	3.160
CCW	10	3.940
	15	5.910
	20	7.884
	25	9.830
	30	11.05

Scale factor 0.395 volt/deg/sec

TABLE 2

Sensor Calibration

monitoring the amplitude of this frequency component in the sensor output voltage. In general, the results are a large dependence between sensor noise and mechanical null setting. Reductions of up to 10 to 1 in sensor output noise can be achieved by choosing the correct operating point. Two distinct operating points, which are of interest, are the electrical null where the sensor output is trimmed using the split drive transducer to 0 volt dc, and the mechanical, which is defined as the setting of the two drive voltages, which minimizes the noise in the sensor output. Some typical data for the sensor is plotted in Figure 35.

It shows the sensor output voltage due to a modulation of the drive plane motion at different settings of the ratio of voltages on the split drive transducer. Both axes are calibrated in equivalent deg/sec with an S. F. of 0.4 volt/deg/sec. The ratio of sensor coupling at the cross-coupling null and at electrical null (0 vdc) is approximately -52 db. Operation of the sensor at an offset of ~ 16 deg/sec reduces the sensor output noise at the separation frequency by 100 to 1. The separation frequency was chosen for the data because the sensor is most sensitive to noise at this frequency. The existence of the cross-coupling null is probably due to the high stresses placed on the readout crystal due to the drive motion and results in direct transmission from the drive transducer to the readout transducer. Further work is needed in this area to determine the exact causes of coupling.

Traces of the sensor output voltage, which are an indication of the sensor threshold and resolution, were taken at the various null conditions and for just the electronics. These are shown in Figure 36 and show the improvement obtained by operating at mechanical null.

Frequency responses for the laboratory model were taken with an oscillating rate table for sinusoidal input angular rates of 7 deg/sec peak for the various value of sensor damping. This data is shown in Figure 37 and indicates a natural frequency of 65 Hz and an inherent damping ratio of 0.02, which agrees very closely with the analytical prediction contained in the Theory of Operation. The damping ratio is adjusted by varying the drive amplifier gain and, as indicated, a damping ratio of 0.6 can be achieved. For damping ratio of 0.8 or greater, the larger gains and the chopper mechanization of the damping signal increase the level of sensor output noise.

The laboratory model null characteristics were measured to determine the threshold/resolution and the null uncertainty over a long period. This type of data is shown in Figures 38 and 39. The short-term random fluctuations of the sensor output voltage, similar to those exhibited during the discussion of the cross-coupling characteristics, define the sensor threshold or signal-to-noise ratio. Since the vibrating beam sensor does not have any type of deadband caused by friction or other causes, the threshold depends on noticeable changes in the output noise. The trace in Figure 38 indicates a

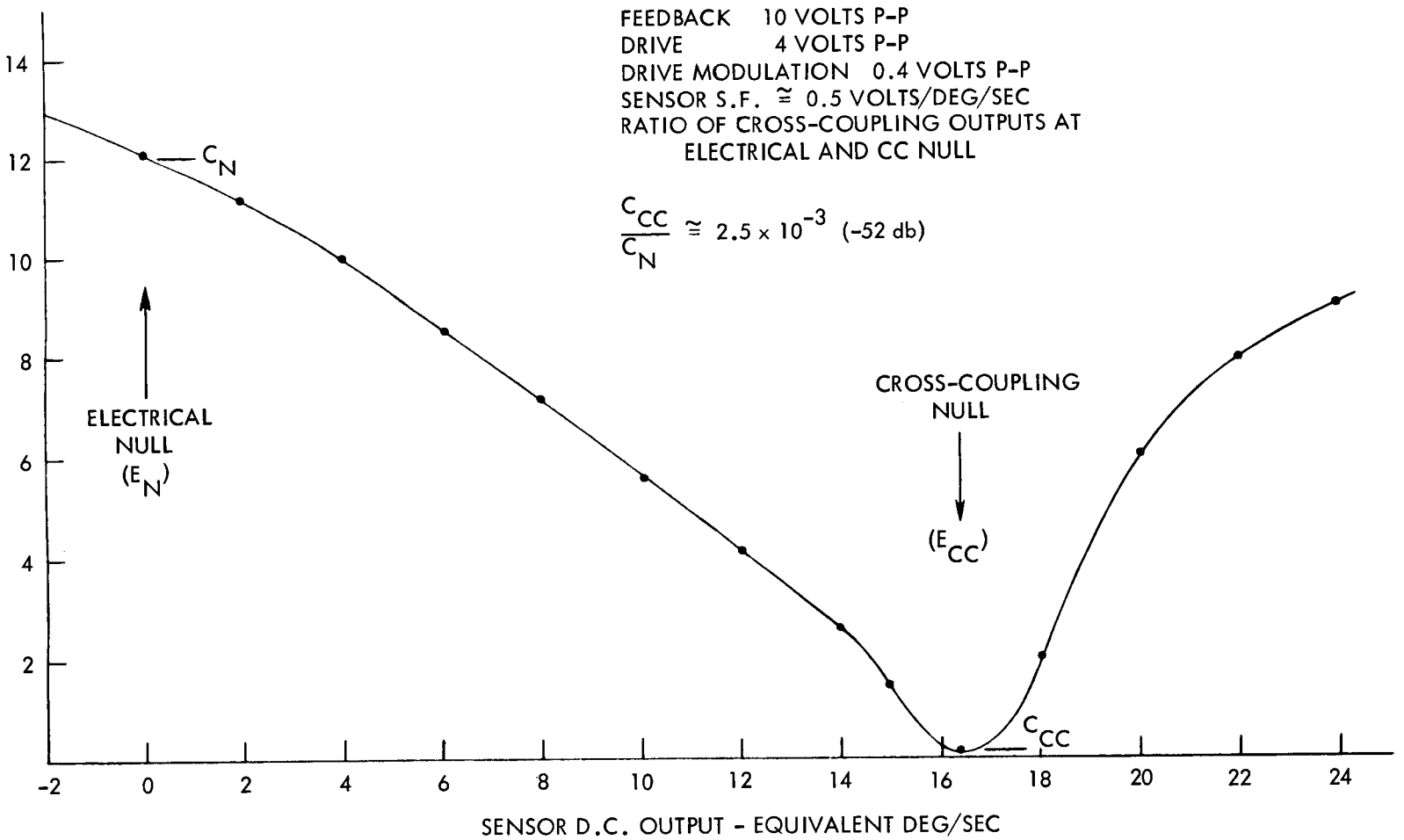

Figure 35. Solid-State Sensor Cross-Coupling Tests

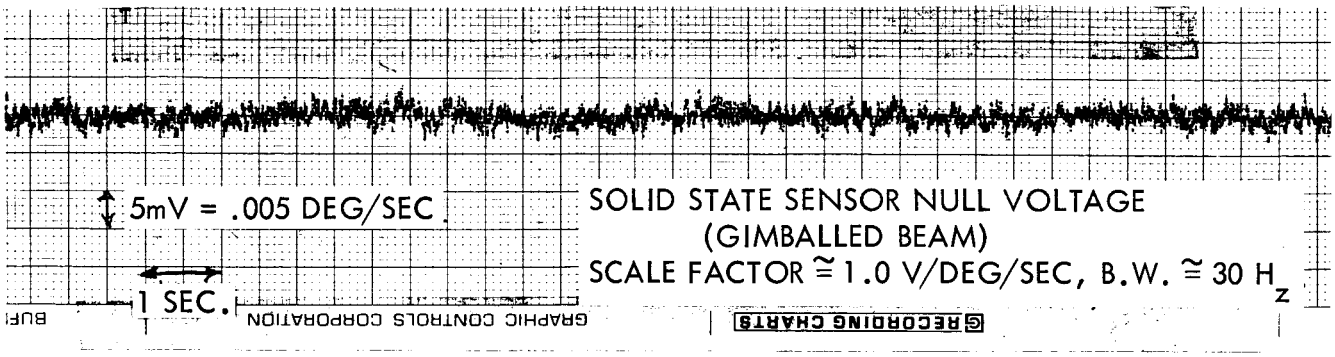

(a)

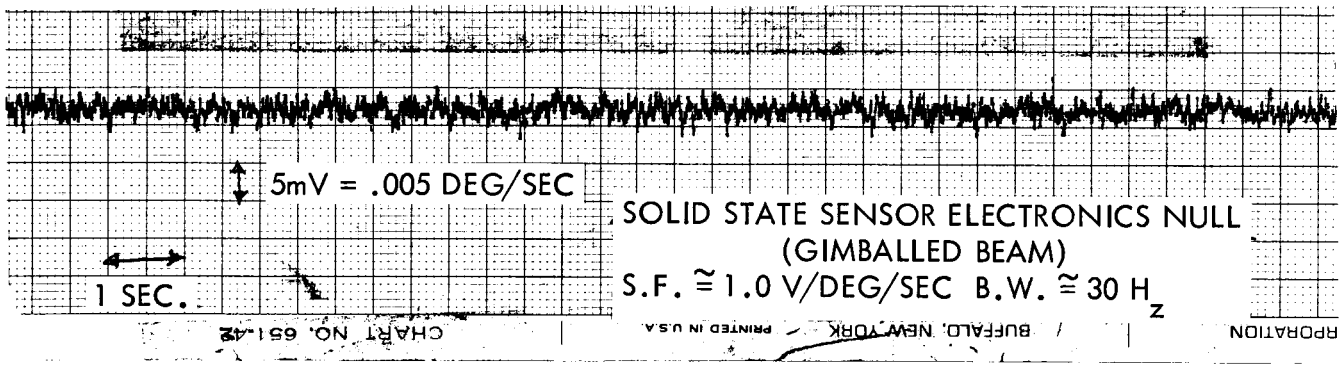

(b)

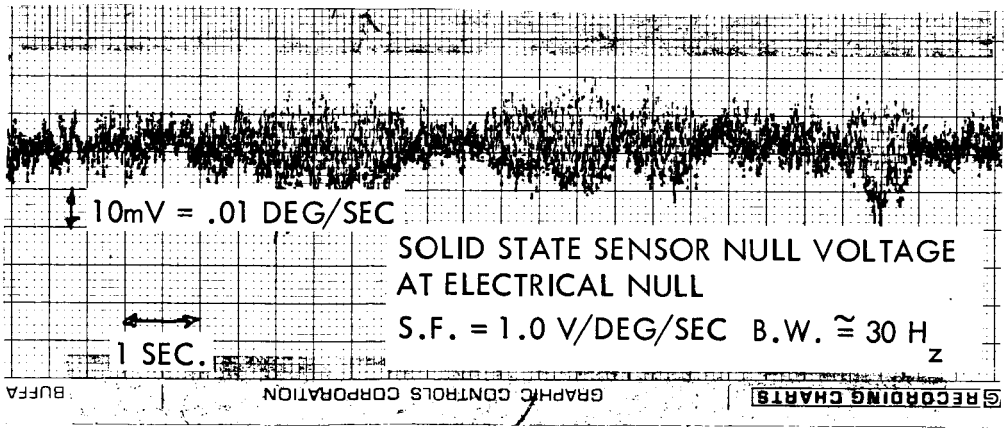

(c)

Figure 36. Sensor Null Traces

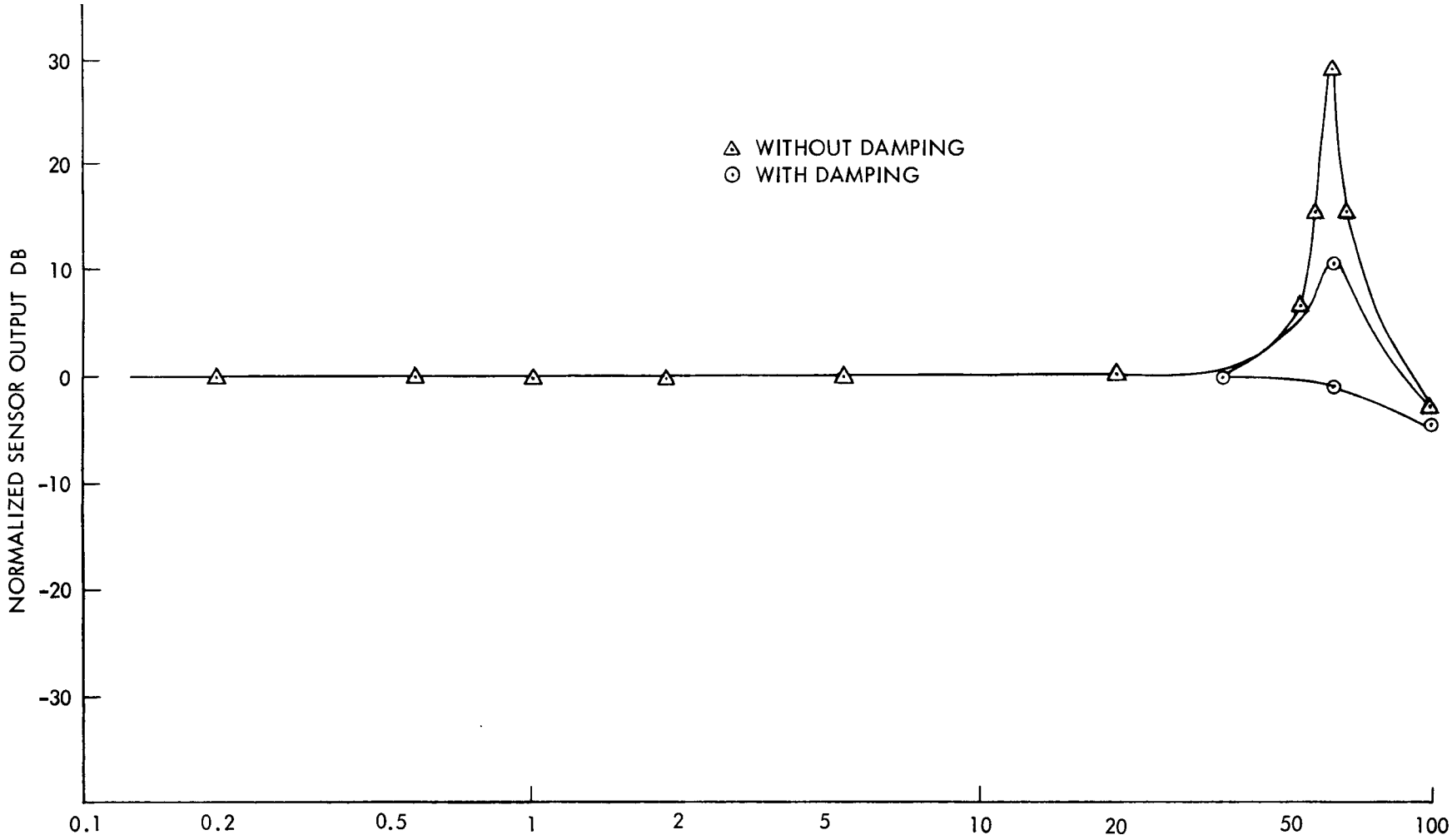

Figure 37. Sensor Frequency Response

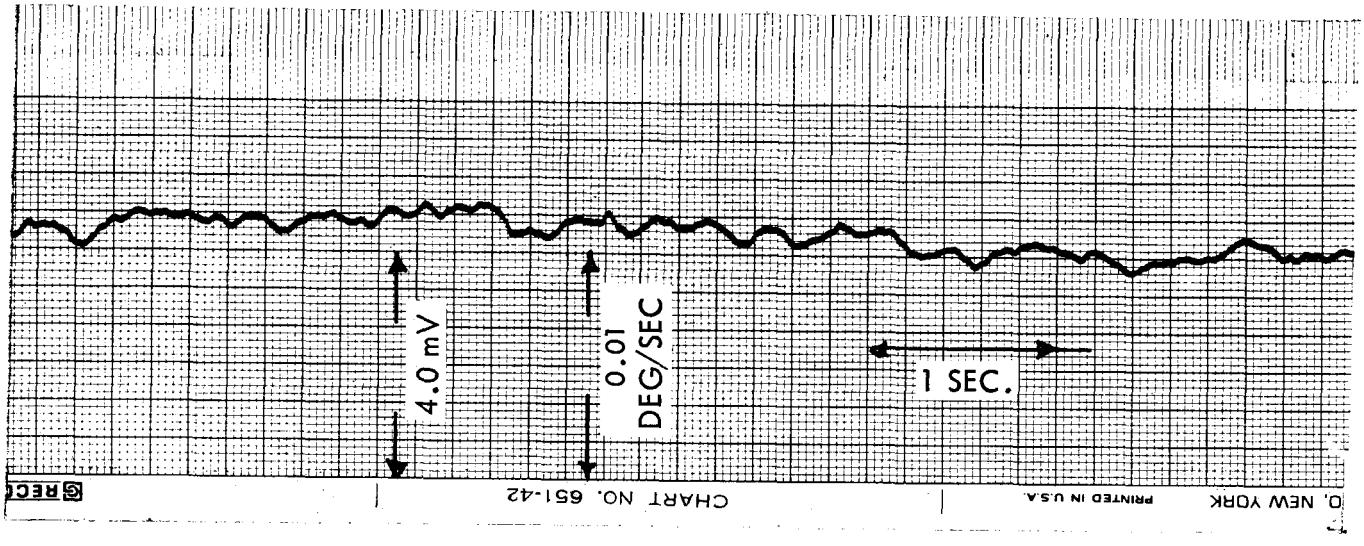

Figure 38. Sensor Output Voltage at Null

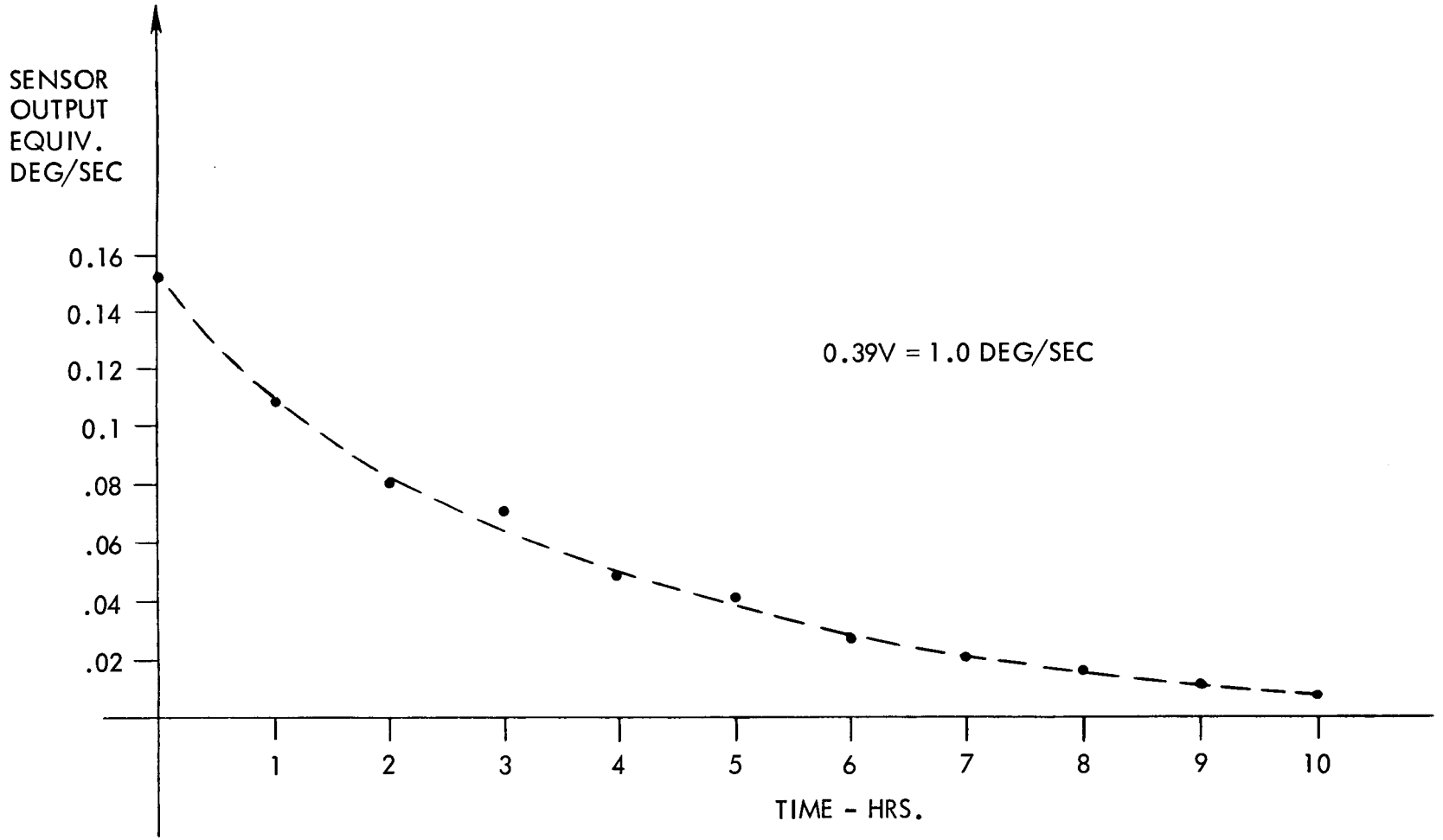

Figure 39. Null Drift of Sensor

peak-to-peak noise voltage of approximately 0.7 millivolts which with a sensor scale factor of 0.4 volt/deg/sec is equivalent to ~ 0.002-0.003 deg/sec. The primary source of the random fluctuations is the electronic noise which results because of the large amplifier gains required. Another source is random modulations of the drive motion which produces separation frequency noise at the output; this source has been minimized by operating at mechanical null. The long term type of data shown in Figure 39 is the null shift of the laboratory model after turn-on. As shown, the sensor has an hourly type of exponential drift with an approximate time constant of 4 to 5 hours. The amplitude of this drift is about 0.15 deg/sec. The cause of this drift is not known exactly but is probably due to a stabilization of transducer and mount parameters. This drift is a function of the time that the sensor has been turned on.

The environmental testing of the sensor laboratory model consisted of temperature tests of the mechanical assembly from -10°C to +70°C and vibration tests of the sensor at 1g from 10 to 2000 Hz. The results of the temperature tests are shown in Figure 40 which is a plot of sensor null in equivalent deg/sec versus temperature. For these tests, the beam and mounting structure were inside the temperature oven and the electronics were outside. The readings at each temperature were made after a half hour soak. As indicated in Figure 40, the null shift due to temperature is approximately ± 6 deg/sec for -10°C to +70°C. The principal cause of these shifts is thought to be the drive transducer and its interface. As pointed out in the section on Theory of Operation, the sensor null is particularly sensitive to changes in the homogeniety of drive transducer coupling. The data shown in Figure 40 consists of a typical run from -10°C to +70°C and the band of data points from five such runs. The variation from run to run is probably due to changes in the transducer characteristics. In addition to this data, the scale factor was checked at various temperatures and was found to vary approximately ± 10% over this range.

The vibration data is shown in Figure 41. The mechanical assembly was vibrated in the output axis which is the most sensitive axis of the sensor to vibration inputs. At low frequencies, below beam resonance, the null shift in equivalent deg/sec due to 1g vibration is less than 0.25 deg/sec. At beam resonance, the null shift increases at least an order of magnitude or two due to Q multiplication and indicates that the nodal points were not exactly correct for this beam. The accuracy of the data at or near resonance is questionable because of the frequency tolerances of the vibration input.

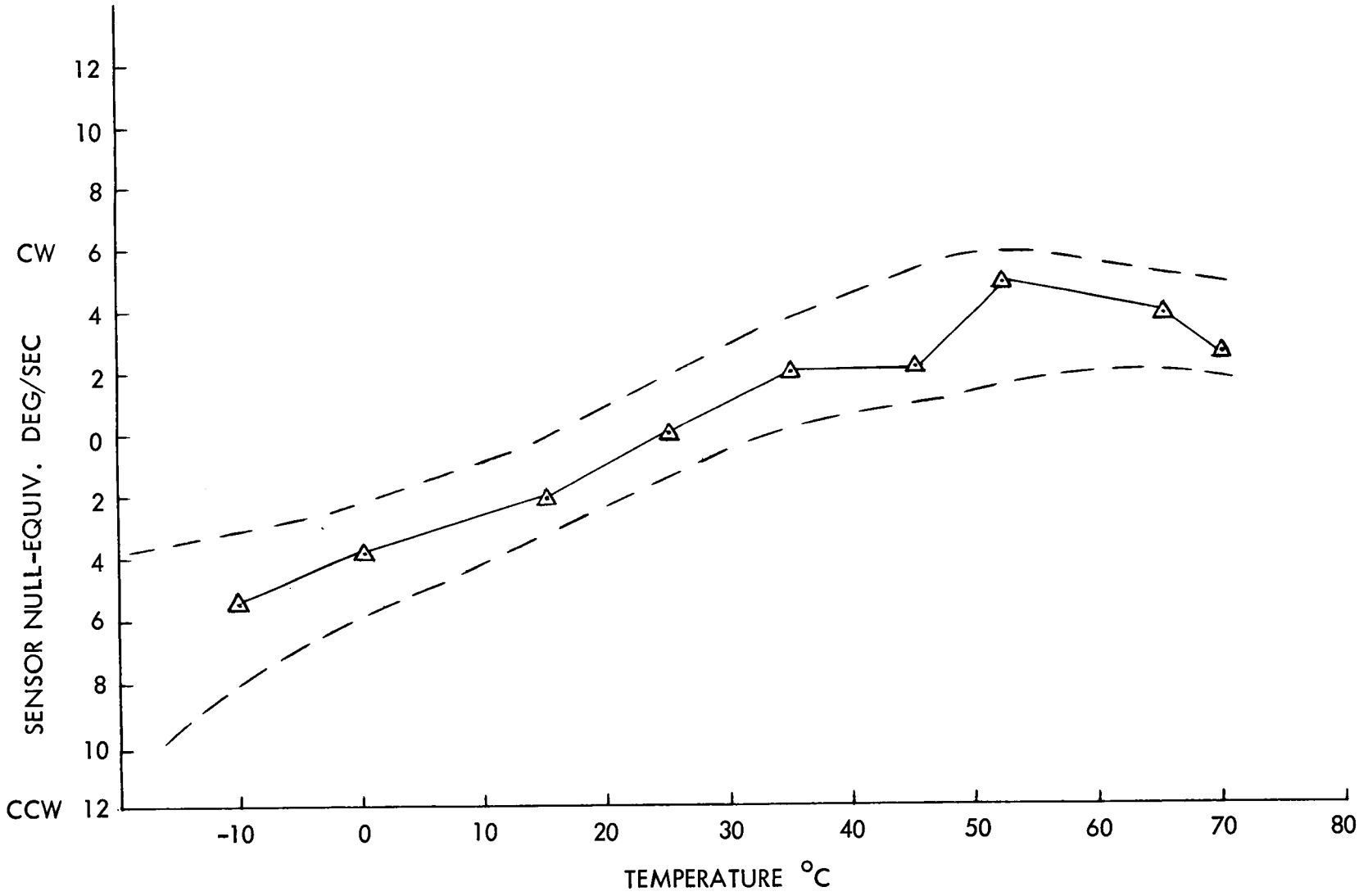

Figure 40. Sensor Null Shift With Temperature

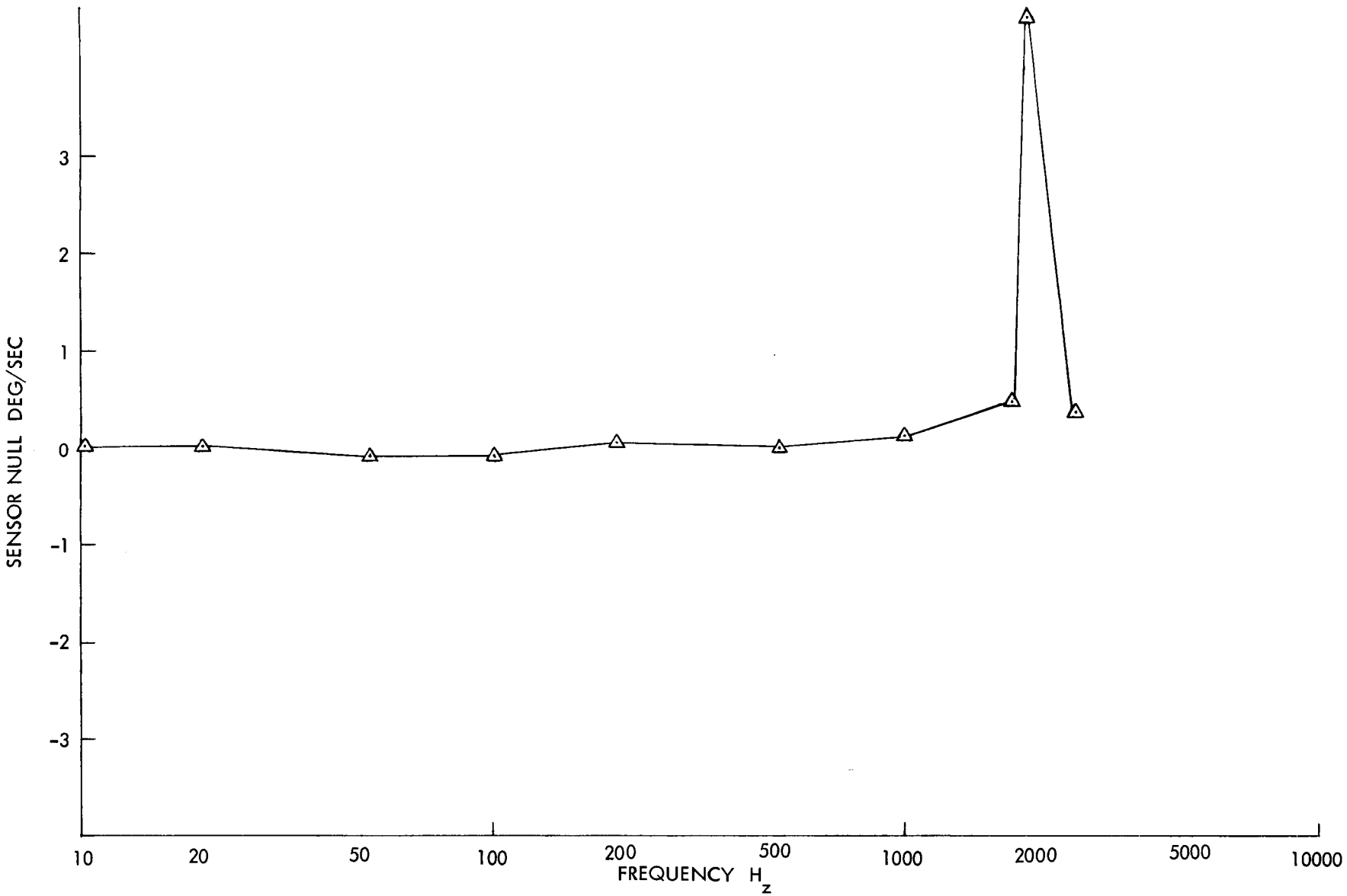

Figure 41. Sensor Vibration Response

Section 5

CONCLUSIONS AND RECOMMENDATIONS

The development and design of the laboratory model for the "free-free" beam, as well as the analysis and testing done on this contract, has shown specifically that improvements in the design of the beam mounting structure and the electronics can improve the null characteristics of the sensor by reducing noise output and stabilizing it. This is accomplished, primarily, by electronically decoupling the vibrations in the sensor and mechanically decoupling the beam vibrations from external accelerations. These improvements are the first step toward the development of a vibratory angular rate sensor of inertial quality. The work on a complete mathematical model for the free-free beam sensor is a start toward the optimization of all sensor design parameters for minimum threshold and null uncertainty.

The "free-free" beam vibratory angular rate angular rate sensor in its present development status is applicable to a wide range of control systems requiring angular rate measurement. These include the damping sensor for a mass expulsion attitude control system for spacecraft and the stability augmentation sensor for aircraft flight control. In particular, for applications where constant rate measurement is not needed and a "canceller" or high pass filter can be used, the sensor can be considered for immediate application. The filter, which may have a time constant of 60 seconds or larger, serves to eliminate the null uncertainty and drift due to turn-on or temperature changes.

Further development of the sensor to attain lower thresholds and null uncertainties should include an investigation of the use of magnetic drive and readout of the beam vibrations, as well as material research. The development of the flexural pivot mount has made it feasible to achieve dimensional stability between the beam and its mounting structure, and thus has made a magnetic drive possible. The principle improvement in sensor performance to be gained from a magnetic mechanization is long-term null stability. Continued development should also include a parameter optimization study and further work on a complete math model for the sensor. The work done on this contract has shown the interrelationships between the sensor design parameters, and further work is needed to be able to systematically select dimensions, frequencies, and gains for minimum sensor threshold.

Appendix A

FREE LATERAL VIBRATION OF A FREE-FREE BEAM

The partial differential equation for the deflection x(z, t) of a vibrating beam of uniform cross-section such as shown in Figure A-1 is

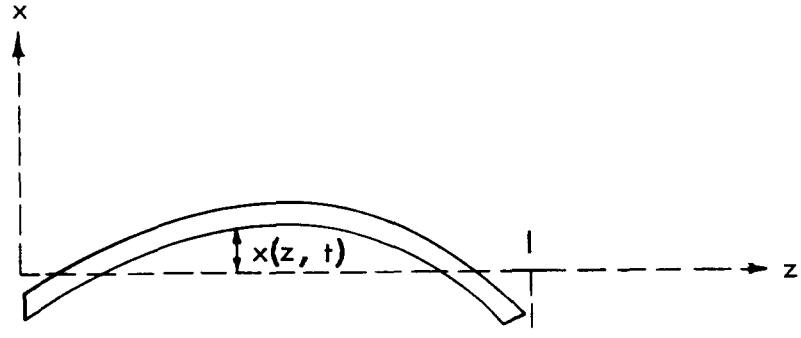

Figure A-1. Free-Free Beam

$$EI \frac{\partial^4 x(z,t)}{\partial z^4} = -\mu \frac{\partial^2 x(z,t)}{\partial t^2}$$ (page 324 of reference 1)

where μ is mass of the beam per unit length and EI is flexural rigidity. The solution of the above equation is found by assuming a solution of the form

$$x(z, t) = H(z) \sin \omega t$$

Therefore

$$EI \frac{d^4H(z)}{dz^4} \sin \omega t = +\omega^2 \mu H(z) \sin \omega t$$

or

$$\frac{d^2H(z)}{dz^4} - \frac{\omega^2 \mu}{EI} H(z) = 0$$

Define $k^4 \equiv \frac{\omega^2 \mu}{EI}$

then $$\frac{d^4H(z)}{dz^4} - k^4 H(z) = 0$$

The general solution of the preceding equation is found by Laplace transform techniques and is

$$H(z) = A_1 \cos kz + A_2 \sin kz + A_3 \cos h\, kz + A_4 \sin h\, kz$$

where the A's are arbitrary constants.

The solution of this problem for the particular case of the free-free beam is found by applying the boundary conditions

(1) $$\left[\frac{d^2H(z)}{dz^2}\right]_{z=0} = 0$$

(2) $$\left[\frac{d^3H(z)}{dz^3}\right]_{z=0} = 0$$

(3) $$\left[\frac{d^2H(z)}{dz^2}\right]_{z=\ell} = 0$$

(4) $$\left[\frac{d^3H(z)}{dz^3}\right]_{z=\ell} = 0$$

The conditions above state that the shape of the beam at any time t must be such that the bending moment and shearing force vanish at the ends. By applying conditions (1) and (2), we find that

$$A_1 = A_3 \text{ and } A_2 = A_4$$

so that

$$H(z) = A_1 (\cos kz + \cos h\, kz) + A_2 (\sin kz + \sin h\, kz)$$

Applying conditions (3) and (4), we obtain the two equations

$$A_1 (\cosh k\ell - \cos k\ell) + A_2 (\sinh k\ell - \sin k\ell) = 0$$

$$A_1 (\sinh k\ell + \sin k\ell) + A_2 (\cosh k\ell - \cos k\ell) = 0$$

A non-trivial solution of these equations for the constants A_1 and A_2 requires that the determinant of the coefficient matrix be equal to zero.

$$(\cosh k\ell - \cos k\ell)^2 - (\sinh^2 k\ell - \sin^2 k\ell) = 0$$

or $$\cos k\ell \cosh k\ell = 1$$

The roots of this equation are the eigenvalues of the problem which determine the resonant frequencies of the beam. The first six roots of the equation are

$$k\ell = 0,\ 4.730,\ 7.853,\ 10.996,\ 14.137,\ 17.279$$

For $$k\ell = 0,\ k = 0 \text{ and } \omega = k^2 \left(\frac{EI}{\mu}\right)^{1/2} = 0$$

$$H(z) = 2A_1 = \text{constant}$$

$$x(z,t) = H(z) \sin \omega t = 0$$

For $$k\ell = 4.73,\ k = \frac{4.73}{\ell},\ \omega = \frac{22.4}{\ell^2} \left(\frac{EI}{\mu}\right)^{1/2}$$

$$\frac{A_2}{A_1} = \frac{\cosh 4.73 - \cos 4.73}{\sin 4.73 - \sinh 4.73} \cong -1$$

$$H(z) = A_1 \left(\cos \frac{4.73z}{\ell} + \cosh \frac{4.73z}{\ell} - \sin \frac{4.73z}{\ell} - \sinh \frac{4.73z}{\ell}\right)$$

The above shape of the beam for the first bending mode as given by H(z) is the normal elastic curve for a free-free beam. Note that the curve has a translation and rotation with respect to the z-axis due to constant and first degree terms in z which are also solutions of the partial differential equation.

An approximation to the elastic curve with the rotational terms removed is

$$H(z) = x_o \sin \frac{\pi z}{\ell} - a$$

The approximate solution for x(z, t) for the first mode is

$$x(z,t) = H(z) \sin \omega t$$

$$x(z,t) = \left(x_o \sin \frac{\pi z}{\ell} - a\right) \sin \omega t$$

where $$\omega = \frac{22.4}{\ell^2} \left(\frac{EI}{\mu}\right)^{1/2}$$

and a is a constant that determines the location of the nodes.

The actual value of 'a' can be found from the fact that since no external alternating force is acting on the beam, its total vertical momentum must be zero. When the beam passes through its equilibrium position, the ends have downward velocities and the middle has an upward velocity. The total momentum is zero for all t if the areas above and below the z-axis are equal.

For $$\omega t = \frac{\pi}{2}$$

$$0 = \int_o^\ell x(z)dz = x_o \int_o^\ell \sin \frac{\pi z}{\ell} \, dz - \int_o^\ell a \, dz$$

Therefore,

$$a = \frac{2x_o}{\pi}$$

and

$$x(z,t) = x_o \left[\sin \frac{\pi z}{\ell} - \frac{2}{\pi}\right] \sin \omega t$$

The nodes are located at the points where

$$\sin \frac{\pi z}{\ell} = \frac{2}{\pi}$$

or $z = 0.22\ell$

$z = 0.78\ell$

REFERENCES

1. Timoshenko, S., "Vibration Problems in Engineering," 3rd Edition.
2. DenHartog, J. P., "Mechanical Vibrations," 4th Edition 1956.